INFORMATION TO USERS

This was produced from a copy of a document sent to us for microfilming. While the most advanced technological means to photograph and reproduce this document have been used, the quality is heavily dependent upon the quality of the material submitted.

The following explanation of techniques is provided to help you understand markings or notations which may appear on this reproduction.

1. The sign or "target" for pages apparently lacking from the document photographed is "Missing Page(s)". If it was possible to obtain the missing page(s) or section, they are spliced into the film along with adjacent pages. This may have necessitated cutting through an image and duplicating adjacent pages to assure you of complete continuity.

2. When an image on the film is obliterated with a round black mark it is an indication that the film inspector noticed either blurred copy because of movement during exposure, or duplicate copy. Unless we meant to delete copyrighted materials that should not have been filmed, you will find a good image of the page in the adjacent frame. If copyrighted materials were deleted you will find a target note listing the pages in the adjacent frame.

3. When a map, drawing or chart, etc., is part of the material being photographed the photographer has followed a definite method in "sectioning" the material. It is customary to begin filming at the upper left hand corner of a large sheet and to continue from left to right in equal sections with small overlaps. If necessary, sectioning is continued again—beginning below the first row and continuing on until complete.

4. For any illustrations that cannot be reproduced satisfactorily by xerography, photographic prints can be purchased at additional cost and tipped into your xerographic copy. Requests can be made to our Dissertations Customer Services Department.

5. Some pages in any document may have indistinct print. In all cases we have filmed the best available copy.

University
Microfilms
International

300 N. ZEEB RD., ANN ARBOR, MI 48106

Downloaded from SHAREOK. Persistent Handle URL: https://hdl.handle.net/11244/4947

8215781

Allam, Awad Moustafa

NUMERICAL SIMULATION OF HETEROGENEOUS FRACTURED GAS RESERVOIR SYSTEMS WITH TURBULENCE AND CLOSURE STRESS EFFECTS

The University of Oklahoma PH.D. 1982

University
Microfilms
International 300 N. Zeeb Road, Ann Arbor, MI 48106

Copyright 1982

by

Allam, Awad Moustafa

All Rights Reserved

PLEASE NOTE:

In all cases this material has been filmed in the best possible way from the available copy. Problems encountered with this document have been identified here with a check mark __√__.

1. Glossy photographs or pages _____
2. Colored illustrations, paper or print _____
3. Photographs with dark background _____
4. Illustrations are poor copy _____
5. Pages with black marks, not original copy _____
6. Print shows through as there is text on both sides of page _____
7. Indistinct, broken or small print on several pages ✓
8. Print exceeds margin requirements _____
9. Tightly bound copy with print lost in spine _____
10. Computer printout pages with indistinct print ✓
11. Page(s) _____ lacking when material received, and not available from school or author.
12. Page(s) _____ seem to be missing in numbering only as text follows.
13. Two pages numbered _____. Text follows.
14. Curling an vrinkled pages _____
15. Other _____

University
Microfilms
International

THE UNIVERSITY OF OKLAHOMA

GRADUATE COLLEGE

NUMERICAL SIMULATION OF HETEROGENEOUS FRACTURED GAS RESERVOIR SYSTEMS WITH TURBULENCE AND CLOSURE STRESS EFFECTS

A DISSERTATION

SUBMITTED TO THE GRADUATE FACULTY

in partial fulfillment of the requirements for the

degree of

DOCTOR OF PHILOSOPHY

BY

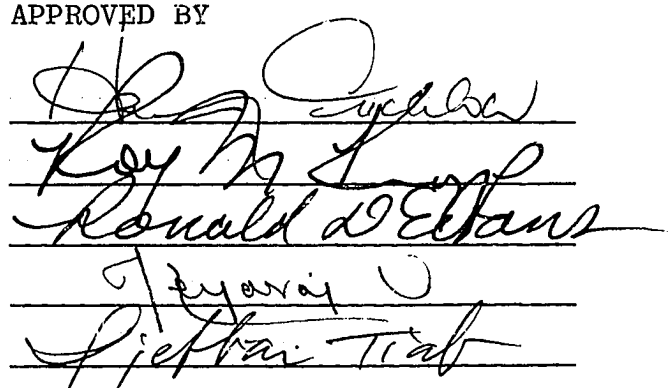
AWAD M. ALLAM

Norman, Oklahoma

1982

NUMERICAL SIMULATION OF HETEROGENEOUS FRACTURED GAS RESERVOIR SYSTEMS WITH TURBULENCE AND CLOSURE STRESS EFFECTS

APPROVED BY



DISSERTATION COMMITTEE

ABSTRACT

Although techniques for designing a fracture treatment are available, the intended results of these techniques are often not attained. The evaluation of fracturing treatments on low permeability gas wells is required to both optimize the fracturing design and form prediction calculations of a treatments effect.

This study primarily investigates the effect of fracture height on the performance of vertically fractured wells. The effects of layered media, turbulance, and closure pressure are included in this work.

Consider that a well, intercepted by a vertical fracture, is in the center of a squared drainage system with closed outer boundary. Any increase in well productivity will be determined by fracture parameters, which are: fracture length, height, fracture conductivity, and location of the fracture in the formation.

On the basis of the analysis of fluid flow in porous media, the problem solving technique used in this study is the numerical method. A three-dimensional finite difference fully implicit model was written for this. In addition, the Sparse Matrix technique was used as a solver. Furthermore,

Slices Source Over Relaxation was used as an iterative method for solving routines.

Presented here are the numerical results of the three-dimensional model for a well intercepting a vertical fracture with finite conductivity. The results are presented in the general form of dimensionless variables. Type curves considering the effect of fracture height on well performance are included. In addition, type curves for turbulent flow in the fracture are also obtained. Finally, other important contributions of this work are the data showing the effect of layered formation on fractured well performance.

Dedicated to my daughter Hannah, my twin sons Mohamed and Ahmed, and my wife Wafaa.

TABLE OF CONTENTS

		Page
ABSTRACT		iii
ACKNOWLEDGMENTS		v
TABLE OF CONTENTS		vi
LIST OF FIGURES		viii
LIST OF TABLES		xii
Chapter		
I.	INTRODUCTION	1
	1. Fracture Geometry	2
	2. Theoretical Consideration	3
	3. Numerical Model Studies	3
	4. Objectives	4
II.	PREVIOUS WORK	5
	1. Analytical Methods	5
	2. Experimental Methods	14
	3. Numerical Methods	19
III.	STATEMENT OF PROBLEM	24
IV.	HYDRAULIC FRACTURE GEOMETRY	26
	1. Fracture Forming and Propping	27
	2. Fracture Area	29
	3. Fracture Width	32
	4. Fracture Conductivity	33
V.	MATHEMATICAL FORMULATION	36
	1. Single Phase Gas Flow Equations	37
	2. Real Gas Potential	42
	3. Non-Darcy Flow	46
	4. Closure Pressure Effects	49

Chapter Page

VI. NUMERICAL MODEL 63

1. Finite Difference Equations . . . 64
2. Methods of Solution 72

A. Sparse Matrix Technique . . . 72
B. SSOR Technique. 74

3. Computer Program. 76
4. Validity of the Model 78

VII. DISCUSSION OF RESULTS 87

1. Effect of Fracture Height 88
2. Effect of Non-Darcy Flow in the Fracture. 94
3. Closure Pressure Effect 110
4. Layered Formations. 114

VIII. CONCLUSIONS 122

NOMENCLATURE 125

REFERENCES 127

APPENDIX A 132

Mathematical Formulation. 133

APPENDIX B 139

Finite-Difference Model 140

APPENDIX C 146

Flow Charts 147

APPENDIX D 153

Example Output. 154

LIST OF FIGURES

FIGURE		Page
4-1	Fracture Plane Related to the Least Principal Stress.	28
4-2	Fracture Orientation.	30
4-3	Proppant Concentration in the Fracture versus Fracture Width	34
5-1	A Schematic View of a Vertically Fractured Well in the Center of Squared Drainage Area	38
5-2	A Two-Dimensional View of the Fractured System.	39
5-3	A Three-Dimensional View of One-Fourth of the Drainage Volume of Vertically Fractured Well in Layered Formation	40
5-4	The Symmetry Element and Boundary Conditions.	44
5-5	The Symmetry Element and Other Boundary Conditions	45
5-6	Flow Capacity Data for 8-12 Mesh Sand	51
5-7	Flow Capacity Data for 10-20 Mesh Sand	52
5-8	Flow Capacity Data for 20-40 Mesh Sand	53
5-9	Flow Capacity Data for 40-60 Mesh Sand	54
5-10	Flow Capacity Data for 50% 20-40 Ottawa Sand and 50% 12-10 Super Prop.	55

FIGURE		Page
5-11	Flow Capacity Data for 75% 20-40 Ottawa Sand and 25% Super Prop.	56
5-12	Flow Capacity Data for 50% 20-40 Ottawa Sand and 50% Super Prop.	57
5-13	Flow Capacity Data for 75% 20-40 Ottawa Sand and 25% 20-40 Super Prop.	58
5-14	Flow Capacity Data for 12-20 Super Prop.	59
5-15	Flow Capacity Data for 20-40 Super Prop.	60
5-16	Flow Capacity Data for 20-40 Ottawa Sand	61
5-17	Flow Capacity Data for 40-60 Super Prop.	62
6-1	Diagram of Grid Distribution. . . .	67
6-2	3-D Model Results Against the Type Curve for Finite Conductivity Fracture (h_f=h).	85
7-1	Log-Log Type Curve for Finite Conductivity Vertical Fracture, F_{cD}=1	90
7-2	Log-Log Type Curve for Finite Conductivity Vertical Fracture, F_{cD}=5	91
7-3	Log-Log Type Curve for Finite Conductivity Vertical Fracture, F_{cd}=10.	92
7-4	Log-Log Type Curve for Finite Conductivity Vertical Fracture, F_{cD}=50.	93

FIGURE		Page
7-5	Log-Log Type Curve for Finite Conductivity Vertical Fracture--Effect of Boundary, X_e/X_f=5	95
7-6	Log-Log Type Curve for Finite Conductivity Vertical Fracture--Effect of Boundary, X_e/X_f=10	96
7-7	Log-Log Type Curves for F_{cD}=1, h_f/h=0.5--Effect of Turbulent Flow	98
7-8	Log-Log Type Curves for F_{cD}=1, h_f/h=0.75--Effect of Turbulent Flow	99
7-9	Log-Log Type Curves for F_{cD}=1, h_f/h=1--Effect of Turbulent Flow	100
7-10	Log-Log Type Curves for F_{cD}=10, h_f/h=1--Effect of Turbulent Flow	101
7-11	Log-Log Type Curves for F_{cD}=10, h_f/h=0.5--Effect of Turbulent Flow	102
7-12	Log-Log Type Curves for F_{cD}=10, h_f/h=0.75--Effect of Turbulent Flow	103
7-13	Log-Log Type Curves for F_{cD}=50, h_f/h=1--Effect of Turbulent Flow	104
7-14	Log-Log Type Curves for F_{cD}=50, h_f/h=0.75--Effect of Turbulent Flow	105
7-15	Log-Log Type Curves for F_{cD}=50, h_f/h=0.5--Effect of Turbulent Flow	106

FIGURE		Page
7-16	Log-Log Type Curves for F_{cD}=100, h_f/h=1--Effect of Turbulent Flow.	107
7-17	Log-Log Type Curves for F_{cD}=100, h_f/h=0.75--Effect of Turbulent Flow.	108
7-18	Log-Log Type Curves for F_{cD}=100, h_f/h=0.5--Effect of Turbulent Flow.	109
7-19	Predicted Flow Rate Versus Time--Effect of Closure Pressure.	113
7-20	Type Curves for Layered Formation with Cross Flow--Using Average Parameters ($\overline{kh}$)	116
7-21	Type Curves for Layered Formation --Boundary Effect	117
7-22	Effect of Reservoir Heterogeneity on the Production Rate.	119
7-23	Effect of Thickness Ratio on the Production Rate	120
A-1	Gas Mass Balance on Element	138

LIST OF TABLES

TABLE		Page
6-1	Constants a and b for Calculating the B Factor	69
6-2	Comparison Between Analytical and Numerical Solutions for F_{cD}=10, h_f/h=1 and M_{DT}=0.	81
6-3	Comparison Between Analytical and Numerical Solutions for F_{cD}=50, h_f/h=1 and M_{DT}=0.	82
6-4	Comparison Between Analytical and Numerical Solutions for F_{cD}=1, h_f/h=1 and M_{DT}=0	83
6-5	Comparison Between Analytical and Numerical Solutions for F_{cD}=5, h_f/h=1 and M_{DT}=0	84
7-1	Reservoir and Fluid Property Data.	112

NUMERICAL SIMULATION OF HETEROGENEOUS FRACTURED GAS RESERVOIR SYSTEMS WITH TURBULENCE AND CLOSURE STRESS EFFECTS

CHAPTER I

INTRODUCTION

Hydraulic fracturing has proven to be one of the most effective means currently available for increasing the productivity of damaged wells or wells producing from low permeability reservoirs. This process has been applied as a well completion technique for about thirty years. In some cases, this technique has been used to improve the injectivity of wells in injection processes. Massive hydraulic fracturis a recent application, differing from hydraulic fracturing in that much larger quantities of fluid and proppant are pumped to create extensive fractures in the reservoir. Essentially, the hydraulic fracture causes a high permeability condiut within the formation to allow a large drainage area around the wellbore. With the introduction of massive hydraulic fracturing techniques, it is now possible to exploit economically low permeability gas reservoirs.

Application of massive hydraulic fracturing to increase

production from low permeability formations has provided unsatisfactory results, in many cases. In addition, pressure analysis techniques often indicate the result of fracturing differ from the designed parameters. Calculated fracture lengths from actual well performance are much shorter than the designed fracture lengths. In most cases, the assumption was made that the permeability of the fracture is infinite and the fracture height equals the formation height. Initially, these assumptions seemed to be realistic, but in time, the analysis of pressure data including these assumptions produced unreasonable results. Recently, solutions have been presented which develop techniques for analyzing fractured systems with finite conductivities.

The main purpose of this study is to determine fracture performance using computer simulation techniques. Also, the effect of fracture height on the productivity increase is to be closely examined. In addition, the effects of non-Darcy flow within the fracture is to be considered. Furthermore, effects of closure pressure for a finite conductivity fracture are considered. The phases of the study in this dissertation are outlined in the following:

1.1 Fracture Geometry

Section IV provides a brief description of the vertical fracture system. Fracture forming and propping is reviewed

in this section. Fracture area is defined as the product of fracture length and fracture height. It was always assumed that fracture height equals formation height. In this work, such an assumption is not made. Thus, fracture geometry is determined by fracture length, height, and width. Fracture height is limited by the upper and lower boundary of fractured formation. Fracture width as well as fracture length depend on formation characteristics and treating parameters. Finally, a very important factor which effects the fracture system is fractue conductivity. The effectiveness of a certain fracture is determined by the actual fracture flow capacity.

1.2 Theoretical Considerations

Section V deals with the mathematical formulation of the problem. The real gas potential is used instead of pressure in developing the governing partial differential equations for the system. In addition, the turbulent effect of non-Darcy flow is considered for the fractured cells only. The flow in the formation obeys Darcy's law. Finally, the change of fracture conductivity with time and distance is included in this study.

1.3 Numerical Model Studies

A finite difference fully implicit numerical computer program is written. The finite difference model is three-dimensional one phase simulator. The sparse matrix technique

is used to obtain a direct solution. Further, the Slices Successive Over Relaxation is also used as an iterative solution scheme in this model. Section VI includes the finite difference equation, boundary conditions, and methods of solution. The validity of the model is also checked in this section.

1.4 Objectives

The objectives of this work include the following:

1. Develop a three-dimensional simulator to model vertical fractured wells in layered formations.
2. Determination of well productivity for vertically fractured wells in heterogenous reservoirs.
3. Effect of fracture height on well performance for vertically fractured wells with finite conductivity fracture.
4. Effect of non-Darcy flow in the fracture on well performance for vertically fractured wells.

CHAPTER II

PREVIOUS WORK

To obtain commercial production of hydrocarbon fluids from low permeable reservoirs, most of these formations must be hydraulically fractured. One of the most important processes developed in the petroleum industry is hydraulic fracturing. The importance of this process is indicated by the increasing need for more energy sources every day. Ever since hydraulic fracturing was first presented to the petroleum industry,[1] it has been known that this process will increase the productivity of a stimulated well. Hydraulic fracturing has been the subject of many studies. Several methods, analytical, experimental and numerical analysis, have been used to investigate this process.

2.1 Analytical Solution

A vertical fracture is the most likely outcome of a fracturing treatment. Thus, most of the attention in the literature has been directed toward vertical fractures. Much of the early work on fractured wells was concerned with the study of steady state behavior using analytical models. In 1961, Prats[2] studied the production response and pressure

behavior of a closed cylindrical reservoir producing an incompressible fluid through a single, vertical fracture located at the center of the cylinder. Prats' study considers the effect that fracture capacity, as well as the formation damage from fracture treatments, have on the productive capacity of vertically fractured wells. In addition, the study gives the equivalent well radius of a fracture having different lengths and capacities and, also, includes pressure distribution in and around the fractures. The effect of a damaged zone around a fracture on the production response was not found to be as great as reported earlier in the literature by Van Poolen.[3] This difference probably stems from the fact that Prats considers a damaged zone which is widest near the fracture, while, VanPoolen considers a damaged zone having a uniform width for the entire fracture length.

Prats found that the production rate decline increases as the fracture length increases. He suggested that the lateral extent of the fracture can be determined from comparison of production rate declines before and after fracturing, or it can be determined from the rate decline if the fluid and formation properties are known. It is found that extensive damage to the formation around a fracture (99 percent permeability reduction for a depth of 1 inch) may not necessarily result in appreciably poorer production rate response. It is concluded that the improvement in production rate due to a high-capacity fracture is equal to the

improvement in production rate due to an acid treatment which results in an effective well radius of one-fourth the fracture length. This suggests that fracturing is to be preferred to acidizing if the creation of long fractures appears probable.

Prats also found that if the ratio of reservoir radius to fracture radius was greater than two, then the production behavior of such a fractured system can be represented by an equivalent radial flow system having an effective well radius equal to one-fourth of the total fracture length.

Muskat[4] arrived at a similar conclusion earlier when he examined a fractured well in an infinite reservoir. In petroleum engineering literature, this observation is known as the "effective wellbore radius concept."

In 1962, Prats et al,[5] studied the effect of vertical fractures on reservoirs producing a compressible fluid. The pressure and production behavior of a homogeneous cylindrical reservoir producing a single fluid through a centrally located vertical fracture of limited lateral extent was investigated. The appropriate partial differential equations were solved by using mathematical methods. It is assumed that there is no pressure drop within the fracture, that is to say, that the fracture capacity is infinite.

They found that the production rate decline of such a fractured reservoir is constant when the flowing bottomhole pressure remains constant. This decline increases as the fracture length increases. Thus, the lateral extent

of fractures can be determined from the production rate declines before and after fracturing. They also concluded that the production behavior over most of the productive life of such a fractured reservoir can be represented by an equivalent radial flow reservoir of equal volume. The effective well radius of this equivalent reservoir would be equal to one-fourth of the total fracture length. Therefore, it appears that the behavior of vertically fractured reservoirs can be interpreted in terms of simple radial flow reservoirs of large wellbore.

In 1971, Van Everdingen and Myer[6] studied buildup curves obtained after well treatment. They concluded that the point source solution can be used in analyzing pressure data from normally completed wells. However, either an acidizing or fracture treatment invalidates this conclusion because of the fact that the duration of one dimensionless time unit is substantially increased.

Although interest in wells intercepting vertical fractures dates back a quarter of a century, the first comprehensive study of the pressure transient response of such well, was performed by Gringarten *et al.*[7] They studied the case flow to an infinitely conducting vertical fracture in infinite reservoirs.

In 1974, Gringarten, Ramey, and Raghavan found it necessary to re-examine the solutions presented by Russell and Truitt. (This will be discussed in the following section

in more detail). The Russell-Truitt solution was not intended for short time analysis. They examined the problem analytically by using Green's functions and the Newman[8] product method which had been discussed earlier by Gringarten and Ramey.[9] Gringarten, et al, were also the first to present a complete and comprehensive view of the pressure behavior of a infinite-conductivity vertical fracture. They modeled a plane (zero-thickness) vertical fracture which is totally penetrating a horizontal, homogeneous, and isotropic formation. A single-phase, slightly compressible fluid flows from the reservoir into the fracture at a constant rate. The producing pressure is uniform over the fracture rate. The producing pressure is uniform over the fracture (infinite fracture conductivity). This pressure remains constant and equal to the initial pressure as distance from the well becomes infinitely large.

An analytical solution was obtained by Gringarten, et al, called the uniform-flux solution. The uniform-flux solution gives the appearance of a high, but not infinite, conductivity fracture. Thus, unlike infinite conductivity boundary conditions, the pressure varies along the length of the fracture at any given time. Application of these solutions to field data indicates that the uniform-flux solution usually matches pressure behavior of wells intersecting natural fractures better than the infinite-conductivity solution. On the other hand, the infinite-conductivity solution

matches the behavior of hydraulically fractured propped wells better than the uniform-flux solution.

Gringarten, et al, also proposed that log-log type curve matching (actually Ramey[10] suggested this approach in 1970) be used to calculate permeability and fracture length. The basis for the type curve matching procedure is well known in petroleum industry literature. They, also, provide a comparison of the analytical solution results for vertically fractured wells with the Russell-Truitt data.

Application of the Gringarten, et al, type curves to hydraulically fractured wells, in many instances, produces results that are compatible with reservoir performance and design calculations prior to treatment. But, in some instances, the results are not compatible with design calculations or production performance, even though field data matched the type curve very well. One of the reasons for this anomaly appears to be the finite flow capacity of the vertical fracture.

Refering back to the study of Prats, which was published nearly twenty years ago, he described the effect of finite fracture capacity as, "the product of fracture permeability and fracture width." This is defined and presented in this paper. But unfortunately, its importance has been ignored for many years. Prats showed that three parameters controlled the pressure distribution around a fractured well. They are, (A) the ratio of the fracture length to the well

radius, (B) the ratio of the reservoir drainage radius to the well radius, and (C) the dimensionless fracture flow capacity. The first two parameters describe the geometry of the system and the third is the measure of the ability of the fracture to carry fluids from the formation into the well. The most important contribution of Prats' paper is the dimensionless fracture flow capacity. This determines that well performance and productivity increase - not the fracture length. Hence, for a long fracture to be as efficient as a short one, the fracture flow capacity would have to be much higher for the longer one.

Agarwal, Carter, and Pollock[11] report that for practical purposes, the infinite-conductivity solution obtained by Gringarten, et al, can be used if the fracture flow capacity is greater than five hundred. They strongly recommend, however, when this is done, that prefracture pressure data be measured whenever possible. Type curve match analysis can be performed with considerable ease and a match can be obtained. Agarwal, et al, have empirically correlated the dimensionless pressure intercept as a function of dimensionless fracture flow capacity. Thus, this correlation may be used to determine fracture flow capacity.

Cinco and Samaniego[12,13] have presented a methodical explanation for the pressure behavior of a vertically fractured well of finite fracture capacity. They have shown that, initially, there is a fractured linear flow period when

the pressure behavior is controlled principally by the fracture. During this period, the formation has no effect on pressure behavior since most of the fluid entering the wellbore comes from fluid expansion within the fracture.

Subsequent to the fracture linear flow period, Cinco and Samaniego have shown that another distinctive flow period exists. They call this flow period a bilinear flow period. During this period, the flow in the fracture is linear incompressible flow, and that which is within the formation is a linear compressible flow. This flow period exists whenever most of the fluid entering the wellbore comes from the reservoir when the effect of the fracture tip is negligible. For the high fracture capacity solution, we see that the bilinear flow period may or may not exist. Cinco and Samaniego have presented a technique to analyze data on the bilinear flow period. It was shown that during this flow period, a graph of bottom-hole pressure versus fourth root of time yields a straight line with slope related to the fracture flow capacity and fracture height.

The next characteristic flow period, according to Cinco and Samaniego, is a linear flow period in the formation. A graph of bottom=hole pressure versus square root time yields a straight line whose slope is related to the fracture length. If boundary effects do not become dominant, then the pseudoradial flow regime will govern pressure behavior.

In 1978, Raghavan, Uraiet, and Thomas[14] studied the effect of vertical fracture height on transient flow behavior analytically. Their work presents an analytical study of the pressure behavior of a well producing at a constant rate through one vertical fracture from an infinitely large reservoir. The fracture height is less than the formation thickness. They examine both the uniform-flux and infinite-conductivity fractures and considered two fracture locations (center and top) in the producing interval. In addition, they present information regarding production rate changes as a function of fracture height.

Raghavan, et al, have discussed methods for determining horizontal permeability, vertical permeability, fracture length, and entry ratio from drawdown and buildup tests. They concluded that at early times, a linear flow period which controls pressure behavior does exist. The duration of this period is governed by the fracture location, fracture length, vertical permeability, and the fracture type (infinite conductivity or uniform-flux). If the fracture is located at the top (or bottom) of the formation, the length of this flow period is almost the same as entry ratio equals one case. During this period, the well behaves as if the formation thickness is equal to the fracture height. Following the linear flow period is the transitional flow period. After this period, a pseudo-radial flow period controls pressure behavior. The onset of the pseudo-radial flow period depends

on the reservoir thickness, fracture length, the ratio of vertical-to-horizontal permeability, and is independent of the location of the fracture.

Raghavan, et al, also concluded that the magnitude of the pressure drops for the limited-entry case and is larger for the complete-entry case because of the converging nature of the flow. This additional pressure drop is time dependent and stabilizes after the onset of pseudo-radial flow. The pressure drop increases as the fracture departs from the center line of the formation. This implies that the productive capacity of a fractured well also depends on the fracture location.

2.2 Experimental Solution

In 1958, Dyes, Kemp, and Caudle[15] were the first to investigate the effect of a vertical fracture on Horner plot straight line. They used the x-ray shadowgraph technique, using miscible displacement in porous models, while studying the influence of fractures on pattern sweep-out efficiency. Fractures were represented by leaving the proper portion of the model surface which was exposed to either injection or production. The types of models were to represent vertical fractures in the five-spot flood.

The pool unit of a Carter electric analyzer was used in studying the influence of fractures on productivity and buildup behavior. The square drainage system of a well was represented by a network of over five hundred elements of

equal volume and resistance. Vertical fractures were represented by a shunt directed from the well perpendicular to the drainage boundary. Horizontal fractures were represented by a circular shunt.

Dyes, et al, concluded that short fractures can be used in flooding operations to gain an increase in injectivity or productivity. A long fracture does not harm the sweep if it is directed between producers. Productivity and pressure buildup tests obtained prior to and following a fracture treatment on a well can be used to differentiate between a short or long fracture in the reservoir.

Most of the experimental work in the area of vertically fractured wells is done because of the great interest in the productivity increase that would result from a fracture treatment. Unfortunately, the results are not in good agreement.

In 1960, McGuire and Sikora[16] were studying the effect of vertical fractures on well productivity by using an electric analogue. This study considers fractures which extend in a vertical plane with equal distance on both sides of the wellbore and through the entire height of the reservoir. The well of six-inch diameter drained 40 acres in a square drainage area. They used the pool unit electric analyzer in their study. By scaling, the results were applied to all combinations of well diameter and spacings.

Sikora provided a family of curves for productivity

increase in fractured wells under steady state conditions. They showed us, experimentally, that the fractures can be made more effective by increasing their relative conductivity. This can be done by propping the fracture with large high strength particles.

In contrast, little improvement in the productivity of the well is gained by increasing the relative conductivity of short fractures. This is because of the undistributed formation beyond the end of the fracture controls the rate of flow.

In 1963, Scott[17] examined the transient pressure behavior of wells intersected by a vertical fracture; he used a heat flow analogy. Results are correlated in terms of dimensionless pressure change and dimensionless transient time. Use of Scott's curves provide a means of determining reservoir permeability, effective wellbore radius, and fracture length.

A heat flow model was constructed to determine the applicability of the pressure transient theory to vertically fractured wells. A complete description of the model is presented in reference 17. For the test, the simulated fracture well was inserted into the reservoir container. Then, granular material of low conductivity was poured into the container and vibrated to a uniform packing. There the reservoir was brought to a uniform temperature in an air bath.

Scott found, as Prats also found, that for high capacity

fractures, the effective wellbore radius is about one-fourth of the total fracture length. Effective wellbore radii in Scott's experiments were found to be higher than those computed by Prats for low conductivity fractures. He attributed that difference to the physical size of the heating wires used in the experiment. It was concluded that the vertical fracture causes a changing slope of the transient pressure curve in fractured wells. In addition, transient pressure behavior of vertically fractured wells may be related to dimensionless pressure curves to determine formation permeability, effective wellbore radius, and fracture length.

Tinsley, Williams, Tiner and Malone[18] have investigated the effect of fracture height on staedy-state production increase by use of electrolytic analogue, in which a conductive solution represents a uniform isotropic porous media. They considered a vertical fracture with constant width in a homogeneous formation producing a single incompressible fluid under a steady-state condition. The model constructed for these experiments was geometrically similar to a producing well with a circular boundary drainage. The model was built with all dimensions scaled to 1/100 of the prototype. The diameter wall was a non-conductive sheet of acrylic plastic, and the semicircular conductive well was aluminum. The wellbore was represented by a vertical wire .031 inch diameter. The fractures to be tested were constructed on a sheet of plastic. This sheet could be inserted vertically into the

model and clamped against the diameter wall. The fluid used in the model for all tests was distilled water.

Tinsley, et al, concluded that productivity increase is a function of the ratio of fracture height to formation height. Steady state productivity curves of this function showed lower porductivity increase values than the unsteady-state published curves. In addition, the productivity increase ratio for a given fracture decreases as the fracture location departs from the center line of the formation interval. However, for fractures less than five hundred feet in length, the effect of fracture location upon productivity index is negligible.

In 1977, Ming Mao[19] studied the performance of vertically fractured wells with finite conductivity fractures by relating potentiometric and computed results. By assuming a well intercepted by vertical fracture is in the center of a drainage system with constant pressure on the outer boundary, potentiometric model was constructed similar to the model presented by Tinsley, et al. Studies were also made from a staedy-state finite-element computer model.

Mao concluded that the productivity of vertically fractured wells are best presented in terms of effective wellbore radius versus fracture conductivity. This appears to correlate effects of fracture length to drainage radius for each value of fracture height to formation height ratio. He also concluded that the studies by McGuire, et al, and

Raymond and Binder[20] appear to be rough approximations. Results of Mao's study from both the potentiometric model and the finite-element model, fit between Prats analytical solutions and the Tinsley, et al, electrolytic model studies.

2.3 Numerical Solution

The first comprehensive treatment of the pressure behavior of a fractured well was presented by Russell and Truitt[21] in 1964. They examined the pressure behavior of fractured wells of infinite conductivity located in a closed square reservoir using a finite difference model. They considered a homogeneous, isotropic formation in the form of a closed square completely filled with a slightly compressible fluid of constant viscosity. Pressure gradients were to be small everywhere and gravity effects were neglected. The plane of the fracture was located symetrically within the reservoir and parallel to one of the sides of the square boundary. The fracture extended throughout the vertical extent of the formation and production at a constant rate was only through the fracture. The boundary conditions which describe the physical situation of interest were specified. Since it is difficult to solve the problem analytically for the boundary conditions, the two-dimension-finite difference analog was written, and the problem was solved numerically.

Russell and Truitt computed the pressure at the wellbore as a function of time and fracture penetration ratio. They demonstrated the effect of fracture length on the drawdown

and buildup behavior of a vertically fractured well for a wide variety of conditions. They concluded that in a vertically fractured system, the transient flow regime is characterized by a region near the fracture where the flow is practically linear. Thus, pressure analysis methods based on radial flow theory are somewhat inaccurate. The degree of inaccuracy involved depends on the magnitude of the linear flow region, i.e., the depth of penetration of the fracture into the formation. The amount of fracture penetration also effects the calculation of fracture length and the determination of average reservoir pressure. In 1968, Clark[22] extended this study to determinations of fracture length.

In 1969, Wattenbarger and Ramey[23] extended the theory of fractured gas well testing to the flow of real gases. They determined the effects of wellbore storage and turbulence on welltest interpretation by using a finite difference model to simulate welltest conditions. The emphasis has been put on the early transient behavior before the effects of outer boundary are noticable at the wellbore. Their mathematical model considers the well is centered in a circular uniform reservoir. A vertical fracture of infinite flow capacity penetrates the formation and passes through the wellbore. The equation for the flow of real gas (pseudo-pressure m(p)) is used. Before applying finite differences to the model, a coordinate transformation was made. The coordinate transformation is a conformed mapping that has certain computational

advantages.

Wattenbarger and Ramey concluded that the drawdown testing for vertically fractured wells can be extended to the real gas case by using the pseudo-pressure function. The stabilized turbulence can be directly related to the effective wellbore radius of a fractured well. They, also, added that turbulence within the fracture itself is sometimes more important than turbulence within the formation.

Morse and Van Gonten[24] studied the productivity of vertically fractured wells prior to stabilized flow. Numerical simulation was used to solve the relationship between the production rate and time. They considered both constant rate and constant wellbore pressure, a squared drainage area with closed boundary, and fractures of various lengths. They concluded that the estimates of semi-steady state production rates for fractured reservoirs are adequate where the formation permeability is more than ten md. For reservoirs of very low permeability, production rates will be grossly pessimistic during the first years of production.

Locke and Sawyer[25, 26] studied the transient pressure behavior of finite-conductivity vertical fractures in gas wells in 1973. They used the numerical simulation and type curve analysis to perform the study. Their solutions cannot be used to analyze transient pressure data in fractured wells becausde only specific cases were presented.

Cinco, et al., studied the transient pressure behavior

for a well with a finite-conductivity vertical fracture in 1978. They developed a mathematical model to study the pressure behavior of a vertically fractured well with finite conductivity in an infinite reservoir. They considered the reservoir contains a slightly compressible fluid with constant viscosity and the fluid produced through the finite conductivity fracture which is fully penetrating the formation.

Cinco, et al, provided a general solution that could be applied to analyze transient pressure data for wells with a finite conductivity vertical fracture. The solution can be correlated as a function of dimensionless fracture conductivity. A decrease in dimensionless fracture conductivity may be caused by either increase in fracture length or decrease in fracture permeability or both. For dimensionless fracture conductivity values greater than 300, the finite conductivity solutions are identical to the infinite conductivity vertical fracture solution of Gringarten, et al.

They, also, concluded that the uniform flux solution of Gringarten, et al, follows a finite fracture conductivity solution of dimensionless conductivity equals a 4.4 at large values of time. Pressure data for a well with a low fracture conductivity does not exhibit a one-half slope straight line on log-log graph.

Narasimhan and Polen[28] studied fluid flow to a well intercepting a vertical fracture. A numerical method, based

on an integral finite difference approach is used. The investigated well intercepting fractures, in general, and vertical fractures, in particular. Finite conductivity, wellbore storage, damage, and fracture deformability are handled. They provide a general purpose tool for studying the pressure response in finite diameter wellbores which is the integral numerical method described in their paper. Results are already published in some of the literature.

CHAPTER III

STATEMENT OF THE PROBLEM

The well is vertically fractured in the center of a square reservoir and producing at constant bottom hole pressure under unsteady-state conditions. The reservoir is heterogenous, i.e., includes two layers, different porosity, and permeability in each layer. Further, the inner boundary between the two layers can be either a cross-flow or no cross flow boundary. The above, below, and outer square boundaries of the reservoir are no flow boundaries. The fracture extends an equal distances on both sides from the wellbore. The fracture is propped and has a finite flow capacity of (wk_f) and height h_f which is different from the total formation height (h).

The problem is to determine the well performance in layered formations after the fracturing treatment considering non-Darcy flow and fracture closure effects. In addition, the effect of fracture height on well performance is to be investigated. The results are to be determined using a numerical model.

The system may be further simplified by the following assumptions:

1) Single phase flow exists.

2) Gravity forces are neglected.

CHAPTER IV

HYDRAULIC FRACTURE GEOMETRY

Hydraulic fracturing is the creation, propogation and preservation of a fracture in a reservoir formation. In the process of hydraulic fracturing treatments, the fracturing fluid is injected into the bore hole and pressurized. When the bottom hole pressure reaches the designed treating pressure, reservoir rocks break down and a hydraulic fracture is initiated. Further injection of fracturing fluids results in fracture extension. The fracture growth depends on treatment, formation properties, injection rate, and total injected volume. In order to keep the fracture open, the propping agent is pumped into the formation. Several different proppants are used depending on the closure stress in the fracture. In deep wells where closure stress is severe, the super prop is usually the only alternative to sand. In addition to preventing the fracture from closing, the propping agents also provide a highly conductive conduit for the reservoir fluids to flow. The final result of a hydraulic fracturing process is a propped fracture.

Effectiveness of hydraulically created fracture is evaluated by the real extent of the fracture and by the

fracture flow capacity. In addition, the post-fracturing production is an important factor to justify a successful fracturing treatment. At the present time, no one can determine exactly the fracture configuration. One of the best ways to obtain some information about fracture length and its conductivity is from pressure and production analysis. The laboratory tests and simulations are another important source for obtaining information about hydraulic fracturing by means of modeling the reservoir conditions. The SPE Monograph, Volume 2, "Hydraulic Fracturing," by Howard and Fast, is a good source of pertinent information.[28] This section provides a description of vertical fracture system as well as a brief review of the effect of treatment parameters on the fracture configuration.

4.1 Fracture Forming and Propping

Essentially, the process of hydraulic fracturing consists of injecting a fluid into the wellbore and pressurizing it until the induced streeses exceed the in-situ stresses of the formation. At this point, a sudden major pressure drop will be observed which indicate a fracture initiation. Hubbert and Willis,[29] studied comprehensively the mechanics of hydraulic fracturing. It was suggested that a fracture is initiated and extended in a plane perpendicular to the least in-situ compression principle stress as shown in Figure 4.1. In general, the plane of hydraulic fracture is either parallel, inclined, or perpendicular to the axis

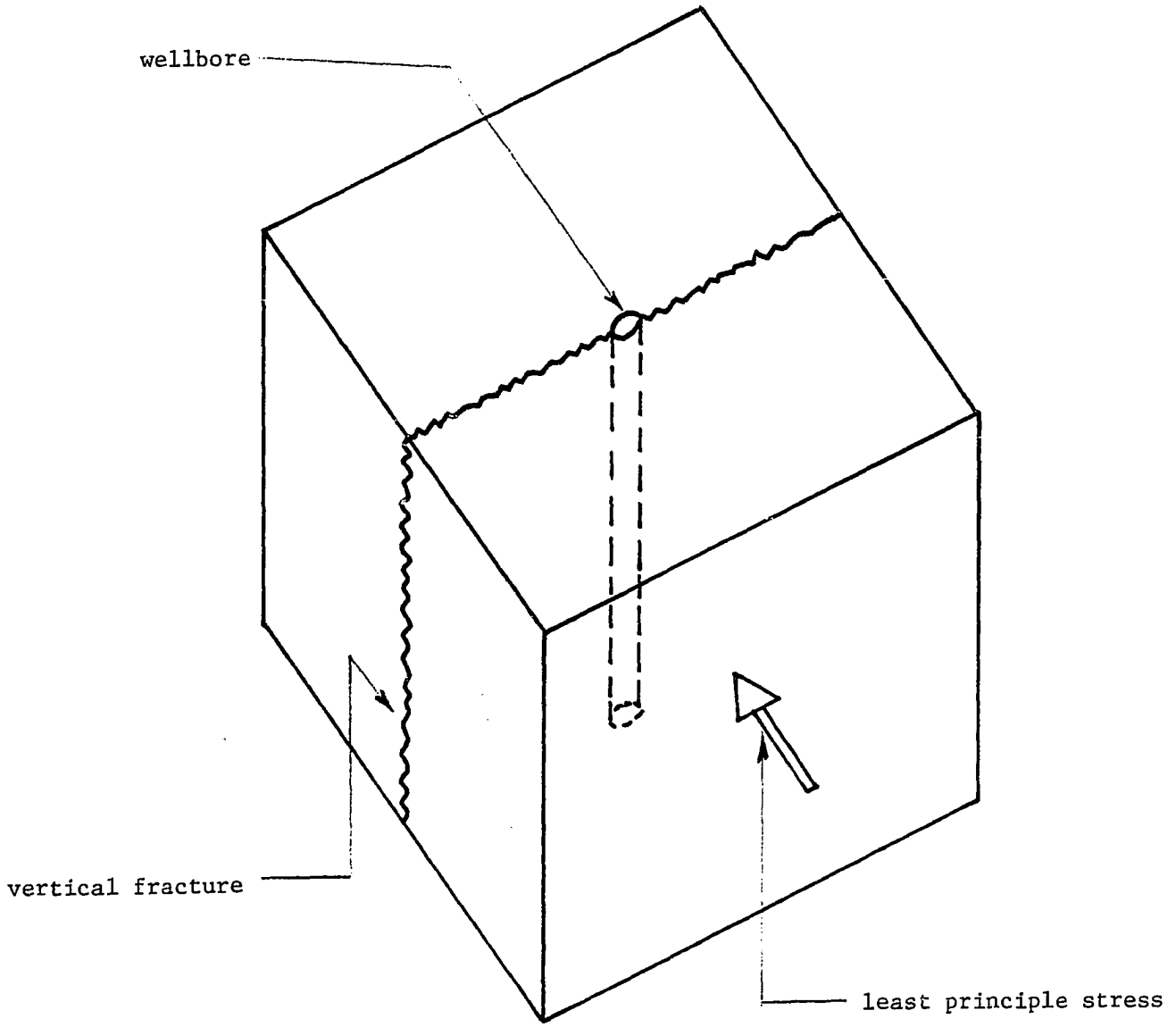


Figure 4.1 Fracture plane related to the least principle stress

of the borehole. Thus, these fractures will be vertical, angular, and horizontal fracture respectively as shown in Figure 4.2.

Daneshy[30] extended this work on the subject of fracture geometry and its orientation by means of mathematical models and experimental tests. It was concluded that both initiation and extension of vertical fractures are caused by purely tensile failure of the borehole wall and the surrounding formation. It was concluded that the appearance of a vertical fracture at the wellbore is not sufficient to insure a vertical fracture, and that a fracture can change direction away from the wellbore. This change of direction can prevent a smooth fracture and cause sand-outs.

Following fracture initiation is the fracture extension stage. At this point, hydraulic pressure is continuously applied to the fracture face to hold the fracture open. In this stage, the fracture geometry changes with the increase of the total injected volume. This geometric change depends on treatment parameters (viscosity, leak-off, injection rate, etc.) and formation properties. The fracture will continue to extend as long as the pressure applied at the tip of the fracture. The final stage is propping the created fracture. The main purpose for using the propping agent is to prevent the fracture from closing.

4.2 Fracture Area

Fracture area is defined as the product of fracture

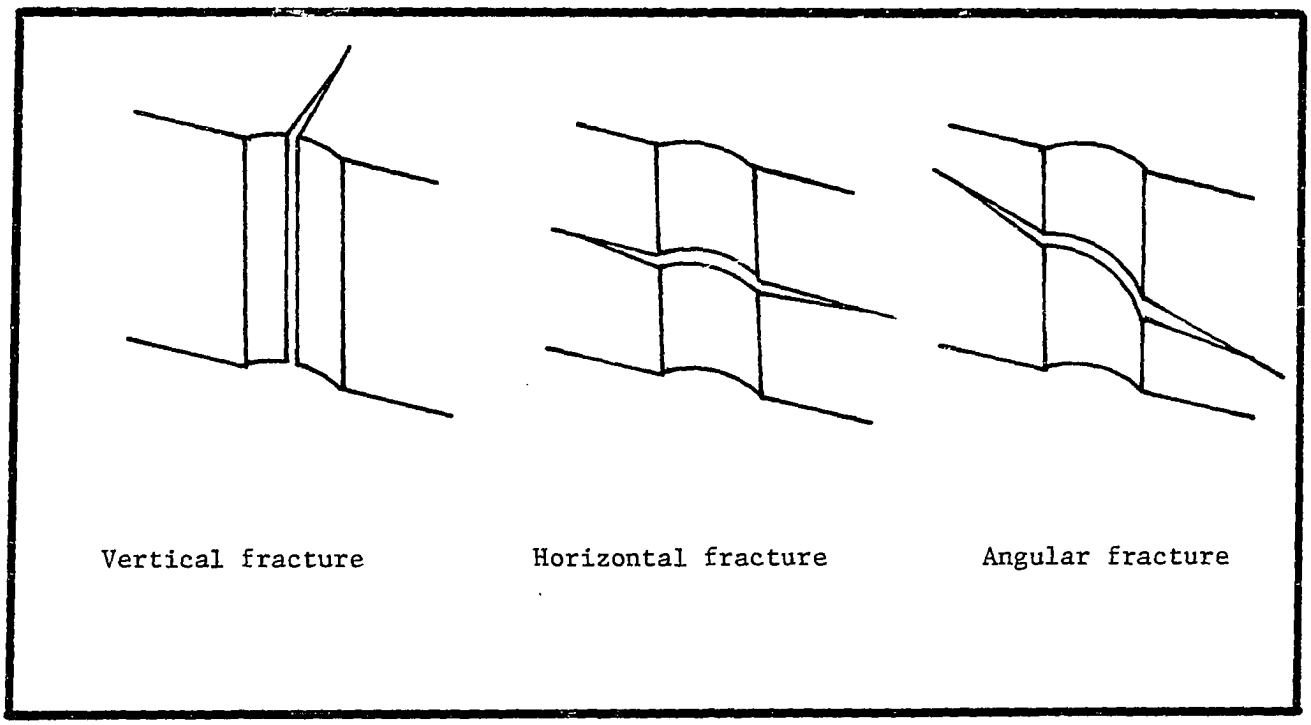


Figure 4.2 Fracture Orientation

length and fracture height. Since the extent of fracture increases with time, the fracture area is a function of time. For a certain fracture area, fracture length depends on fracture height. For most cases, fracture height is determined by the upper and lower boundary of the fractured formation. For simplicity, it was always assumed that fracture height equals formation height. In the present work, this assumption is no longer held.

One of the treating parameters which effects fracture extent greatly is the injection rate. High injection rate will often increase injection treating pressure and extent fracture area. Senddon[31] presented a mathematical expression for hydraulic fracture extension. This expression is given as:

$$P-S = \left[\frac{2 E \gamma}{\pi L_f (1-v^2)} \right]^{\frac{1}{2}} \quad \ldots\ldots\ldots\ldots\ldots\ldots \quad (4.1)$$

in which:

v = Poisson's ratio of the material

S = Least principle stress

P = Pressure needed for propagation of the fracture

γ = Specific gravity of fracturing fluid.

Obviously, the above equation is based on some assumptions. The formation is assumed to be homogeneous, isotropic, lineraly elastic, and impermeable to fracturing fluids. The last assumption made the use of this equation limited in field applications. The effect of fracture height is not

included in the above expression which is a two dimensional representation of the fracture.

4.3 Fracture Width

Generally, fracture width calculations aid in establishing the required injection rate for a certain treatment. It is also an important factor in optimizing fracturing design. Fracture width is a function of both formation characteristics and treating parameters. In other words, fracture width depends on rock elasticity, injection rate, fracturing fluid properties, and fracture area.

Perkins and Kern[32] were first to derive the expression for calculating fracture width in a vertical fracture; for Newtonian fluids in laminar flow:

$$W = 0.02 \left[\frac{q_I \mu L_f}{E} \right]^{\frac{1}{4}} \quad \ldots\ldots\ldots\ldots\ldots\ldots (4.2)$$

Newtonian fluids in turbulent flow:

$$W = 0.033 \left[\frac{q_I^2 \gamma L_f}{E h_f} \right]^{\frac{1}{4}} \quad \ldots\ldots\ldots\ldots\ldots\ldots (4.3)$$

Conditions for laminar and turbulent flow:

$$\frac{q_I^2 \gamma}{h_f \mu} \leq 0.32 \text{ laminar} \quad \ldots\ldots\ldots\ldots\ldots\ldots (4.4)$$

$$\frac{q_I \gamma}{h_f \mu} > 0.32 \text{ turbulent} \quad \ldots\ldots\ldots\ldots\ldots\ldots (4.5)$$

in which

W = Maximum fracture width at the wellbore, ft.

q_I = Injection rate, bbl/min.

Several assumptions were made in developing the above expression of fracture width. These assumptions are:

1) Homogeneous, lineraly elastic and isotropic formation
2) The rocks are assumed to be impermeable to fracturing fluid, i.e., there is no leak-off taking place.
3) It is either assumed that the fracture originates from a point source (penny shaped crack) or that it has a constant height.

γ = specific gravity of fracturing fluid

h_f = fracture height, ft.

Fracture width can be also calculated as a function of proppant concentration. Figure 4.3 represents an experimental correlation between fracture width and proppant concentration. The following equation was derived from the above correlation:

$$W = 0.104 \times 10^{-4} S_c \quad \ldots\ldots\ldots\ldots\ldots\ldots \quad (4.6)$$

where

S_c = proppant concentration in lb/1000 ft.^{2}

Basically, the actual fracture length could be reduced considerably from the designed value due to crushing or embedding of propant agent in the fracture.

4.4 Fracture Conductivity

Fracture conductivity is a very important factor in designing and evaluating a hydraulic fracturing treatment. The increase of well productivity following a fracturing

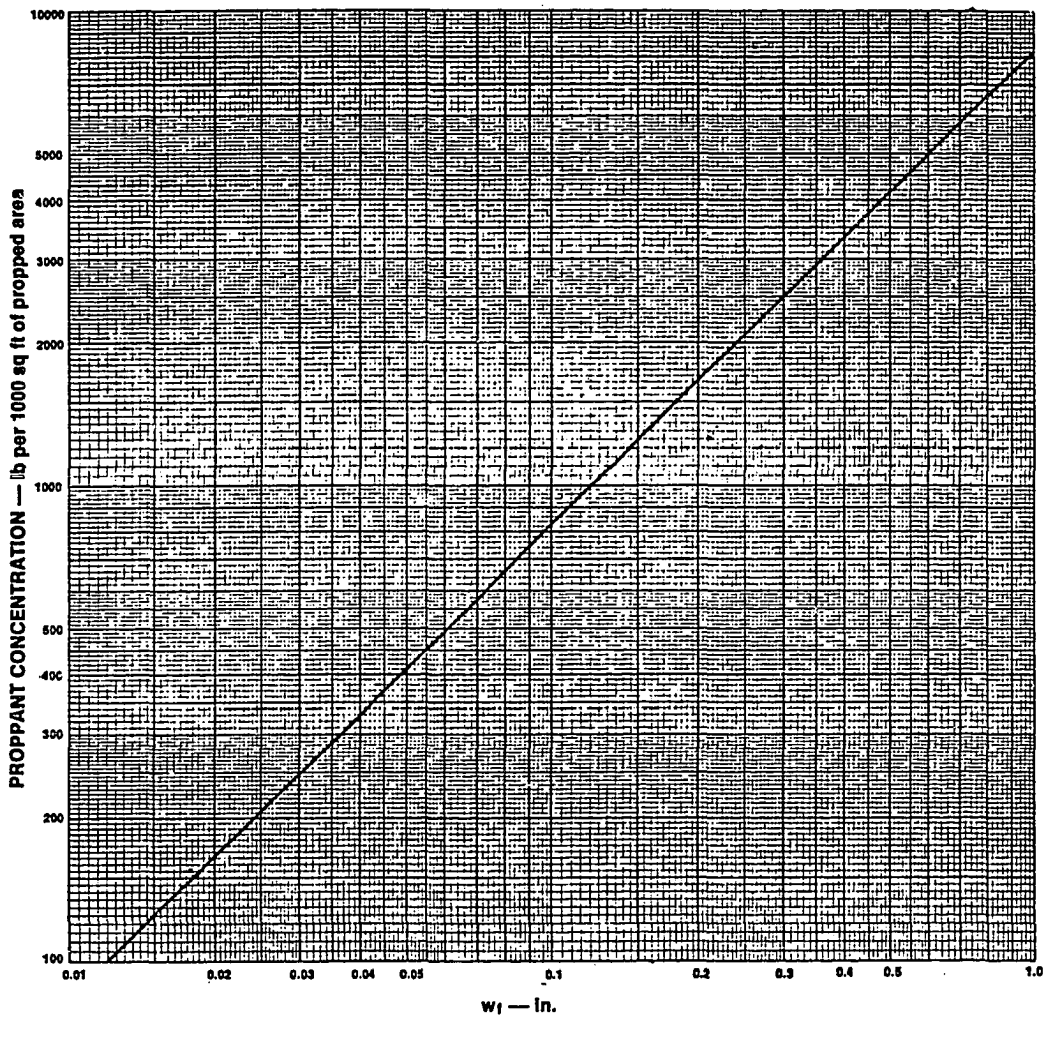


Figure 4.3 Proppant Concentration in the Fracture versus Fracture width.

treatment depends greatly on the fracture conductivity as well as fracture extent. The fracture conductivity is defined by the fracture permeability and its width. An analytical solution for fracture permeability is not available as yet in the literature. However, the laboratory data on fracture flow capacity for different proppant agents are available.

Now, let us discuss in the following section the formulation of the mathematical model of a vertically fractured well in layered media.

CHAPTER V

MATHEMATICAL FORMULATION

The problem of a vertically fractured well in the center of a squared drainage area with no flow boundaries will be formulated. In addition, the model will consider a formation of two layers with different permeability and porosity values. The inner boundary between the two layers can accomodate cross flow as well as no flow except through the fracture. The well is producing at constant bottom hole flowing pressure.

This study investigates the problem of a vertically fractured well producing a single-phase which is gas. The real gas potential will be used instead of pressure in the real gas flow equations. The pseudo-pressure function of Al-Husseiny *et al*[33] is used in developing the governing partial differential equations. The turbulent effect in the fractured cells is considered. The flow in the rest of the formation cells is laminar and Darcy's formula is applicable. Finally, the change of fracture conductivity with time and distance is included.

5.1 Single-phase Gas Flow Equations

Figure 5.1 shows a schematic view of a vertically-fractured well in the center of a square drainage area. The fracture partially penetrates the reservoir formation to a fraction of the total height of the two zones. This provides a three-dimensional fluid flow problem. If the fracture height is assumed to be equal to the total height, the problem becomes two-dimensional. The fracture can be in any location between the upper and lower boundaries of the two zones.

To reduce the computational time considerably, it is convienient to take advantage of the symmetry of this type system shown in figures 5.2 and 5.3. Unsteady-state gas flow through a porous media is governed by nonlinear partial differential equations which can not be solved by analytical means. To solve the nonlinear terms in a vigorous way rather than making simplifying assumptions, the finite difference scheme must be used to solve such a problem. In addition, the pseudo-pressure function simplified the problem and the nonlinear terms no longer appear in the partial differential equations.

The equation for flow of a real gas in the porous medium can be derived using Darcy's law and the principle of conservation of mass. Appendix A includes this derivation in more details. Considering one cubic unit of reservoir formation through which, a single phase is flowing in

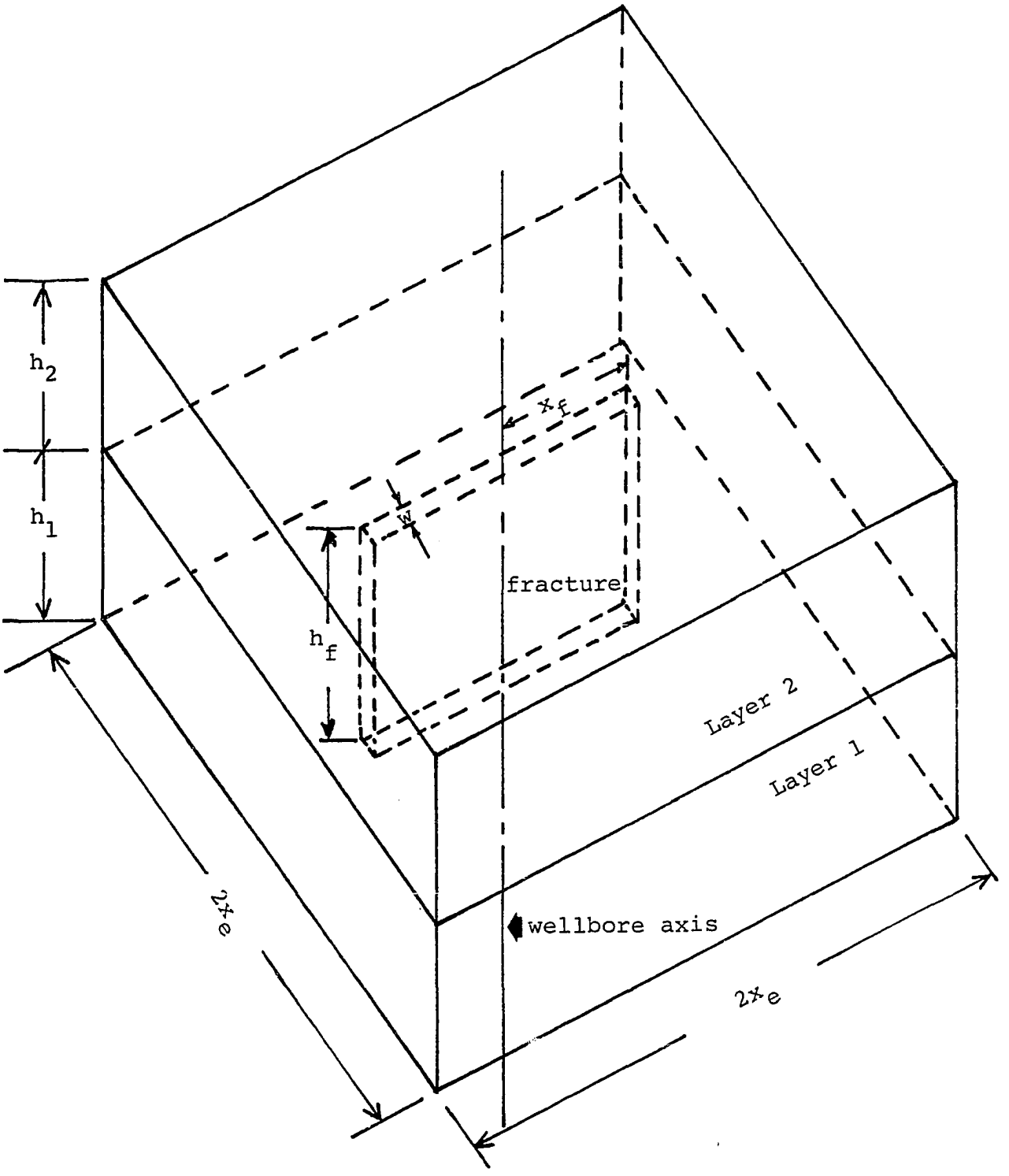


Figure 5.1 A schematic view of a vertically fractured well in the center of squared drainage area.

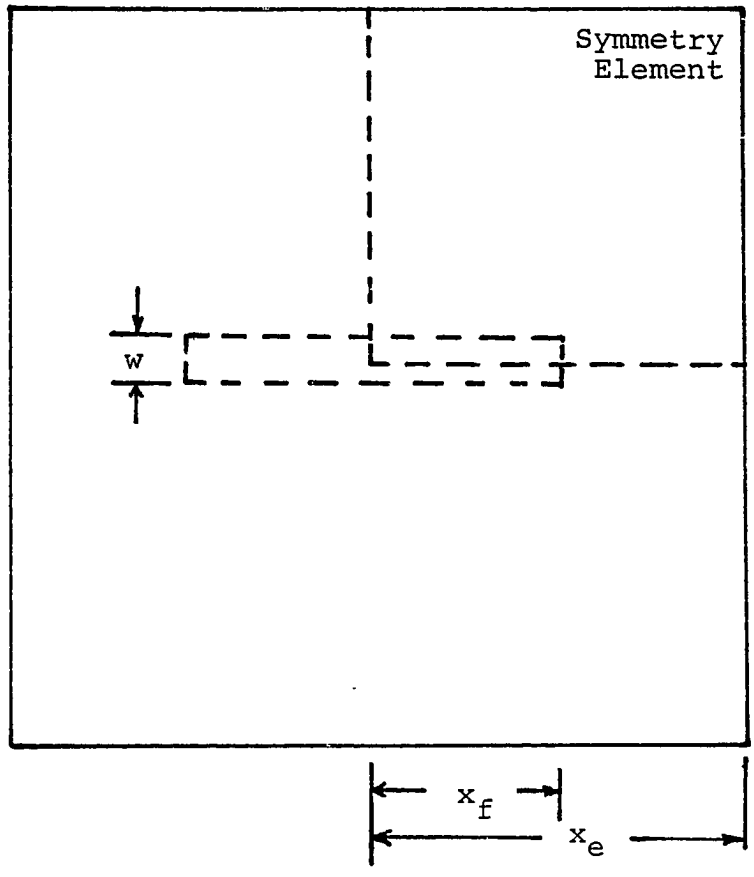


Figure 5.2 A two-dimensional view of the fractured system.

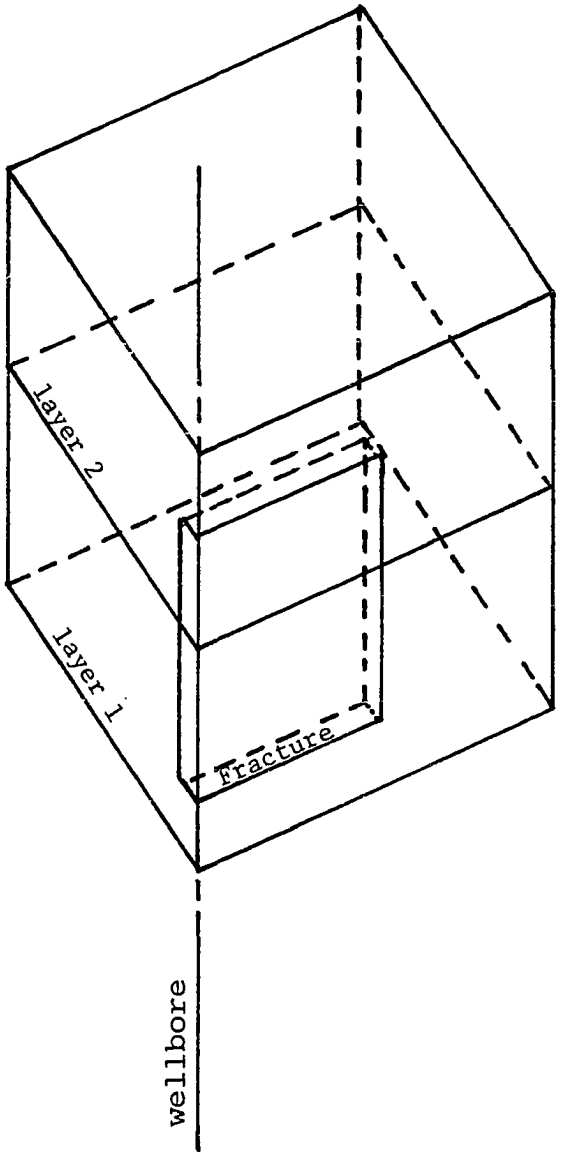


Figure 5.3 A three-dimensional view of one-fourth of the drainage volume of vertically fractured well in layered formation.

one direction, from the equation of state:

$$\frac{\partial (\rho v)}{\partial x} = - \phi \frac{\partial \rho}{\partial t} \quad \ldots\ldots\ldots\ldots\ldots\ldots \quad (5.1)$$

but from Darcy's law:

$$v = -\frac{k}{\mu} \frac{\partial P}{\partial x} \quad \ldots\ldots\ldots\ldots\ldots\ldots\ldots\ldots \quad (5.2)$$

substituting equation (1) in (2), we have:

$$\frac{\partial \left(-\frac{k}{v} \frac{\partial P}{\partial x} \rho \right)}{\partial x} = -\phi \frac{\partial \rho}{\partial t} \quad \ldots\ldots\ldots\ldots\ldots \quad (5.3)$$

using the gas law for real gases;

$$\rho = \frac{PM}{ZRT} \quad \ldots\ldots\ldots\ldots\ldots\ldots\ldots\ldots \quad (5.4)$$

from equations 3 and 4:

$$\frac{\partial \left(-\frac{k}{v} \frac{PM}{ZRT} \frac{\partial P}{\partial Z} \right)}{\partial x} = -\phi \frac{\partial}{\partial t} \left(\frac{PM}{ZRT} \right) \quad \ldots\ldots\ldots \quad (5.5)$$

dividing by M/RT which is assumed to be constant for isothermal formation:

$$\frac{\partial}{\partial x} \left(\frac{kP}{\mu Z} \frac{\partial P}{\partial x} \right) = \phi \frac{\partial}{\partial t} \left(\frac{P}{Z} \right) \quad \ldots\ldots\ldots\ldots\ldots \quad (5.6)$$

Then, for the three-dimensions, we have in the reservoir:

$$\frac{\partial}{\partial x} \left(\frac{kP}{\mu Z} \frac{\partial P}{\partial x} \right) + \frac{\partial}{\partial y} \left(\frac{kP}{\mu Z} \frac{\partial P}{\partial y} \right) + \frac{\partial}{\partial z} \left(\frac{kP}{\mu Z} \frac{\partial P}{\partial z} \right) = \phi \frac{\partial}{\partial t} \left(\frac{P}{Z} \right) \quad (5.7)$$

and in the fracture:

$$\frac{\partial}{\partial x} \left(\frac{k_f P}{\mu Z} \frac{\partial P}{\partial x} \right) + \frac{\partial}{\partial y} \left(\frac{k_f P}{\mu Z} \frac{\partial P}{\partial y} \right) + \frac{\partial}{\partial z} \left(\frac{k_f P}{\mu Z} \frac{\partial P}{\partial z} \right) = \phi_f \frac{\partial}{\partial t} \left(\frac{P}{Z} \right) \quad (5.8)$$

where k and k_f represent permeability in the reservoir and in the fracture respectivity. All variables are defined in the nomenclature.

5.2 Real Gas Potential Flow Equation

Another approach to solve the problem is to formulate the equations in terms of a real gas potential or pseudo-pressure. The use of this pseudo-pressure function simplifies equations 7 and 8, derived in the previous section. In addition, some of the non linearity in the partial differential equations (5.7) and (5.8), will be removed when the pseudo-pressure function is used instead of pressure. The pseudo-pressure is defined as:

$$m(P) = 2\int_{P_m}^{P} \frac{P}{\mu Z}\, dP \quad \ldots\ldots\ldots\ldots\ldots\ldots \quad (5.9)$$

For convienience m(P) will be abbreviated to m, then:

$$\frac{\partial m}{\partial P} = \frac{\partial P}{\mu Z} \quad \ldots\ldots\ldots\ldots\ldots\ldots\ldots\ldots \quad (5.10)$$

and;

$$\frac{\partial m}{\partial x} = \frac{\partial m}{\partial P}\,\frac{\partial P}{\partial x}$$

From equation (5.10), we have:

$$\frac{\partial m}{\partial x} = \frac{P}{\mu Z}\,\frac{\partial P}{\partial x} \quad \ldots\ldots\ldots\ldots\ldots\ldots\ldots\ldots \quad (5.11)$$

Now, the right hand side of equation (5.7) can be expanded:

$$\phi\,\frac{\partial}{\partial t}\left(\frac{P}{Z}\right) = \phi\,\frac{P}{Z}\left(\frac{1}{P} - \frac{1}{Z}\,\frac{\partial Z}{\partial P}\right)\frac{\partial P}{\partial t} \quad \ldots\ldots\ldots\ldots \quad (5.12)$$

The isothermal gas compressability is defined as:

$$C_g = \frac{1}{P} - \frac{1}{Z}\,\frac{\partial P}{\partial Z} \quad \ldots\ldots\ldots\ldots\ldots\ldots\ldots \quad (5.13)$$

substituting equations (5.11), (5.12), (5.13), in (5.7), we have:

$$\frac{\partial}{\partial x}\left[k\,\frac{\partial m}{\partial x}\right] + \frac{\partial}{\partial y}\left[k\,\frac{\partial m}{\partial y}\right] + \frac{\partial}{\partial z}\left[k\,\frac{\partial m}{\partial z}\right] = \phi\,\mu\,C_g\,\frac{\partial m}{\partial t}. \quad (5.14)$$

similarly, for the fracture;

$$\frac{\partial}{\partial x}\left[k_f\,\frac{\partial m}{\partial x}\right] + \frac{\partial}{\partial y}\left[k_f\,\frac{\partial m}{\partial y}\right] + \frac{\partial}{\partial Z}\left[k_f\,\frac{\partial m}{\partial Z}\right] = \phi\,\mu\,C_g\,\frac{\partial m}{\partial t}. \quad (5.15)$$

The boundary conditions are:

$$\left.\begin{aligned} &\frac{\partial m}{\partial y}(x, o, z) = 0 \\ &\frac{\partial}{\partial y}(x, y_e, z) = 0 \end{aligned}\right\} o \le x \le x_e,\ o \le z \le h$$

$$\left.\begin{aligned} &\frac{\partial}{\partial x}(o, y, z) = 0 \\ &\frac{\partial}{\partial x}(x_e, y, z) = 0 \end{aligned}\right\} o \le y \le y_e,\ o \le z \le h \quad (5.16)$$

$$\left.\begin{aligned} &\frac{\partial}{\partial z}(x, y, o) = 0 \\ &\frac{\partial}{\partial z}(x, y, h) = 0 \end{aligned}\right\} o \le y \le y_e,\ o \le x \le x_e$$

$$\left.\begin{aligned} &m(P) = \text{constant} \quad o \le y \le r_w,\ x = r_w \\ &m(P) = \text{constant} \quad o \le x \le r_w,\ y = r_w \end{aligned}\right\} o \le z \le h$$

$$m(P) = m(P)_I \qquad t = 0$$

Figures 5.4 and 5.5 show the symmetry element and boundaries. The boundary condition between the two layers can be either flowing boundary or no flow boundary. The fluid flow to the wellbore can occur through the fracture and formation cells. When no flow boundary case is considered between the layers, the only connection between them will be through the fracture. The fracture location can be anywhere within the upper and lower out boundaries.

Some usual simplifying assumptions were made in

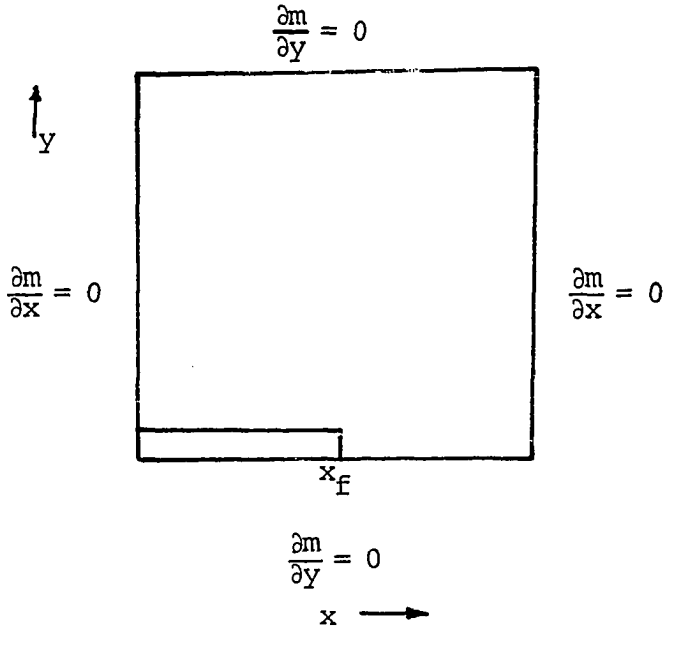


Figure 5.4 The symmetry element and boundary conditions.

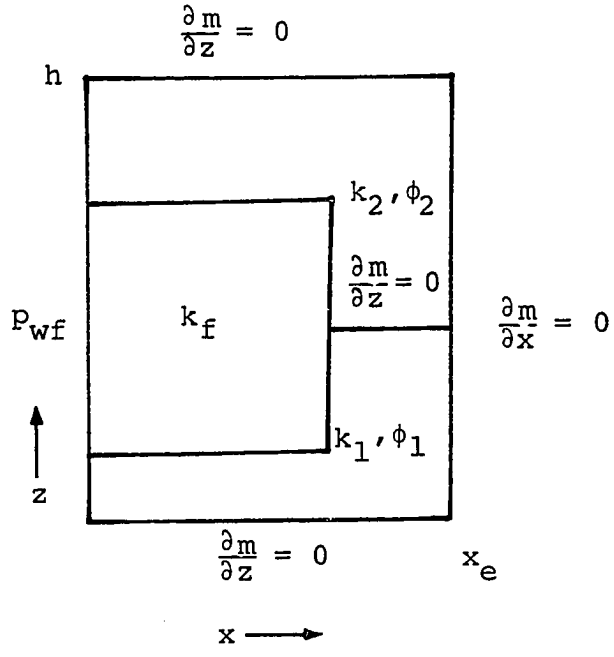


Figure 5.5 The symmetry element and other boundary conditions.

developing this model. They are:

1) Horizontal, isotropic, layered formations.
2) The fracture is vertical and extends an equal distance from both sides of the wellbore.
3) The drainage area is square with no flow across the outer boundaries.
4) Flow is unsteady and turbulence only in the fracture.
5) Gravity forces are neglected.

5.3 Non-Darcy Flow

Thus far, the mathematical formulation of the partial differential equations is based on the assumption that the flow behavior can be described as laminar. This is not true especially in the case of gas wells. At high flow rates, non-Darcy flow occurs more commonly in gas wells. Non-Darcy flow also occurs in flow through high conductivity fractures. Turbulent flow in porus media has been studied for many years. In this section, the non-Darcy flow will be discussed.

Forcheimer[34] suggested a non-linear equation with a velocity squared term to represent the pressure drop in a porous medium with non-Darcy flow.

$$\Delta P/\Delta L = \mu v/k + \beta \rho v^2 \quad . . . . . (5.17)$$

This equation is equivalent to Darcy's equation, except for an extra term which considers the extra pressure drop due to the high velocity. In the Forcheimer equation, beta factor (turbulence factor) was required which is a characteristic

of the porous medium Cornell and Katz[35] measured the porosity and permeability for a number of different sandstone and carbonate formations. They derived a correlation of beta factors as a function of permeability and porosity

The correlations described above are best suited for flow in the formation. The correlation developed by Cooke[36] has the most immediate application to hydraulically induced fractures. He noted that beta factors packed with multiple layers of sand had not been reported and suggested the following equation:

$$\beta = b/(1{,}000\ k)^{a} \quad . \quad . \quad . \quad . \quad . \quad . \quad . \quad . \quad . \quad . \quad . \quad . \quad . \quad . \quad . \quad . \quad . \quad (5.18)$$

where a and b are constants which depend on sand size.

In 1969, Wattenbarger and Ramey,[37] using a finite difference model, studied the effects of turbulence in the formation for a gas well intercepted by an infinitely conductive fracture. They concluded that turbulence in the formation only becomes significant for very small fracture lengths, and that turbulence in the fracture is more common.

Holditch and Morse[38] developed a simulator which included the effects of non-Darcy flow in the fracture. In their study, the beta factor was predicted by Cooke's formula.

Recently, Guppy, Cinco, and Ramey[39, 40] have investigated the effects of non-Darcy flows within the fracture for a vertically fractured system with finite conductivity. They concluded that the fracture conductivity does not have a constant value, but it varies with time.

Non-Darcy Factor

To obtain the correct pressure profile in the reservoir under non-Darcy flow conditions, a correlation factor called turbulent factor (δ) is included in the partial differential equations. δ is derived as follows;

from Darcy's law

$$\Delta P/\Delta L = \mu \nu / k_f \quad \ldots\ldots\ldots\ldots\ldots\ldots \quad (5.19)$$

the flow of fluid in the fracture with non-Darcy flow effect can be represented by Forcheimer's equation.

$$\Delta P/\Delta L = \mu\ \nu/k_f + \rho\ \beta\ \nu^2 \quad \ldots\ldots\ldots\ldots \quad (5.20)$$

from equation (5.20):

$$\Delta P/\Delta L = \mu\ \nu/k_f \left[1 + \frac{\beta\ \rho\ \nu\ k_f}{\mu}\right] \quad \ldots\ldots\ldots \quad (5.21)$$

$$\Delta P/\Delta L = \mu\ \nu/k_T \quad \ldots\ldots\ldots\ldots\ldots\ldots \quad (5.22)$$

where k_f = permeability measured under laminar flow conditions.

$$k_T = \frac{1}{k_f}\left[1 + \frac{\beta\ \rho\ \mu\ k_f}{\mu}\right]^{-1} \quad \ldots\ldots\ldots\ldots \quad (5.23)$$

k_T is the permeability required in Darcy's law to provide correct values under non-Darcy flow conditions. Therefore, from equation 7:

$$\delta = \frac{k_T}{k_f} = \frac{1}{1 + \frac{\beta\ \rho\ \nu\ k_f}{\mu}} \quad \ldots\ldots\ldots\ldots\ldots \quad (5.24)$$

In oil field units:

$$\delta = \frac{1}{1 + \frac{2.97 \times 10^{-10}\ \beta\ \rho\ \nu\ k_f}{\mu}} \quad \ldots\ldots\ldots \quad (5.25)$$

where:

ν = gas velocity in the fracture, ft/day

The turbulent factor is a measure of the degree of non-Darcy flow in the fracture. If β factor or ν approaches zero, then ∂ approaches one and flow is laminar. If the velocity is high, the the value of ∂ will be smaller than one. As the degree of non-Darcy flow increases, the value of the turbulent factor decreases.

Now, for non-Darcy flow, the velocity of a fluid is given by:

$$\nu = - \frac{\delta k_f}{\mu} \frac{\partial P}{\partial x} \quad \ldots\ldots\ldots\ldots\ldots\ldots \quad (5.26)$$

Thus, for the flow in the formation, equation 14 can be used to describe the flow behavior. For non-Darcy flow in the fracture, we have:

$$\frac{\partial}{\partial x}\left[\delta k_f \frac{\partial m}{\partial x}\right] + \frac{\partial}{\partial y}\left[\delta k_f \frac{\partial m}{\partial y}\right] + \frac{\partial}{\partial z}\left[\delta k_f \frac{\partial m}{\partial z}\right] = \phi \mu C_g \frac{\partial m}{\partial t} \quad (5.27)$$

Euqations (5.14) and (5.27) represent the flow of gas in the formation and fracture at any one point in the reservoir for any instant.

5.4 Closure Pressure Effects

Another characteristic of a fractured system that should be considered is the reduction in fracture permeability with increasing closure stress. When a fractured well begins production, the pressure in the fracture is reduced significantly. The closure pressure is the difference between bottom-hole treating pressure and the average pressure in the fracture. The fracture flow capacity decreases as the closure pressure increases. As a result of that, the

fracture permeability decreases with time. Laboratory data on fracture closure pressure as a function of proppant concentration and fracture flow capacity are available in the Halliburton's Frac Theory Book[4] and are presented in Figures (5.6 - 5.17).

Using the laboratory data of these figures, the effect of changing closure pressure can be considered in calculating actual fracture flow capacity and fracture permeability. The model considers the maximum closure pressure at each cell in the fracture. However, a new fracture flow capacity is determined at each time step. From that, a new fracture permeability is calculated.

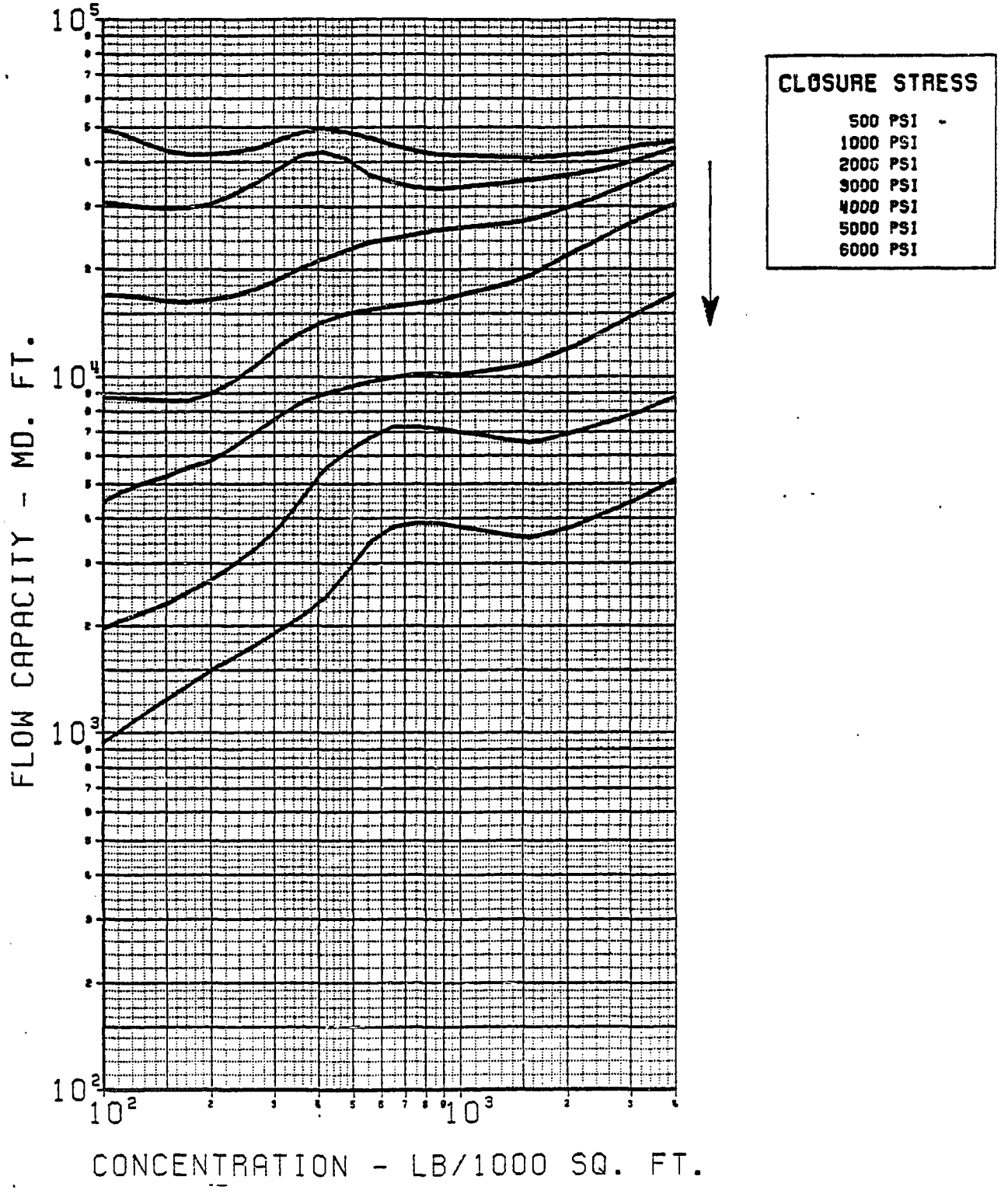


Figure 5-6: Flow Capacity Data for 8-12 Mesh Sand (ref. 41)

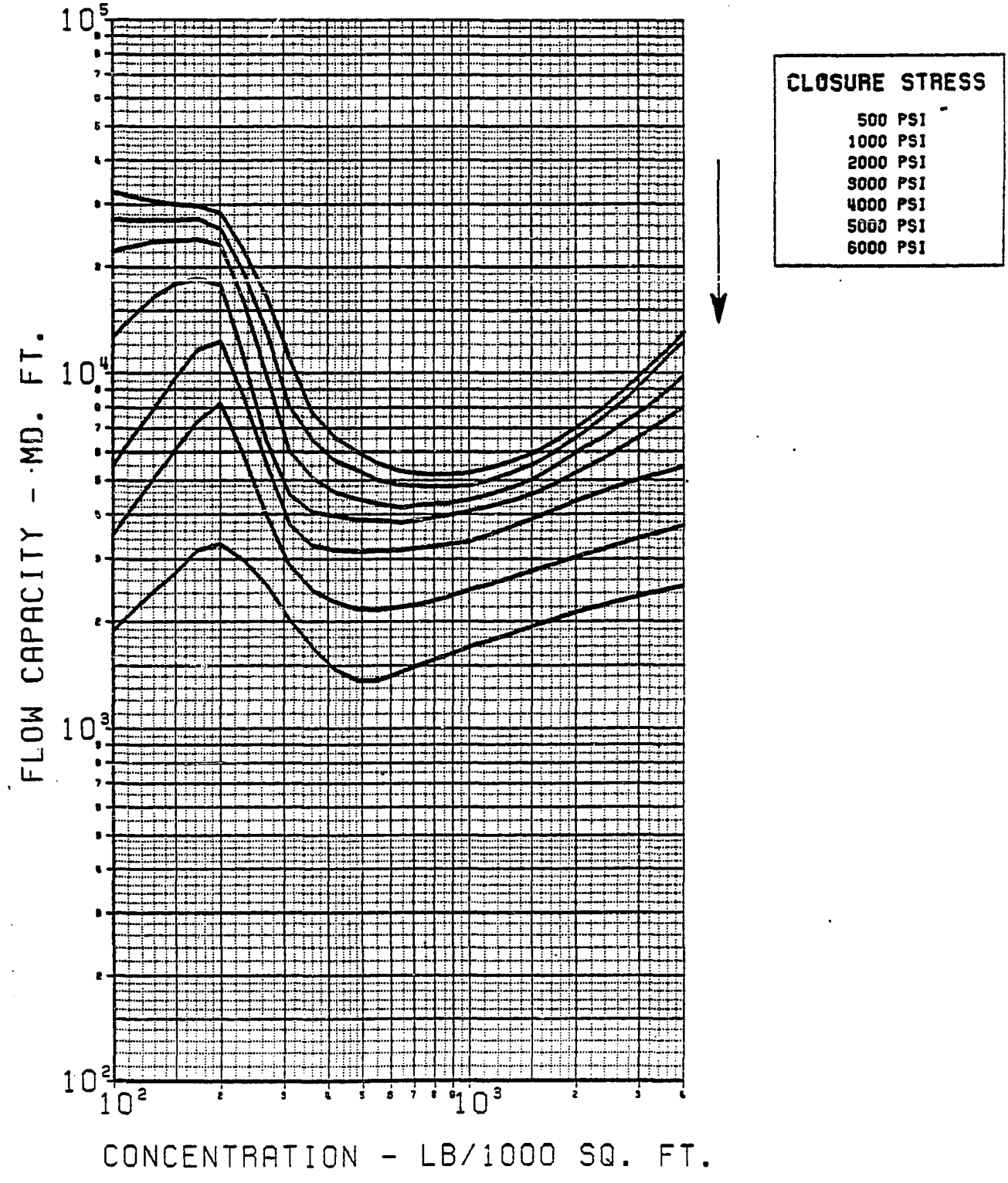


Figure 5-7: Flow Capacity Data for 10-20 Mesh Sand (ref. 41)

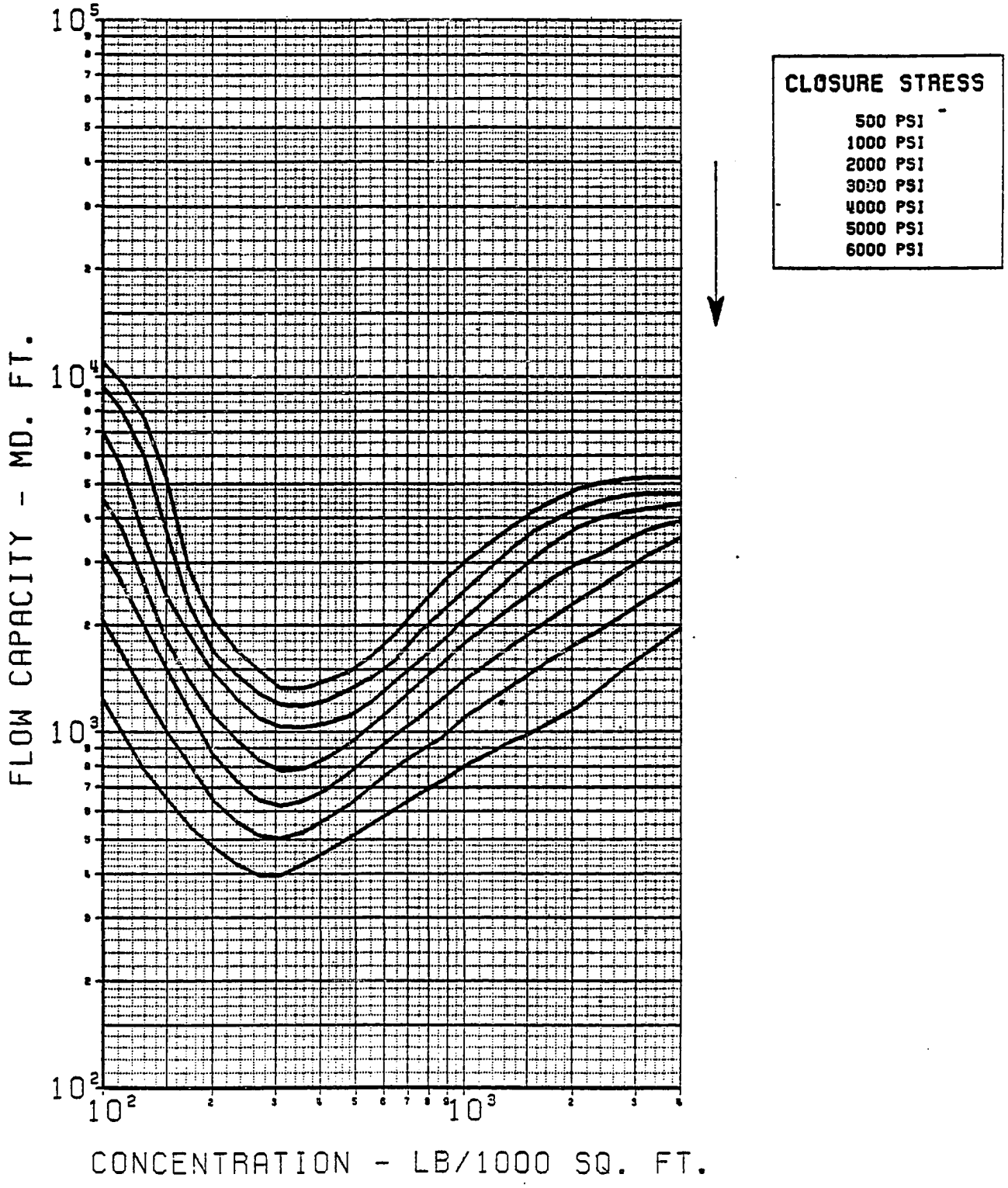


Figure 5-8: Flow Capacity Data for 20-40 Mesh Sand (ref. 41)

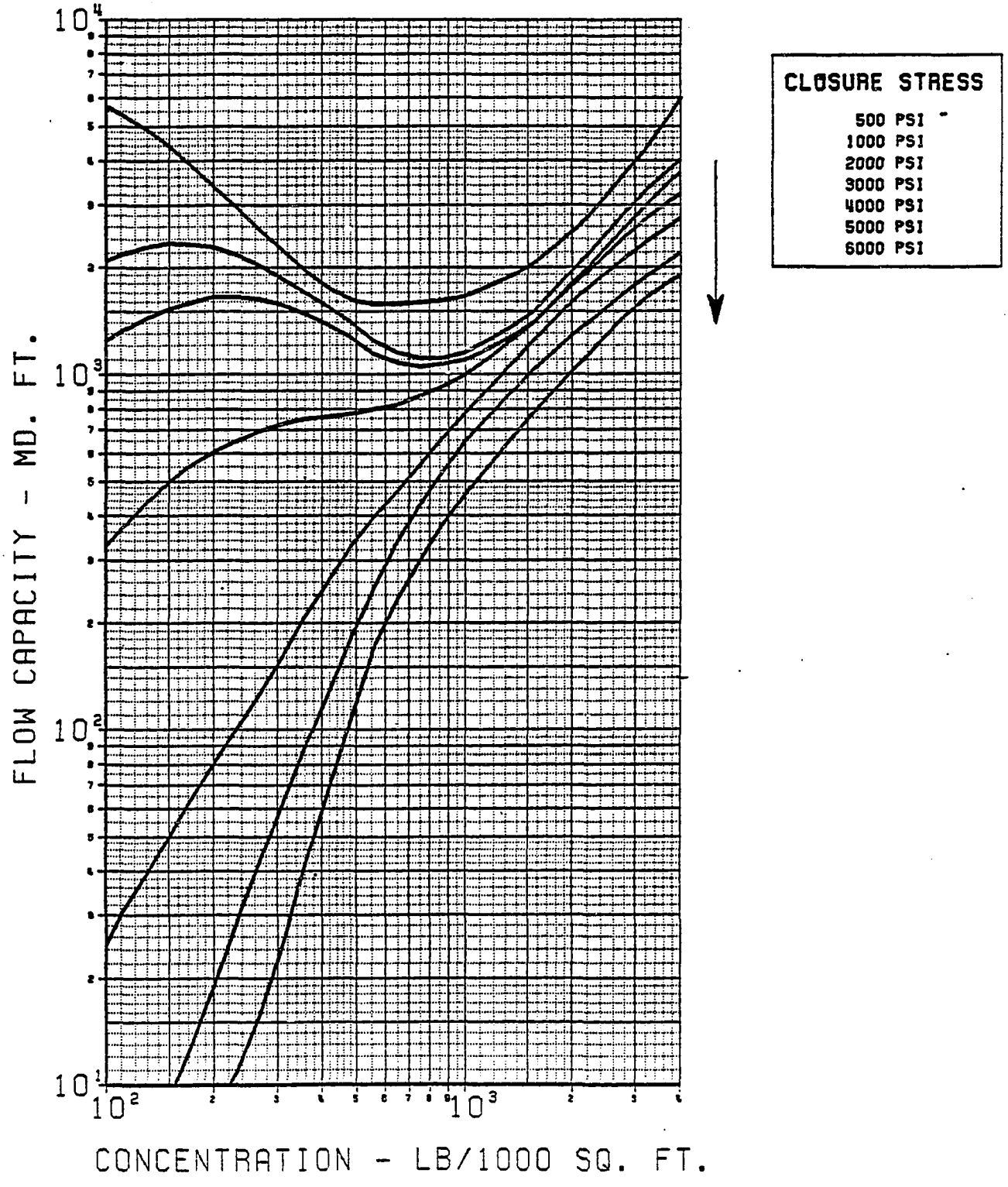


Figure 5-9: Flow Capacity Data for 40-60 Mesh Sand (ref. 41)

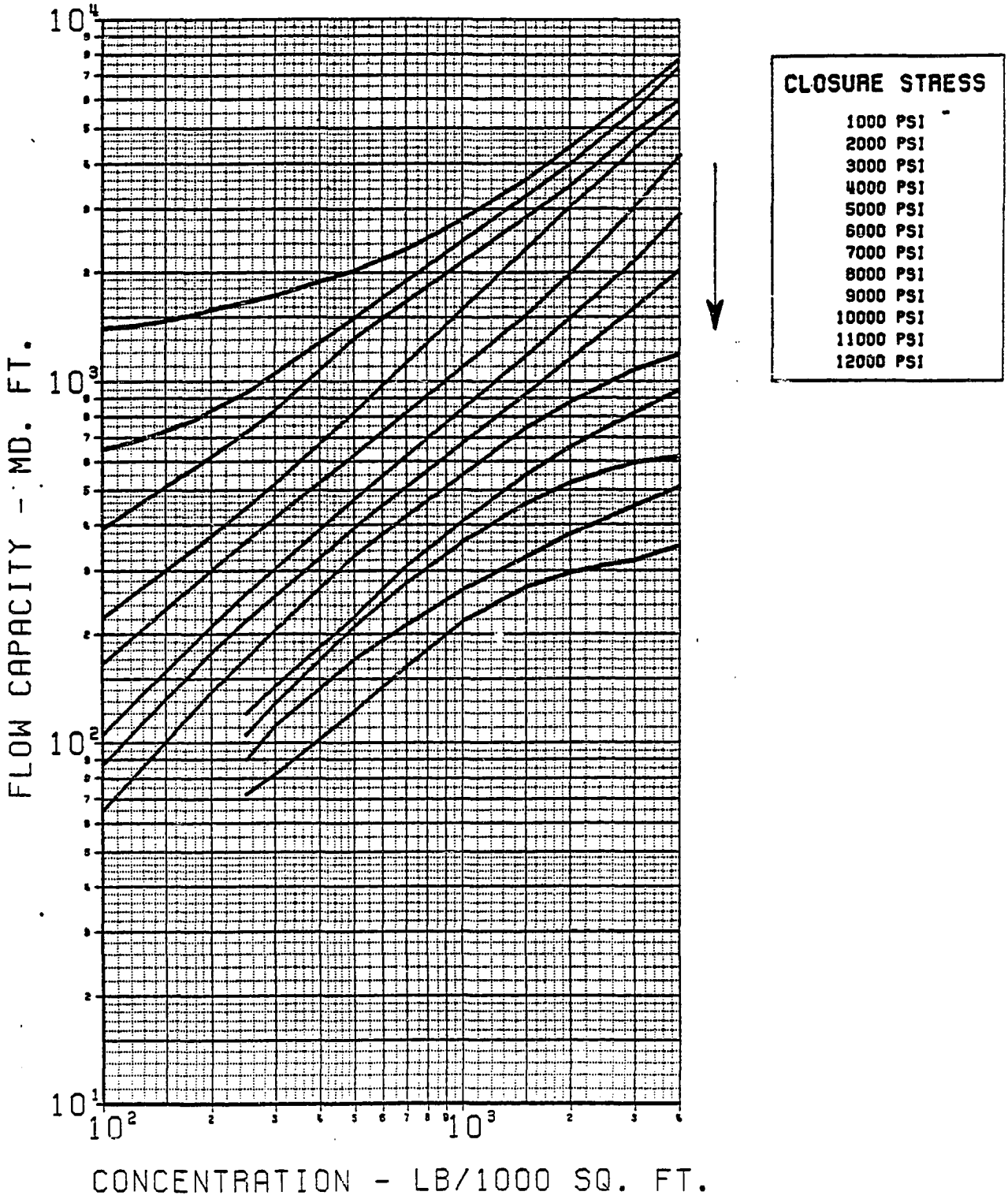


Figure 5-10: Flow Capacity Data for 50% 20-40 Ottawa Sand and 50% 12-20 SUPER PROP (ref. 41)

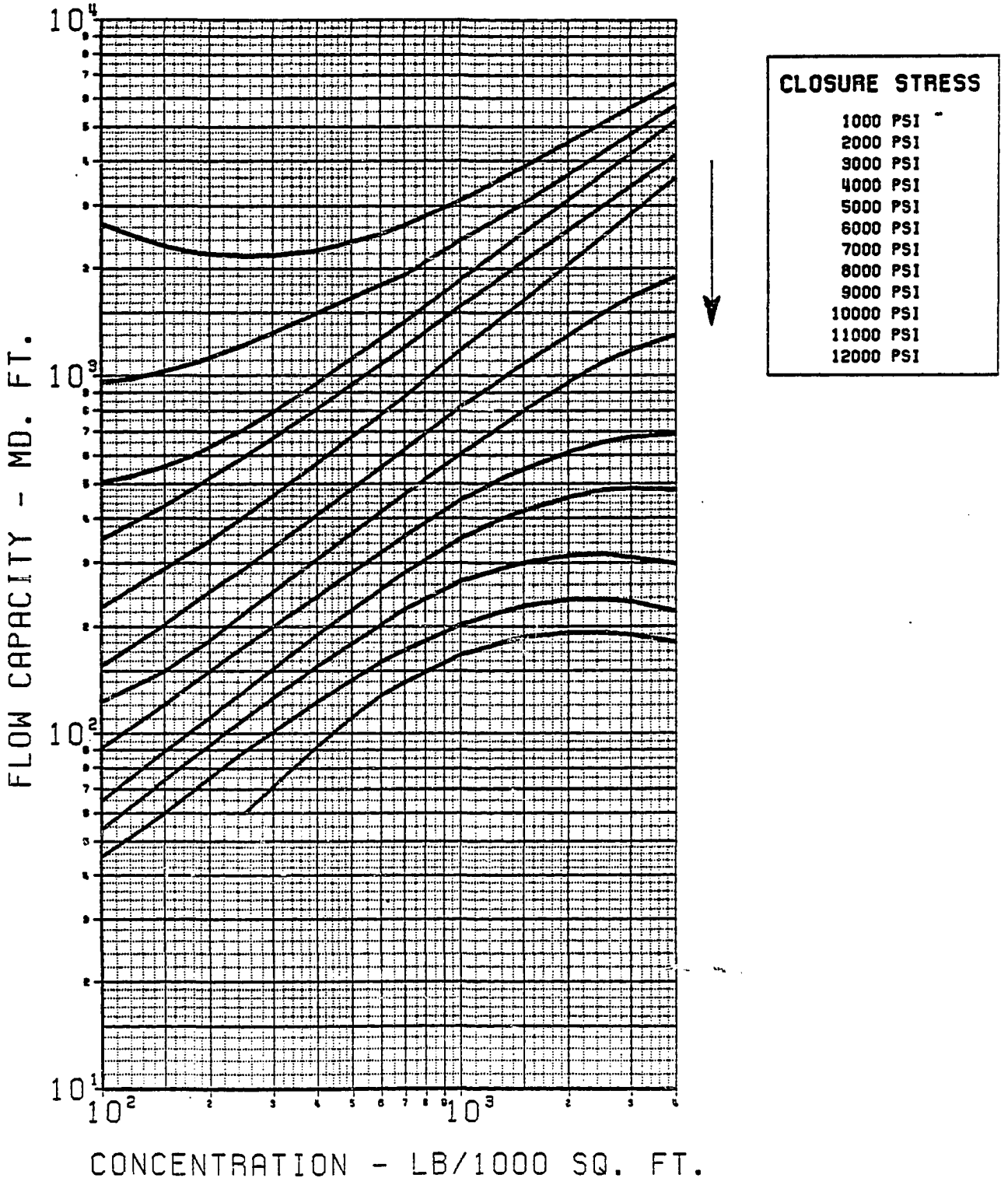


Figure 5-11: Flow Capacity Data for 75% 20-40 Ottawa Sand and 25% SUPER PROP (ref. 41)

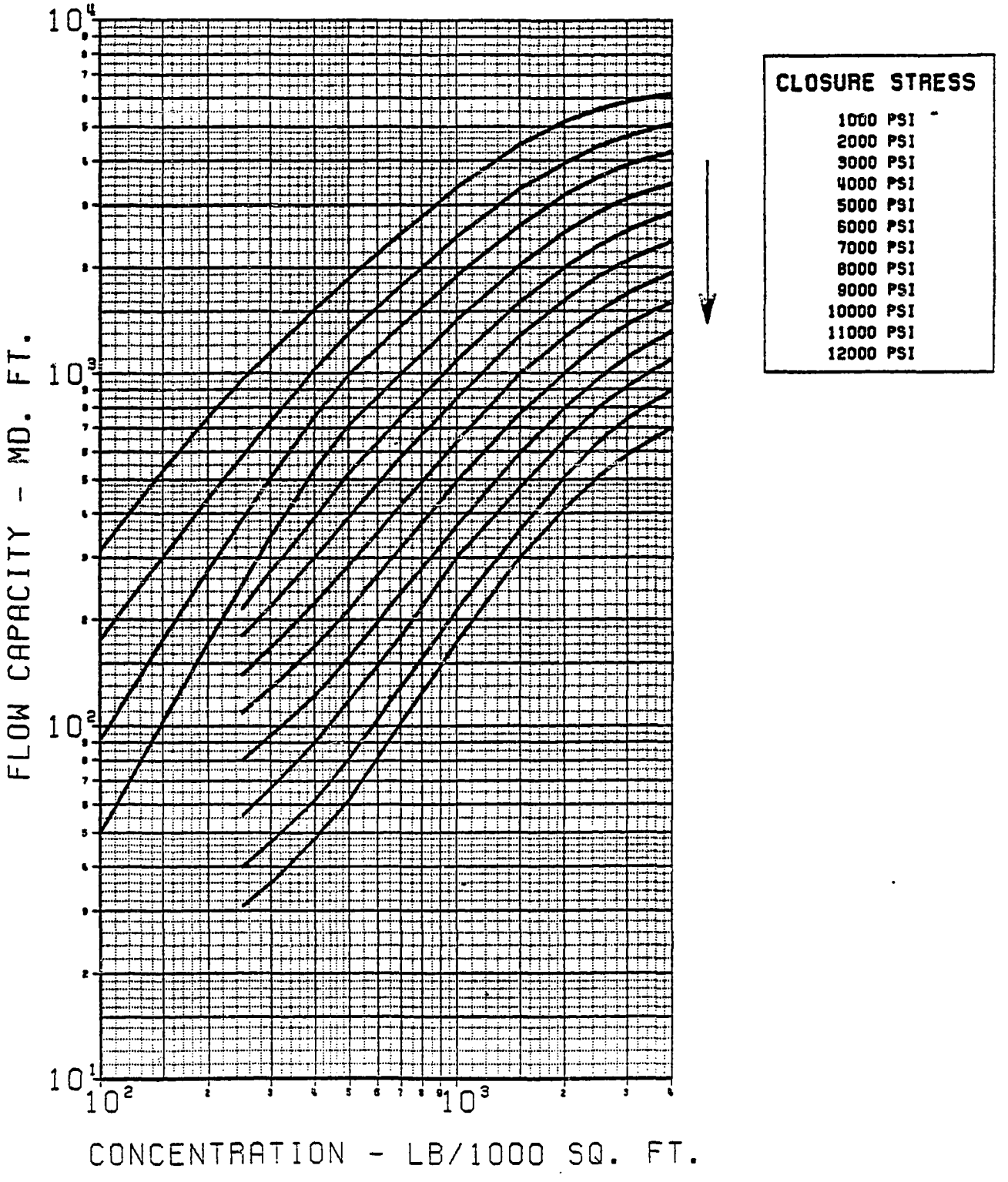


Figure 5-12: Flow Capacity Data for 50% 20-40 Ottawa Sand and 50% SUPER PROP (ref. 41)

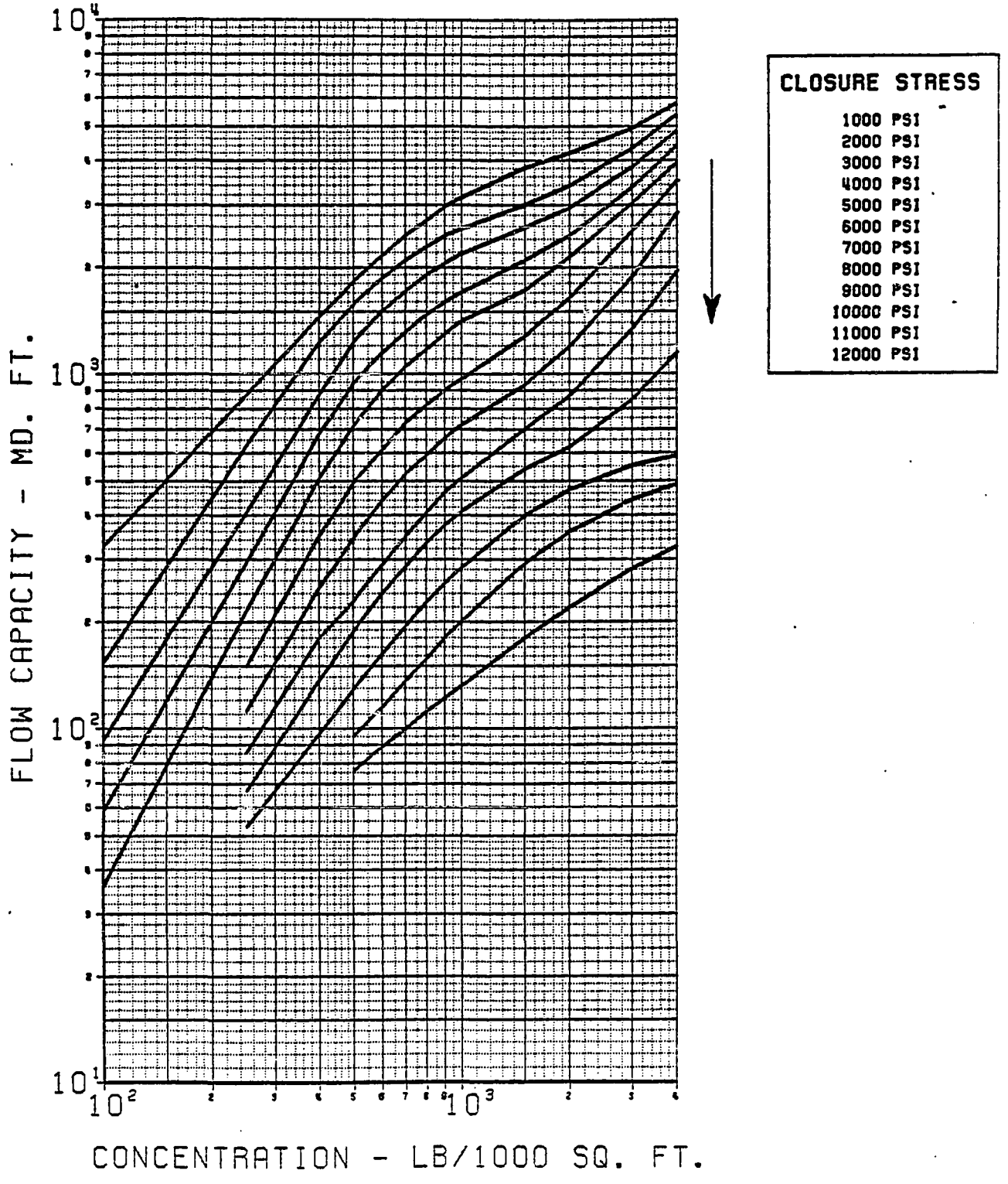


Figure 5-13: Flow Capacity Data for 75% 20-40 Ottawa Sand and 25% 20-40 SUPER PROP (ref. 41)

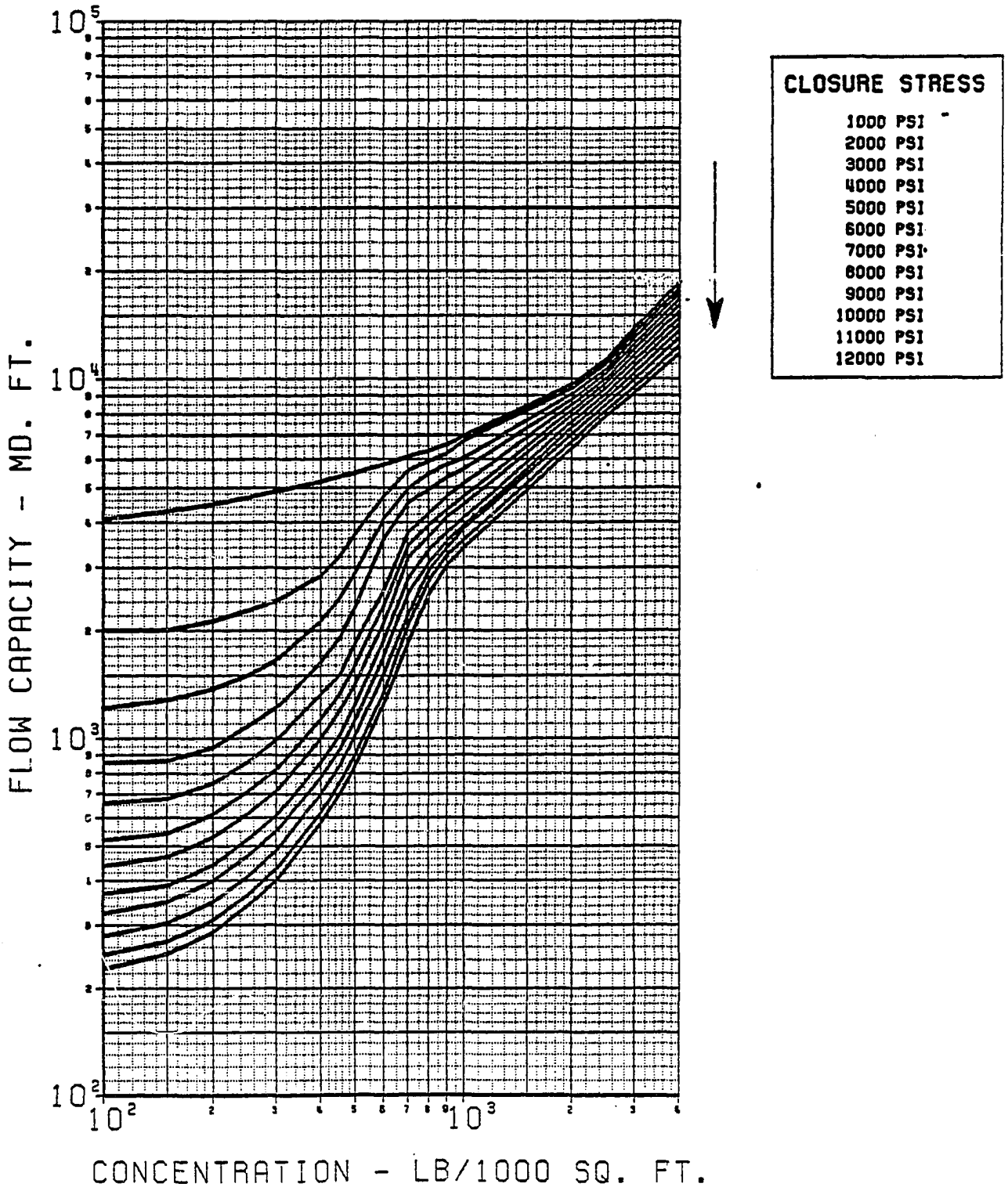


Figure 5-14: Flow Capacity Data for 12-20 SUPER PROP (ref. 41)

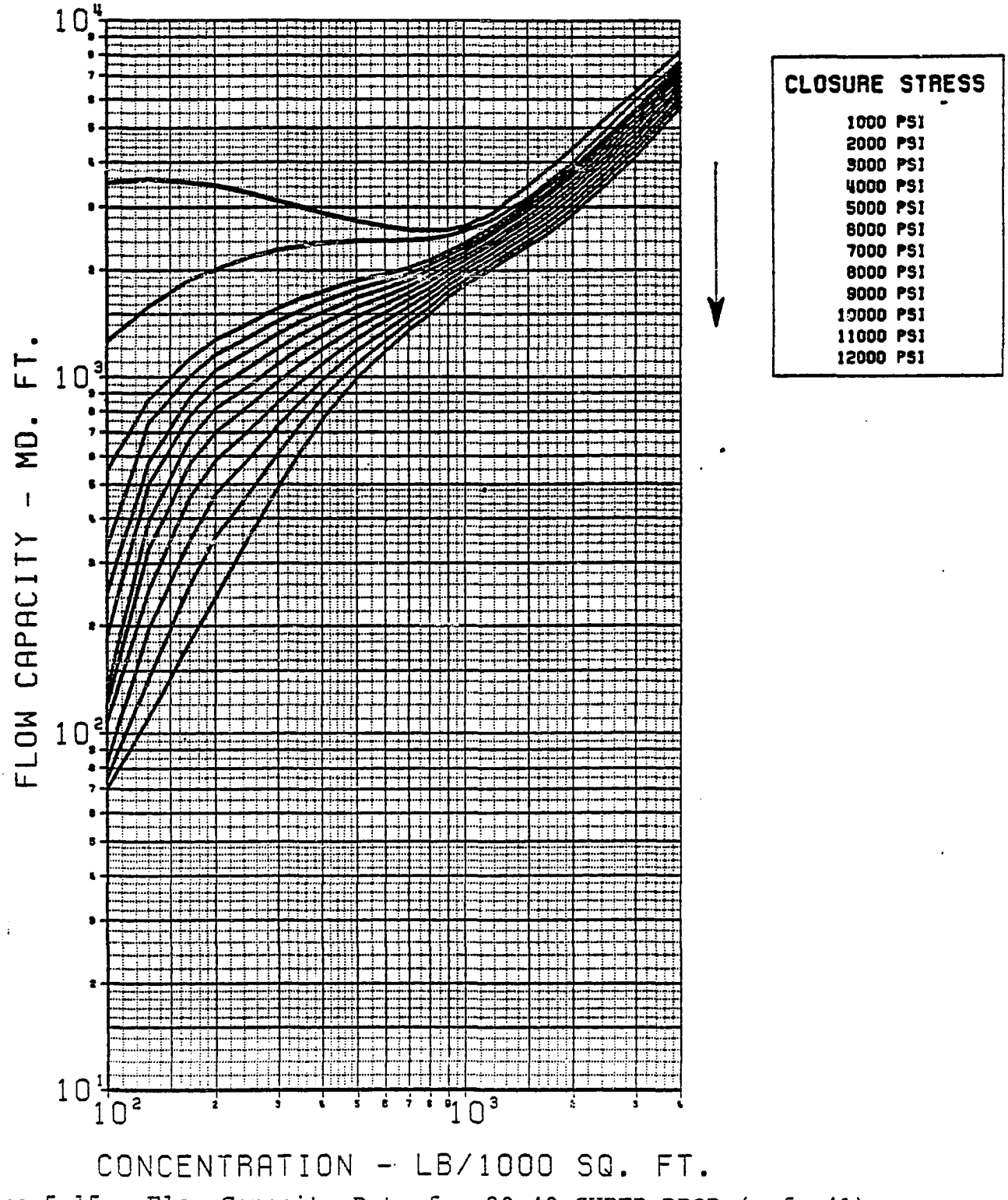


Figure 5-15: Flow Capacity Data for 20-40 SUPER PROP (ref. 41)

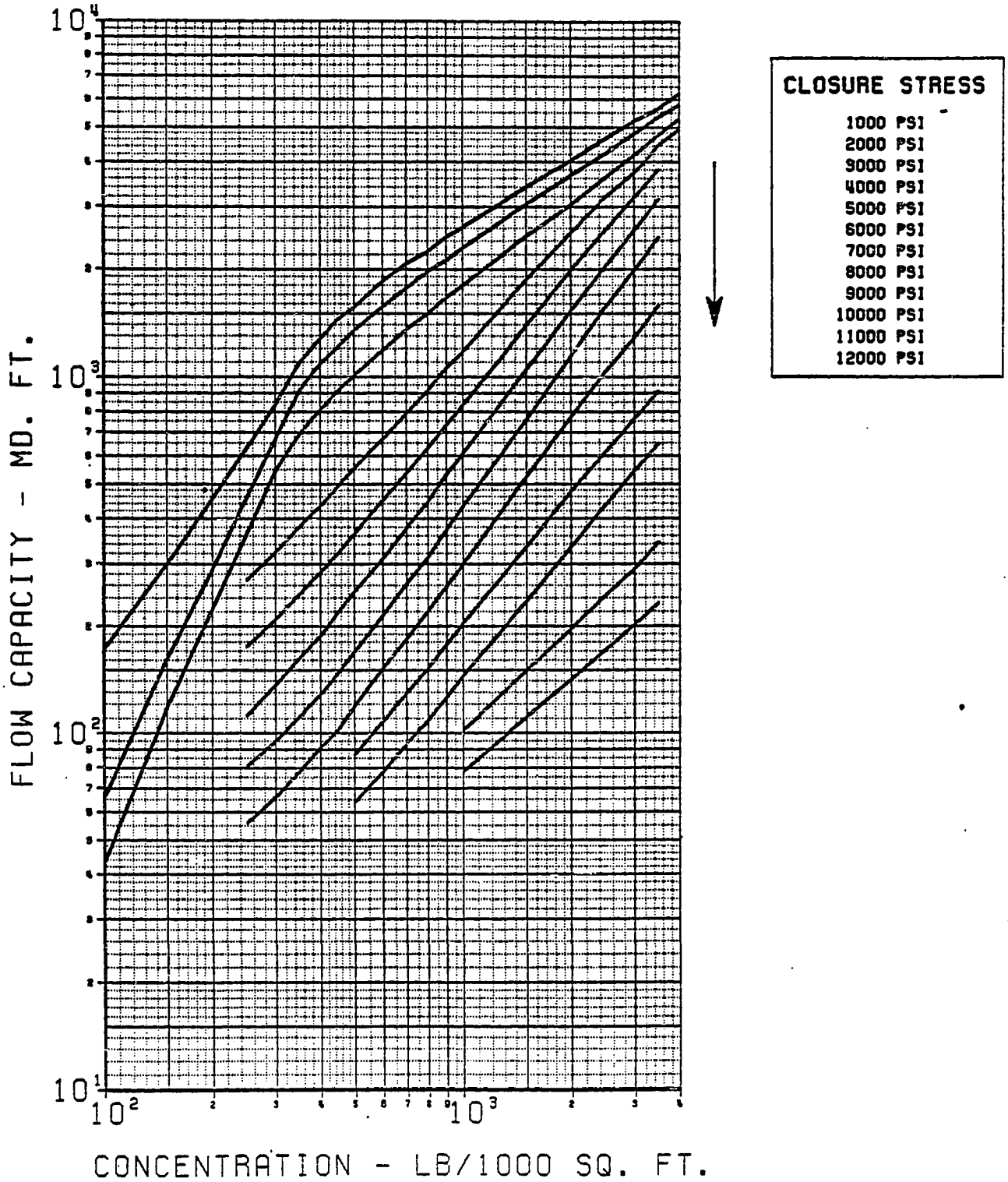


Figure 5-16: Flow Capacity Data for 20-40 Ottawa Sand (ref. 41)

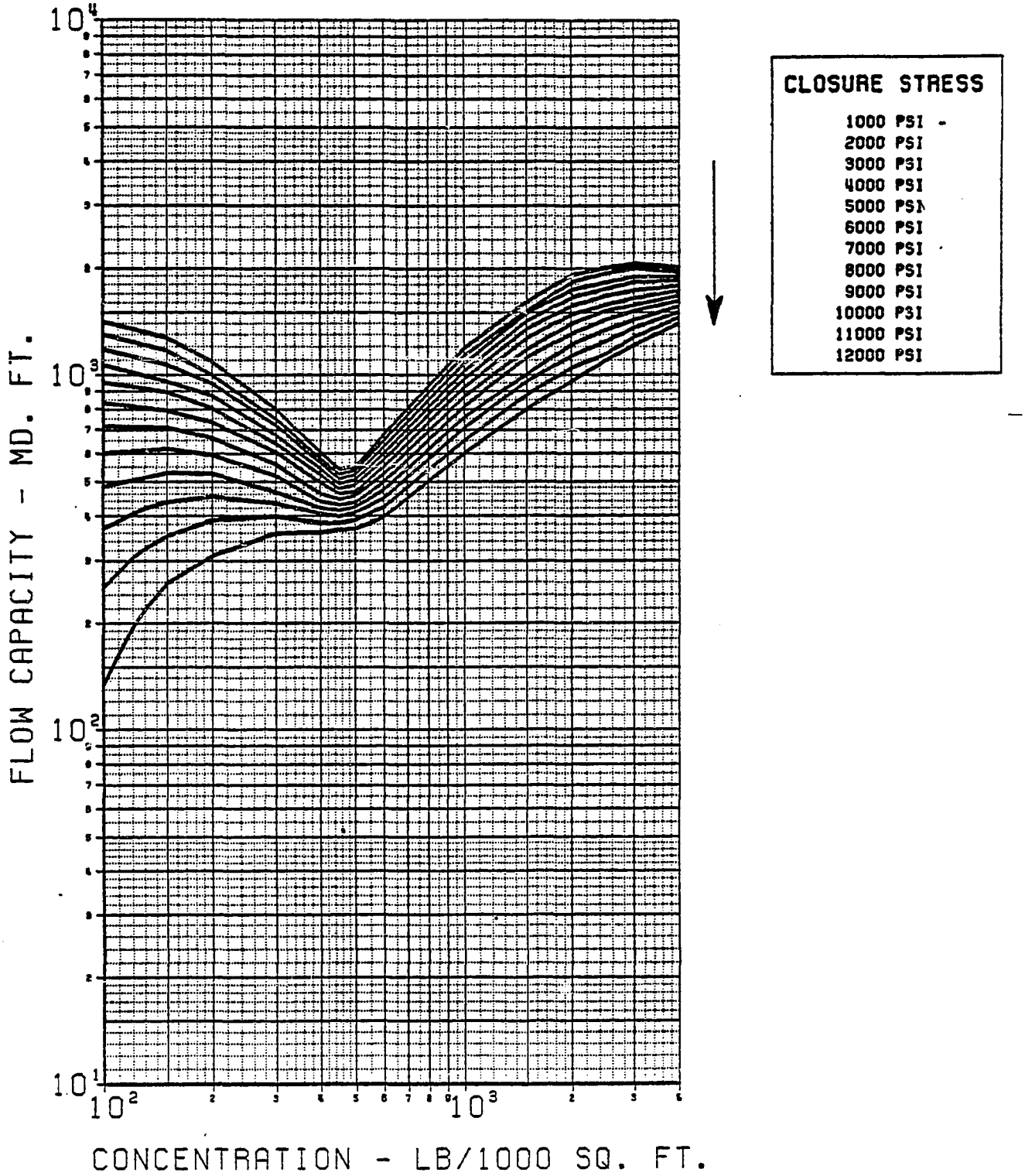


Figure 5-17: Flow Capacity Data for 40-60 SUPER PROP (ref. 41)

CHAPTER VI

NUMERICAL MODEL

Numerical simulators can be used for solving the mathematical equations in petroleum engineering problems. These equations describe the behavior of the fluids in porous media under unsteady state conditions. Peaceman and Rachford[42] were the first to introduce the numerical models to solve the reservoir engineering problems in the 1950's. Since that time, the numerical models have been used extensively to model the most complicated patterns of reservoir behavior. In some cases, the analytical tools are difficult to use or impossible to use because of the complexity of the problems. However, developing a computer model to solve such difficult systems numerically is very essential. For instance, in the cases of vertically fractured wells with finite conductivity fracture, it is very difficult to design a computer model to solve this system. In the past, two important assumptions were made in developing such simulators. One is that the fracture has an infinite permeability. These types of problems can be handled by utilizing analytical means. The second assumption was that the fracture and

formation heights be the same.

In the present work, a vertically fractured well with finite conductivity is simulated. Further, the fracture height is different from the formation height. The formation is layered with no cross-flow between layers. In addition, the non-Darcy flow and closure pressure effects are considered in the fracture. A three-dimensional reservoir model, fully implicit, finite difference, is written. This simulator utilizes both an iterative and a direct solution scheme.

6.1 Finite Difference Equations

The equations which govern the fluid flow in the formation and fracture are derived earlier in the previous section. The numerical solution of these equations can be obtained by the use of the finite difference technique. The equivalent finite difference equations are produced by making the first order Taylor expansion for all derivatives. The solution is obtained at discrete points in space and time. Appendix B includes the finite difference equation formulation. The finite difference equation for flow is given by:

$$\frac{1}{\Delta x_j}\left[k_{j+\frac{1}{2}} \frac{m_{j+1}-m_j}{\Delta x_{j+\frac{1}{2}}} - k_{j-\frac{1}{2}} \frac{m_j - m_{j-1}}{\Delta x_{j-\frac{1}{2}}} \right]^{n+1} +$$

$$\frac{1}{\Delta y_i}\left[k_{i+\frac{1}{2}}\frac{m_{i+1}-m_i}{\Delta y_{i+\frac{1}{2}}}-k_{i-\frac{1}{2}}\frac{m_i-m_{i-1}}{\Delta y_{i-\frac{1}{2}}}\right]^{n+1}+$$

$$\frac{1}{\Delta z_\ell}\left[k_{\ell+\frac{1}{2}}\frac{m_{\ell+1}-m_\ell}{\ell_{+\frac{1}{2}}}-k_{\ell-\frac{1}{2}}\frac{m_\ell-m_{\ell-1}}{Z_{\ell-\frac{1}{2}}}\right]^{n+1}=$$

$$(\phi\mu C_g)^{n+1}\left[\frac{m_{ij}^{n+1}-m_{ij\ell}^{n}}{\Delta t}\right]+Q \quad \text{.....(6.1)}$$

Equation (6.1) can be simplified as:

$$c_1\, m_{j+1}^{n+1}+c_2\, m_{j-1}^{n+1}+c_3\, m_{i+1}^{n+1}+c_4\, m_{i-1}^{n+1}+c_5\, m_{\ell+1}^{n+1}+$$

$$c_6\, m_{\ell-1}^{n+1}-c_7\, m_{ij\ell}^{n+1}=\text{RHS} \quad \text{.....(6.2)}$$

where all coefficients c_1-c_7 and RHS are defined in Appendix B.

For the flow in the fracture cells, the coefficients of equation (2) are calculated based on the fracture permeability (k_f). In addition, these coefficients include another new term called turbulent factor (δ), to consider the effect of non-Darcy flow within the fracture cells. Finite difference equations for fracture blocks are included in Appendix B.

Several points should be noted in formulating the previous equations. First of all, an irregular grid is used. The dependent pseudo-pressure function is calculated

at the center of each block. Figure 6-1 shows the grid size distribution. This grid is used to increase the definition in regions where better control is needed. Cells near the wellbore and fracture are a smaller size than those away from the wellbore. This is done to provide a stable solution.

Secondly, as fluid and reservoir properties are only defined at grid points, some techniques must be used for approximating interblock flow coefficients based on values at the grid points. The term that makes up the flow coefficients is the fluid permeability. At the fracture faces, permeability changes rapidly from grid block to another. These sharp changes in fluid permeability could cause a significant difficulty. The two-points upstream technique[43] appears to be a useful tool in evaluating permeability at the upstream block face. The two-points method provides a reduction in numerical dispersion. Thus, at planes ($i \pm \frac{1}{2}$), the following approximation is used:

For flow in the minus x- direction:

$$k_{j+\frac{1}{2}} \quad k_{j+1} - \frac{\Delta x_{j+1}}{\Delta x_{j+1} + \Delta x_{j+2}} (k_{j+2} - k_{j+1}) \quad \ldots\ldots (6.3)$$

$$k_{j-\frac{1}{2}} = k_j - \frac{\Delta x_j}{\Delta x_j + \Delta x_{j+1}} (k_{j+1} - k_j) \quad \ldots\ldots\ldots\ldots (6.4)$$

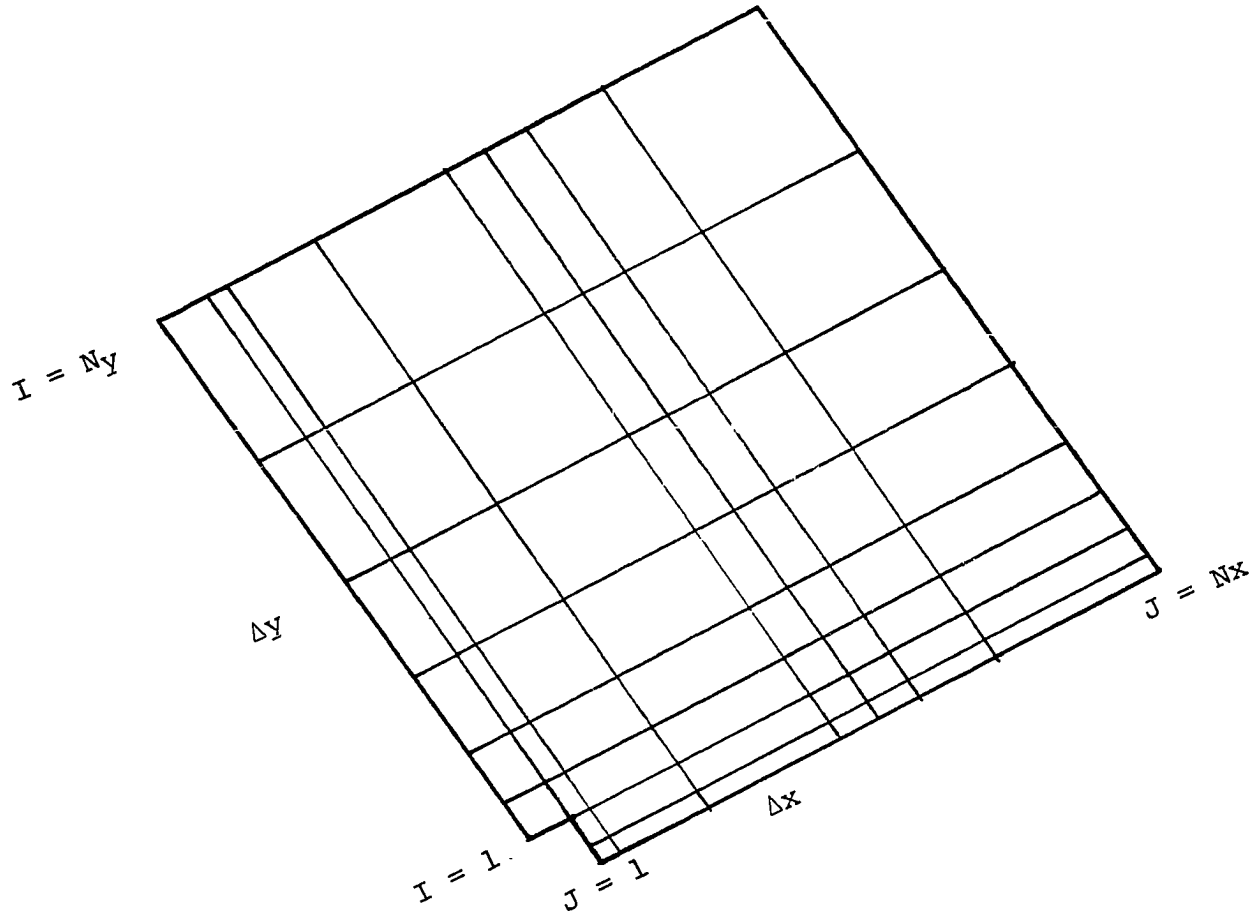


Figure 6.1 Diagram of Grid Distribution

The equations for evaluating upstream permeability for flow in the plus x direction are included in Appendix B. Equations (6.3) and (6.4) can be written for y and z directions.

Thirdly, turbulence and fracture closure effects are calculated in the main program. Equation (5.25) defines the turbulence factor (δ):

$$\delta = \frac{1}{1 + \frac{2.97 \times 10^{-10} \beta \rho v k_f}{\mu}} \quad \ldots\ldots\ldots (6.5)$$

The turbulent flow is considered only in the fracture. The flow in the formation is assumed to obey Darcy's law. Values of density (ρ), velocity ($\bar{v}$), viscosity (μ), and permeability (k_f) are calculared for each fracture cell at each time step. To provide stability, the turbulence factor at time step t^n is averaged with the old value. The following equation is used:

$$\delta_i^n = \frac{0.67}{1 + 2.97 \times 10^{-10} \beta \rho v k_f} + 0.34\, \delta_i^{n-1} \quad \ldots\ldots\ldots (6.6)$$

The value of the β factor is calculated using Cooke's formula:[36]

$$\beta = b/(1000 k_f)^a \quad \ldots\ldots\ldots (6.7)$$

The values of (a) and (b) must be read in the model. These values depend on the size of propping agent. Table 6.1 provides this data.[36]

To consider the effects of fracture closure, the bottom hole treating pressure must be read into the model. The maximum closure pressure which is the difference between bottom hole treating pressure and current pressure is calculated for each cell in the fracture. Using the data of closure pressure versus fracture flow capacity, the new permeability in the fracture cell is determined at each time step. Therefore, the fracture flow capacity is changing with distance and time. These modifications produce a realistic results from the model because the model is more representative to the actual reservoir conditions.

TABLE 6-1

CONSTANTS a AND b FOR CALCULATING THE β FACTOR

Sand Size	a	b
8-12	1.24	3.32
10-20	1.34	2.63
20-40	1.54	2.65
40-60	1.60	1.10

Finally, the finite difference method is a fully implicit formulation. The above equations are set up for each grid block. Therefore, the following number of equations to be solved are defined as:

$$N = NX * NY * NZ$$

where:

NX = Number of blocks in the X-direction

NY = Number of blocks in the Y-direction

NZ = Number of blocks in the Z-direction

These N equations are solved simultaneously for the unknown pseudo-pressures at each time step. All parameters in the left hand side of equation (6.2) are calculated at the future time step (n+1), as are the unknowns in the equation. The collected terms in the right hand side of equation (6.2) are known from the old time step (n). The old pseudo-pressure value is used in the RHS.

The boundary conditions around the entire system are given by assuming zero permeability.

$$\frac{\partial m}{\partial x}\Big|_A = \frac{m_i - m_{j\pm 1}}{\Delta X_j} = 0$$

$$\frac{\partial m}{\partial y}\Big|_B = \frac{m_i - m_{i\pm 1}}{\Delta Y_i} = 0 \quad \text{.....(6.8)}$$

$$\frac{\partial m}{\partial z}\Big|_C = \frac{m - m_{\ell\pm 1}}{\Delta Z_\ell} = 0$$

where:

A - the boundary at ($x=0$, or $x=x_e$)

B - the boundary at ($y=0$, or $y=y_e$)

C - the boundary at ($z=0$, or $z=h$)

The boundary conditions for producing cells (1, 1, ℓ) are set up differently. Since these cells are producing, the RHS of equations (6.2) must include the flux rate term. For a constant bottom hole flowing pressure, the flux rate term can be calcualted as:

$$RHS = RHS + C * PMPW_f \quad \text{.....(6.9)}$$

where $PMPW_f$ is the pseudo-pressure function corresponding to bottom hole flowing pressure; C is defined in Appendix B. The boundary conditions for producing cells are:

$$\left.\frac{\partial m}{\partial X}\right|_{x=r_w} = \frac{m_j - PMPW_f}{\Delta x_j} = \text{non-zero}$$

$$\left.\frac{\partial m}{\partial Y}\right|_{y=r_w} = \frac{m_i - PMPW_f}{\Delta y_i} = \text{non-zero} \quad \text{.....(6.10)}$$

The inner boundary between the two layers can be represented by assuming no flow (k = 0):

$$\left.\frac{\partial m}{\partial z}\right|_{Z=h_i} = \frac{m_\ell - m_{\ell\pm1}}{\Delta Z_\ell} = 0 \quad \text{.....(6.11)}$$

In this case, the only communication between the layers will be via the fracture. On the other hand, the inner boundary can be with cross flowing;

$$\frac{\partial m}{\partial Z}\Big|_{z=h_1} = \frac{m_\ell - m_{\ell\pm1}}{\Delta z_\ell} = \text{non-zero} \quad \ldots\ldots\ldots\ldots\ldots(6.12)$$

6.2 Methods of Solution

At this point, equations were developed to describe the fluid flow in a fractured formation. The finite difference equations are set up in the previous section. Combining all equations for N blocks yield NX * NY * NZ equations with N pseudo-pressure unknowns, where NX, NY, and NZ are the total grids in the X, Y, and Z directions. The matrix formed by the equations appears as a 7-diagonal matrix. The matrix has three central diagonals and four other diagonals There are two basic methods for solving this system of equations. First, the direct Process: in this method, the solution to the system of equations is obtained upon the completion of a fixed number of operations. Second is the iterative process. The latter process is cyclic in nature, and the solution process involves several computations of hopefully better and more exact approximations to the solution at each iteration. One technique of each process is used in developing the model. In the following section, the Sparse Matrix Technique will be discussed as a direct method for solving this system of equations.

A. Sparse Matrix Technique

The banded matrix is solved by a direct method using a sparse matrix solver. The big advantage of the Sparse

Matrix technique is working only on the non-zero elements. The technique involves two approaches. First, the matrix is reordered to preserve its sparsity and to minimize the number of operations involving non-zeros. Second, the reordered matrix is solved by using an efficient Gaussian elimination algorithm. The algorithm operates and stores only non-zeros elements of the matrix plus the new non-zeros that occur during calculations.

The Sparse Matrix algorithm used is similar to that developed by Gustavson[44] and Gustavson, Liniger and Willoughby.[45] The details of the techniques are given in the references. Initially, the matrix algorithm is based on utilizing a Gaussian elimination method which is derived by considering a coefficient matrix M, where the coefficient matrix M is large, sparse, and non symmetrical. This matrix can be factored as a product of L, a lower triangular matrix; D, a diagonal matrix; and U, a unit upper triangular matrix. Thus, the following:

$$M\bar{x} = b$$

$$M = LDU$$

The LDU decomposite of M is found, and the triangular systems are solved as:

$$LY = b,\ DZ = y,\ \text{and}\ Ux = Z$$

Since M is sparse, most entries of M, L, and U are zero,

and there are significant advantages to factoring, storing, or operating on the non-zeros.

B. SSOR Technique

SSOR is an abbreviation for "SLICES SUCCESSIVE OVER-RELAXATION." This is an iterative technique that is also used in the model. Two important factors are required for SSOR to converge. Firstly, the value of the iteration parameter (w) must be less than 2.0. Secondly, the matrix M must be diagonally dominate. Which means, the absolute value of the main diagonal must be greater than or equal to the sum of the absolute values of other coefficients for the same grid point.

The general equation 6.2 is rewritten for a slice as follows:

$$c_1 m_{j+1} + c_2 m_{j-1} + c_3 m_{i+1} + c_4 m_{i-1} - c_7 m_{ij\ell}$$

$$= RHS - c_5 m_{\ell+1} - c_6 m_{\ell-1} \quad \ldots\ldots\ldots\ldots\ldots\ldots (6.13)$$

Equation (6.13) shows that we have five unknowns. If similar equations are formulated for all grid points in level ℓ, the NX * NY equations will have results which have NX * NY unknowns. At this point, old pseudo-pressure values at level $\ell+1$ will be used in Equation (6.13) as knowns. Also, pseudo-pressure values at level $\ell-1$ will be known because they are just calculated from previous iteration.

Now, as for level ℓ, we have a matrix which has the dimension N*N which must be solved, where N equals NX * NY. The alternating diagonal technique has been used in mathematics for years. Price and Coats[46] were the first to improve the technique and apply it to petroleum reservoir simulation. The alternating diagonal technique for two-dimensional, single phase flow is explained in the literature. Thus, the alternating diagonal technique is used to solve this system of equations in one vertical level (ℓ).

To accelerate the convergence after the solution was obtained for one level, the relaxation parameter (w) is used. During over-relaxation, we amplify the magnitude of pseudo-pressure change during each iteration by simply multiplying this pseudo-pressure change by (w). Thus, for a new pseudo-pressure value, we have the following:

$$m_{ij}^{k+1} = m_{ij}^{k} + w\,(m_{ij} - m_{ij}^{k}) \quad \text{.....(6.14)}$$

It should be noted that this step is completed before proceeding to the next level (ℓ+1). In other words, the extrapolated value m^{k+1} is used in the subsequent equations. The optimum value for (w) is obtained by trial and error.

The process is repeated for ℓ+1, ℓ+2, ..., NZ. If the solution doesn't meet the convergence criteria, the iterative process continues until one of the following conditions is met:

1) The solution is obtained within the convergence limit, or
2) Number of iteration exceeds the maximum allowable limit.

For condition 2, the time step is reduced by factor of one half and the process is repeated again. The relative error in the model is defined in equation (6.15).

$$\varepsilon \leq \frac{m^{k+1} - m^{k}}{m^{k+1}} = 0.0001 \quad \text{.....(6.15)}$$

6.3 Computer Program

The computer program consists of main and several subroutines. The main is used for all input, output, and controlling DO LOOP. Appendix C includes a flow chart of the main routine. Initial calculations, such as gas properties table (pseudo-pressure, viscosity, formation volume factor, and compressability), gas inplace are made prior to entering DO LOOP. The program will terminate from DO LOOP when; 1) the gas flow rate drops below a certain limit; 2) total number of cycles have occurred; 3) average reservoir pressure reaches bottom hole flowing pressure; and 4) the total time in days exceeds the time limit. A material balance is kept in main and a summary table is stored for each step and is printed upon termination of the run.

Function PINT is an interpolation subroutine used in several places throughout the program. Subroutine GASP

is used to calculate the gas properties in each cell. This subroutine is called:

1) To utilize all gas properties
2) During each iteration
3) At the end of each time step to update gas properties for material balance calculations.

In subroutine COEFF, the permeability for gas between cells are calculated in x, y, and z directions. The average permeability is chosen based on the two-point upstream cell. The boundary conditions are set up in this subroutine. All coefficients c_1, c_2, c_3, c_4, c_5, c_6, c_7, and RHS are then calculated. The last step in this subroutine is normalizing the coefficients by dividing all of them by c_7. At this time, the matrix is set up and ready to be called for solution subroutine.

Subroutine CONT is used to control the process. Several checks are made at the beginning of CONT. These checks are to determine if the new time stey may be too large. The time step may be reduced based on the maximum pressure change in a cell, and the maximum time step. After any necessary adjustment, GASP is called to update the gas properties in each cell. Then SSOR or NDRV is called for solution. Upon returning to CONT, the values of pseudo-pressure for each cell have been calculated. Using PINT interpolating routine, values of pressure are known at each cell for time $(t + \Delta t)$.

Numerous checks are made near the end of CONT to determine if the calculated values of pressure have met specific limitations. If the pressure drop is too high, another iteration is begun with time step reduced to one half of the previous one. This is necessary to make the program more stable by controlling pressure drop within a certain limit for each time step. Appendix C presents flow charts for the main and several subroutines.

6.4 Validity of the Model

The model was stable and consistent throughout all different validation runs made to verify its accuracy. Some points of interest should be mentioned before any discussions of results. First, it was difficult to design a unique grid-size distribution for all cells. In general, this is one of the most important features in designing a stable simulator. To achieve acceptable results, it was necessary to use irregular grid size. Because of the sharp discontinuity encountered in this problem, especially near the fracture faces, it was necessary to use small dimensions in the vicinity of any discontinuity. Thus, very small cells were considered near the wellbore and the fracture. Larger cells, however, were acceptable at greater distances from these areas of discontinuities.

For the purpose of this study, the drainage area was treated as three-dimensional flow region divided into

irregular flow cells. In addition, the discontinuity encountered in the third dimension is also considered. As a result, a unique grid size structure was chosen with fine grids at some areas.

Second, the described model was stable under a wide range of varying conditions. It was found that a very small initial time step is necessary. This initial time step in the model is 10^{-4} day. The time step can be increased by a factor of two for every new time. The maximum time step size is set equal to 20 days. In fact, it can be larger or smaller than 20 days, as long as the convergence criteria are met. If Δt is too large, the program will cut back Δt by a factor of $\frac{1}{2}$.

In many cases, it was observed that a large initial time step caused oscillating solutions due to numerical instability. In addition, more stability was obtained when a maximum pressure drop for every time step is considered. A maximum pressure drop of 300 psi is allowed for any time step. If the pressure drop for any cell exceeds such a limit, a reduction in the time step is considered. This pressure control factor is very important, particularly at very early time.

In general, the program was very stable because the problem is implicitly treated. It should be mentioned that the execution time was large when the iterative

technique was used compared to the direct method solution. For example, two different computer runs were made using the same input data in both cases. Using the iterative solver (SSOR), the total execution time was 9.92 minutes for modelling the well performance for 10 days of production. In the second computer run, the direct solver (SPARSE) yielded an execution time of 3.2 minutes. This is expected because of the heterogeneity which was involved in the problem. Thus, in all runs, the solver used was sparse matrix technique.

Finally, in this study, the validity of the model is verified by comparing results with the analytical solution of a finite conductivity fracture (constant pressure case). The solution generated for hf/h=1, laminar flow, and the results were compared with the analytical solution for constant bottom hole pressure presented by Agarwal. et al.

The above results of these simulations are presented in Tables 6.1-6.4 and Figure 6.2. Figure 6.2 is a plot of log $1/q_D$ versus log t_{Dxf} for various F_{CD}. In Figure 6.2, solution is presented for four values of F_{CD}: 1, 5, 10, and 50.

Comparison of the analytic and numerical solutions presented reveal two interesting points. First, there is excellent agreement between the numerical solutions and those of Agarwal et al. over most of the range. Second, for $t_{Dxf}<10^{-4}$, the numerical results differ from the

TABLE 6- : COMPARISON BETWEEN ANALYTICAL AND NUMERICAL SOLUTIONS FOR FCD=1 ,HF/H=1 AND MDT=0

TDXF	1/QD ANALYTICAL	NUMERICAL
.105E-04	.164E+00	.232E+00
.180E-04	.190E+00	.252E+00
.292E-04	.200E+00	.271E+00
.460E-04	.221E+00	.281E+00
.712E-04	.247E+00	.310E+00
.109E-03	.283E+00	.353E+00
.166E-03	.306E+00	.372E+00
.251E-03	.355E+00	.400E+00
.378E-03	.390E+00	.430E+00
.570E-03	.446E+00	.452E+00
.856E-03	.481E+00	.511E+00
.129E-02	.510E+00	.530E+00
.193E-02	.570E+00	.603E+00
.290E-02	.621E+00	.641E+00
.435E-02	.692E+00	.695E+00
.653E-02	.760E+00	.766E+00
.980E-02	.820E+00	.825E+00
.147E-01	.940E+00	.940E+00
.221E-01	.101E+01	.100E+01
.331E-01	.110E+01	.110E+01
.496E-01	.125E+01	.125E+01
.745E-01	.137E+01	.137E+01
.112E+00	.154E+01	.154E+01
.168E+00	.166E+01	.166E+01
.251E+00	.181E+01	.180E+01
.377E+00	.196E+01	.196E+01
.565E+00	.213E+01	.213E+01
.787E+00	.230E+01	.230E+01
.100E+01	.243E+01	.243E+01

TABLE 6- : COMPARISON BETWEEN ANALYTICAL AND NUMERICAL SOLUTIONS FOR FCD=5 ,HF/H=1 AND MDT=0

TDXF	1/QD ANALYTICAL	NUMERICAL
.292E-04	.905E-01	.102E+00
.460E-04	.101E+00	.113E+00
.712E-04	.113E+00	.121E+00
.109E-03	.128E+00	.132E+00
.166E-03	.137E+00	.140E+00
.251E-03	.156E+00	.158E+00
.378E-03	.172E+00	.174E+00
.570E-03	.185E+00	.186E+00
.856E-03	.205E+00	.205E+00
.129E-02	.230E+00	.231E+00
.193E-02	.257E+00	.257E+00
.290E-02	.280E+00	.280E+00
.435E-02	.313E+00	.313E+00
.653E-02	.351E+00	.351E+00
.980E-02	.392E+00	.392E+00
.147E-01	.471E+00	.470E+00
.221E-01	.500E+00	.500E+00
.331E-01	.571E+00	.570E+00
.496E-01	.656E+00	.656E+00
.754E-01	.746E+00	.747E+00
.112E+00	.852E+00	.852E+00
.168E+00	.971E+00	.970E+00
.251E+00	.111E+00	.110E+01
.377E+00	.125E+00	.125E+01
.565E+00	.140E+00	.139E+01
.787E+00	.151E+00	.150E+01
.100E+01	.161E+00	.160E+01

TABLE 6- : COMPARISON BETWEEN ANALYTICAL AND NUMERICAL SOLUTIONS FOR FCD=10 ,HF/H=1 AND MDT=0

TDXF	1/QD ANALYTICAL	NUMERICAL
.105E-04	.525E-01	.601E-01
.180E-04	.594E-01	.652E-01
.292E-04	.670E-01	.712E-01
.460E-04	.740E-01	.776E-01
.712E-04	.812E-01	.820E-01
.109E-03	.885E-01	.884E-01
.166E-03	.100E+00	.100E+00
.251E-03	.110E+00	.110E+00
.378E-03	.122E+00	.122E+00
.570E-03	.133E+00	.133E+00
.856E-03	.151E+00	.151E+00
.129E-02	.168E+00	.168E+00
.193E-02	.186E+00	.186E+00
.290E-02	.211E+00	.211E+00
.435E-02	.241E+00	.241E+00
.653E-02	.272E+00	.273E+00
.980E-02	.315E+00	.315E+00
.147E-01	.360E+00	.361E+00
.221E-01	.423E+00	.424E+00
.331E-01	.498E+00	.498E+00
.496E-01	.586E+00	.585E+00
.745E-01	.680E+00	.680E+00
.112E+00	.781E+00	.781E+00
.168E+00	.887E+00	.887E+00
.251E+00	.101E+01	.101E+01
.377E+00	.115E+01	.115E+01
.565E+00	.131E+01	.131E+01
.787E+00	.143E+01	.143E+01
.100E+01	.154E+01	.154E+01

TABLE 6- : COMPARISON BETWEEN ANALYTICAL AND NUMERICAL SOLUTIONS FOR FCD=50 ,HF/H=1 AND MDT=0

TDXF	1/QD ANALYTICAL	NUMERICAL
.105E-04	.250E-01	.300E-01
.180E-04	.271E-01	.310E-01
.292E-04	.300E-01	.321E-01
.460E-04	.340E-01	.340E-01
.712E-04	.381E-01	.390E-01
.109E-03	.431E-01	.430E-01
.166E-03	.482E-01	.480E-01
.251E-03	.570E-01	.570E-01
.378E-03	.652E-01	.650E-01
.570E-03	.761E-01	.760E-01
.856E-03	.890E-01	.890E-01
.129E-02	.105E+00	.104E+00
.193E-02	.126E+00	.125E+00
.290E-02	.150E+00	.150E+00
.435E-02	.175E+00	.175E+00
.653E-02	.210E+00	.211E+00
.980E-02	.246E+00	.246E+00
.147E-01	.287E+00	.287E+00
.221E-01	.346E+00	.346E+00
.331E-01	.421E+00	.421E+00
.496E-01	.507E+00	.507E+00
.745E-01	.593E+00	.593E+00
.112E+00	.704E+00	.701E+00
.168E+00	.820E+00	.810E+00
.251E+00	.950E+00	.950E+00
.377E+00	.108E+01	.107E+01
.565E+00	.125E+01	.1125+01
.787E+00	.137E+01	.136E+01
.100E+01	.145E+01	.145E+01

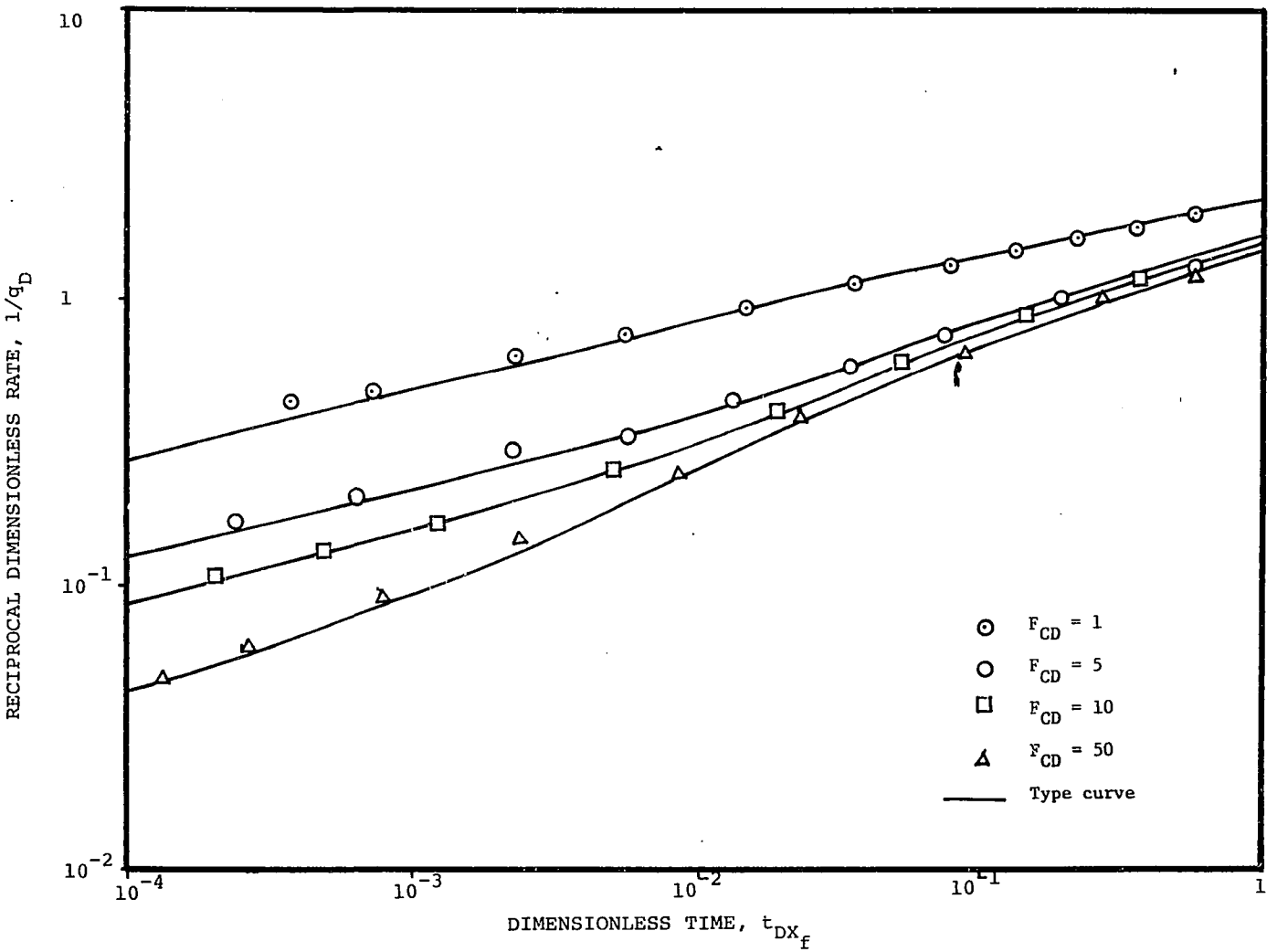


Figure 6.2: The 3-D model results against the type curve for finite conductivity fracture - (h_f = h)

analytical solution. In real life, this dimensionless time corresponds to a few seconds. A smaller initial time step and more iteration per time step will cause a better agreement over that region.

CHAPTER VII

DISCUSSION OF RESULTS

All studies on fractured wells with finite conductivity fracture are based on the assumption that the fracture height and formation height are equal. This is not usually the case. Field studies on fracture height indicate that this assumption is unrealistic. Furthermore, the propped fracture height through which fluid is produced is less than the created fracture height.

In this study the effect of the fracture on the well performance is closely examined for constant pressure case. The well is intercepted by vertical fracture with finite conductivity. Two operating techniques are commonly used by industry for producing wells; constant rate or constant bottom hole flowing pressure. At times, constant flow rates are hard to maintain due to wellhead limitations. Also, if the reservoir is in the depletion phase, the flow rate decreases with time. Generally, the constant bottom hole flowing pressure technique is more likely to be used during production.

In the case of constant pressure, the flow rate changes continuously, and the constant rate solution can not be used. Recently, Raghavan[14] studied the effect of fracture height on transient flow behavior for a uniform flux and infinite conductivity fractures (constant flow rate case). Agarwal, et al. published the results for constant pressure production for finite conductivity fractures. These results demonstrated that a graph of log $1/q_D$ vs log t_{Dxf} can be used to determine fracture length and its conductivity by using the type curve match technique. Cinco, et al.[12] solved the same problem by using semi-analytical methods.

These studies showed that, at early times, a high conductivity fracture gives a higher flow rate at a given pressure than a low conductivity fracture. In the following sections, we shall examine the characteristics of the dimensionless rate as a function of dimensionless time obtained by numerical simulator.

7.1 Effect of Fracture Height

The main purpose of this work is to study the effect of fracture height on productivity of a well intercepting a vertical fracture with finite conductivity. Using the numerical simulator, several runs were made for different fracture conductivities. To compare the results with Agarwal, et al. analytical solution, a Darcy flow in the

fracture is assumed. When the fracture height equals the formation thickness, a good agreement is obtained between our results and numerical solution for all different fracture conductivities. This has been mentioned earlier in the validity of the model section.

Figures 7-1 to 7-4 are graphs of reciprocal dimensionless rate versus dimensionless time and dimensionless fracture conductivity. The term penetration ratio will be used throughout this study which is defined as:

$$b = \frac{h_f}{h}$$

The case of b = 1 is equivalent to the complete fracture penetration throughout the total formation thickness. At this point, it should be mentioned that when b = 1, the problem is reduced to two-dimensional. Thus, the flow in the vertical direction is not significant because of complete penetration. Thus, one may be able to compare the results with the analytical solution for such a case.

As can be seen from Figures 7-1 to 7-4, for all runs when b = 1, the results are comparable with Agarwal, et al. The dimensionless flow decreases as the penetration ratio decreases for any values of dimensionless fracture conductivity. This is expected because larger values of b correspond to a greater fracture area. In general, all results indicate that a fracture with b < 1 behaves as a fully penetrated fracture with lower conductivity.

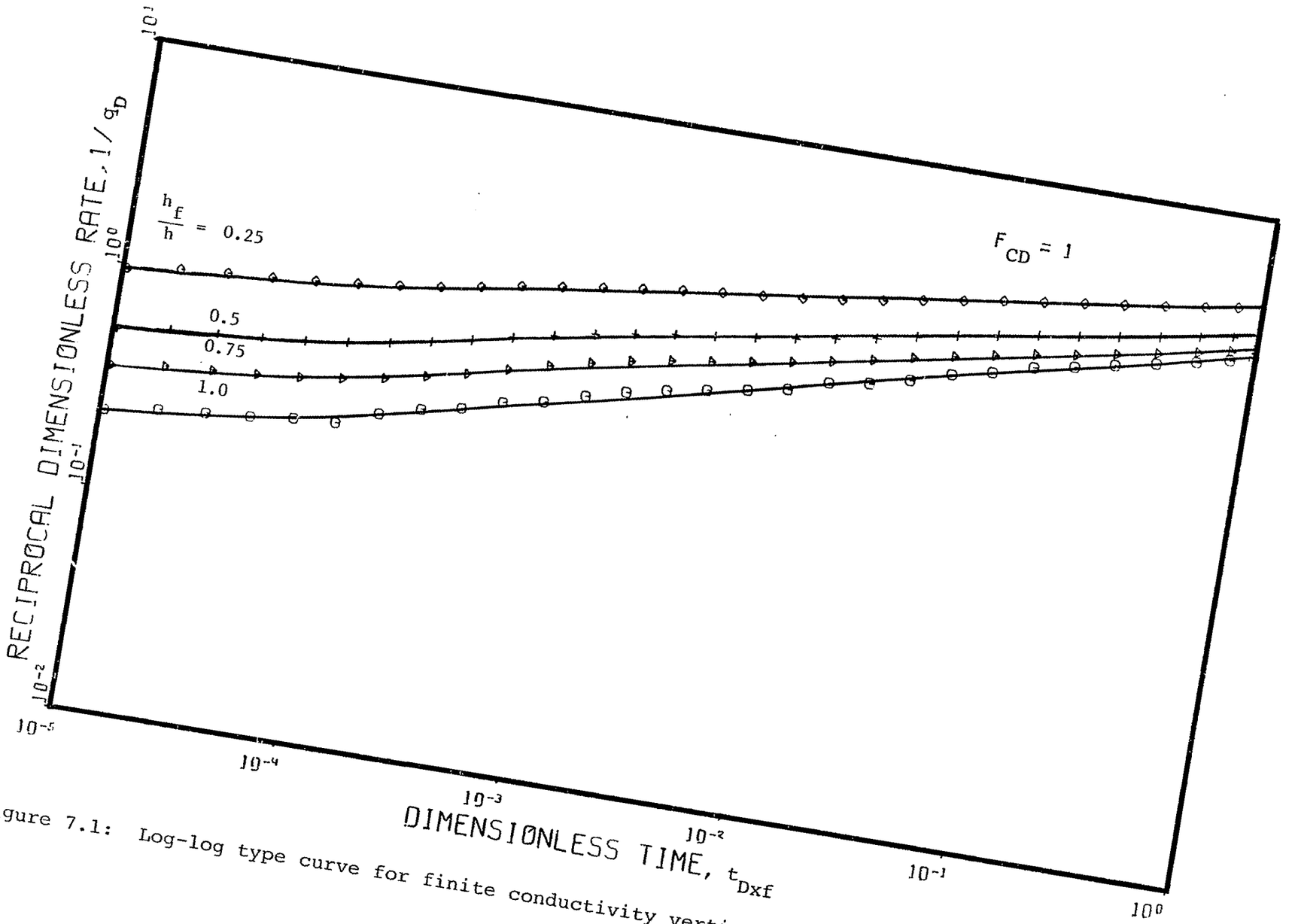


Figure 7.1: Log-log type curve for finite conductivity vertical fracture

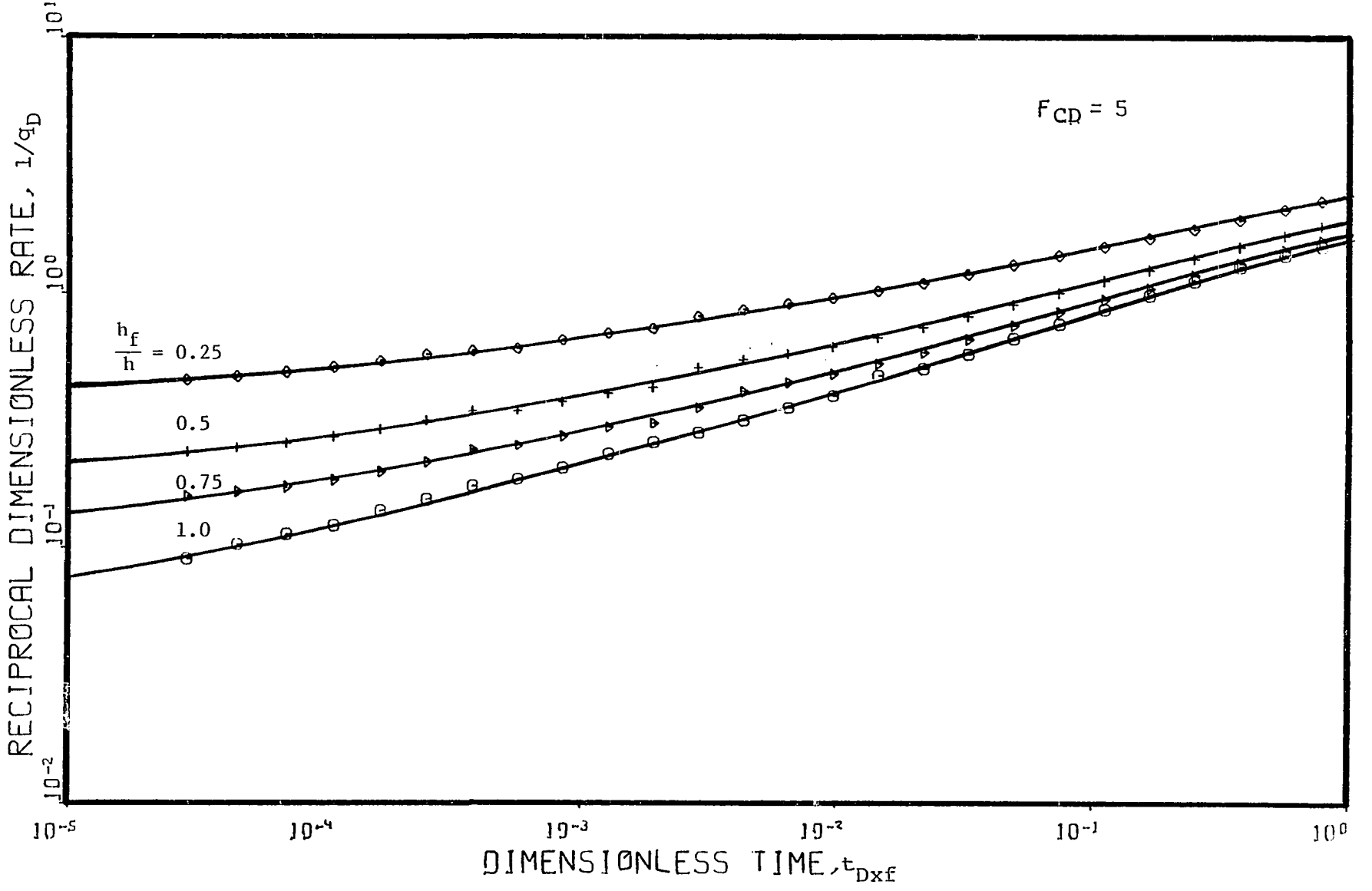


Figure 7.2: Log-lgo type curve for finite conductivity vertical fracture

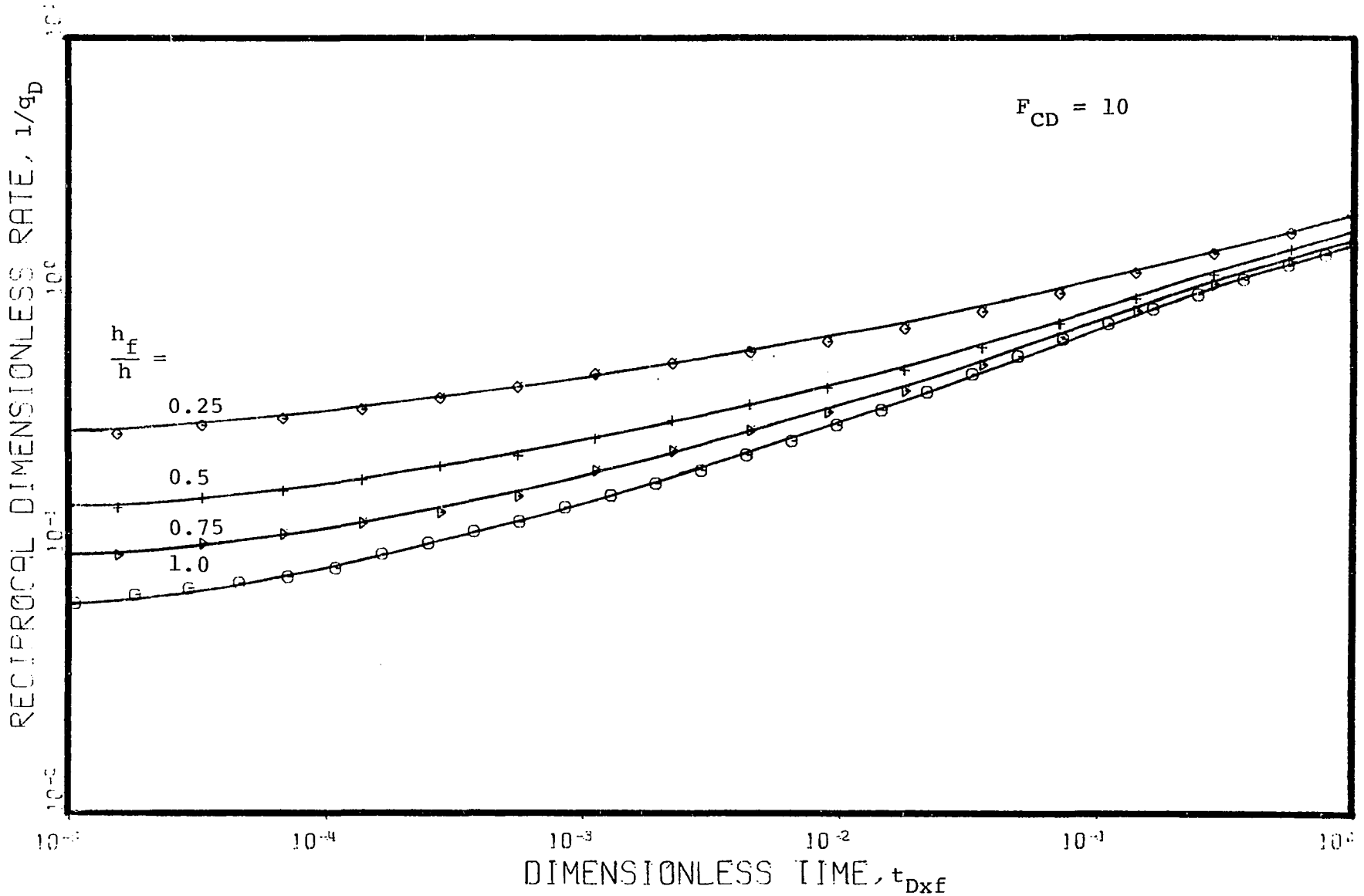


Figure 7.3: Log-log type curve for finite conductivity vertical fracture

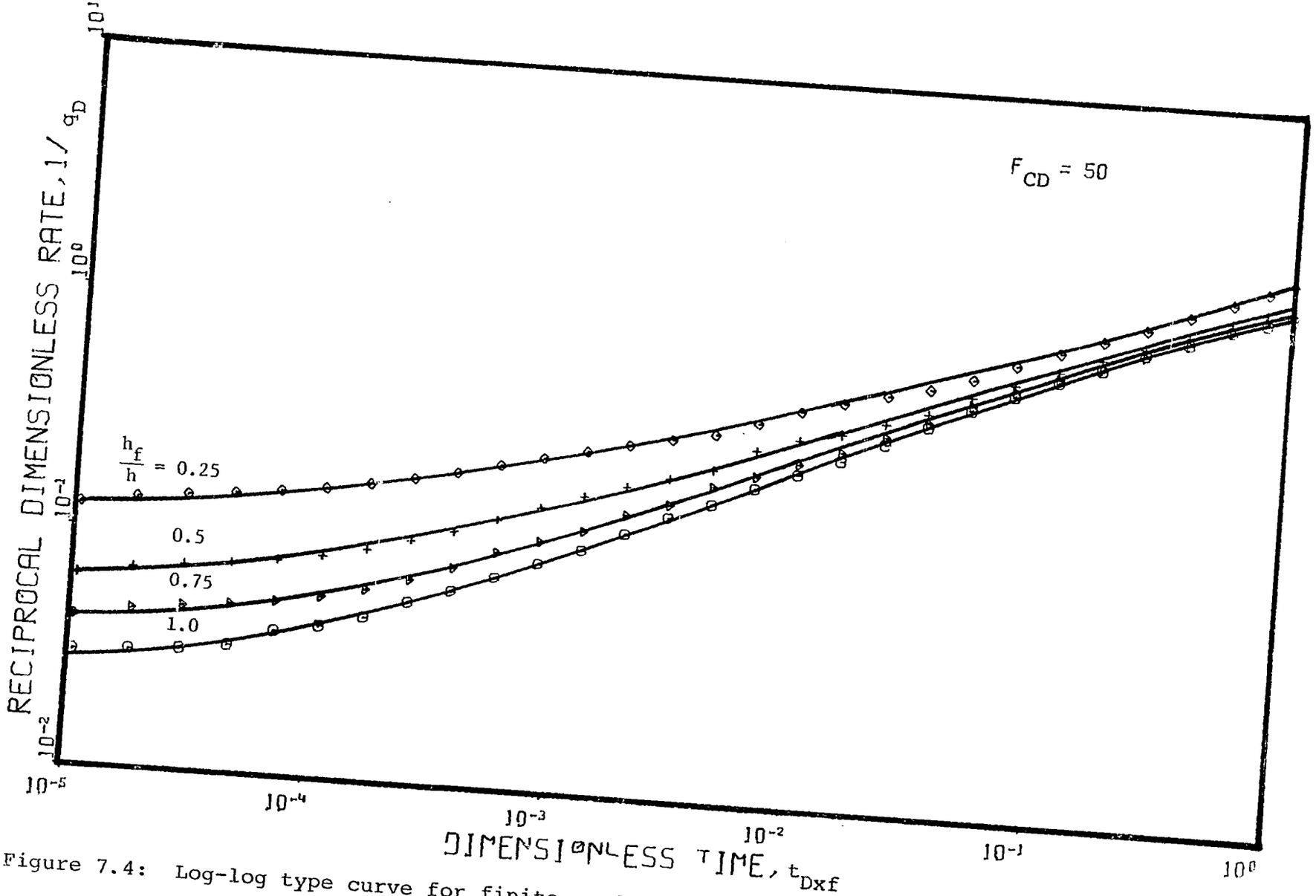


Figure 7.4: Log-log type curve for finite conductivity vertical fracture

Figures 7-5 and 7-6 present the result of long time solution. As is evident from these graphs, the boundary effect appears at the late time period. This is also expected because the model assumes a bounded reservoir. It is noticeable that the curves cross each other at approximately t_{Dxf} of 20 and 100 in Figures 7-5 and 7-6, respectively. This implies that for a partially penetrated reservoir ($b < 1$) is depleted slower than a fully penetrated reservoir. Obviously, such a depletion effect is because a fully penetrated reservoir produces at higher rates at the early time of well life. Figures 7-5 and 7-6 present the late time solution in dimensionless form for two different sets of x_e/x_f ratios of 5 and 10, respectively. A family of graphs can be obtained by varying F_{CD} and x_e/x_f for different b. But for illustration purposes, results for only $F_{CD} = 10$ are presented.

7.2 Effect of Non-Darcy Flow in the Fracture

It is also the objective of this work to study the effect of turbulent flow and fracture height on the productivity of a fractured well. It was shown in a previous section that a turbulent factor (δ) is needed to include the effect of non-Darcy flow within the fracture. Since the results are presented in the dimensionless form, a dimensionless pseudo-pressure drop is presented (m_{DT}). This is similar to the dimensionless constant presented by

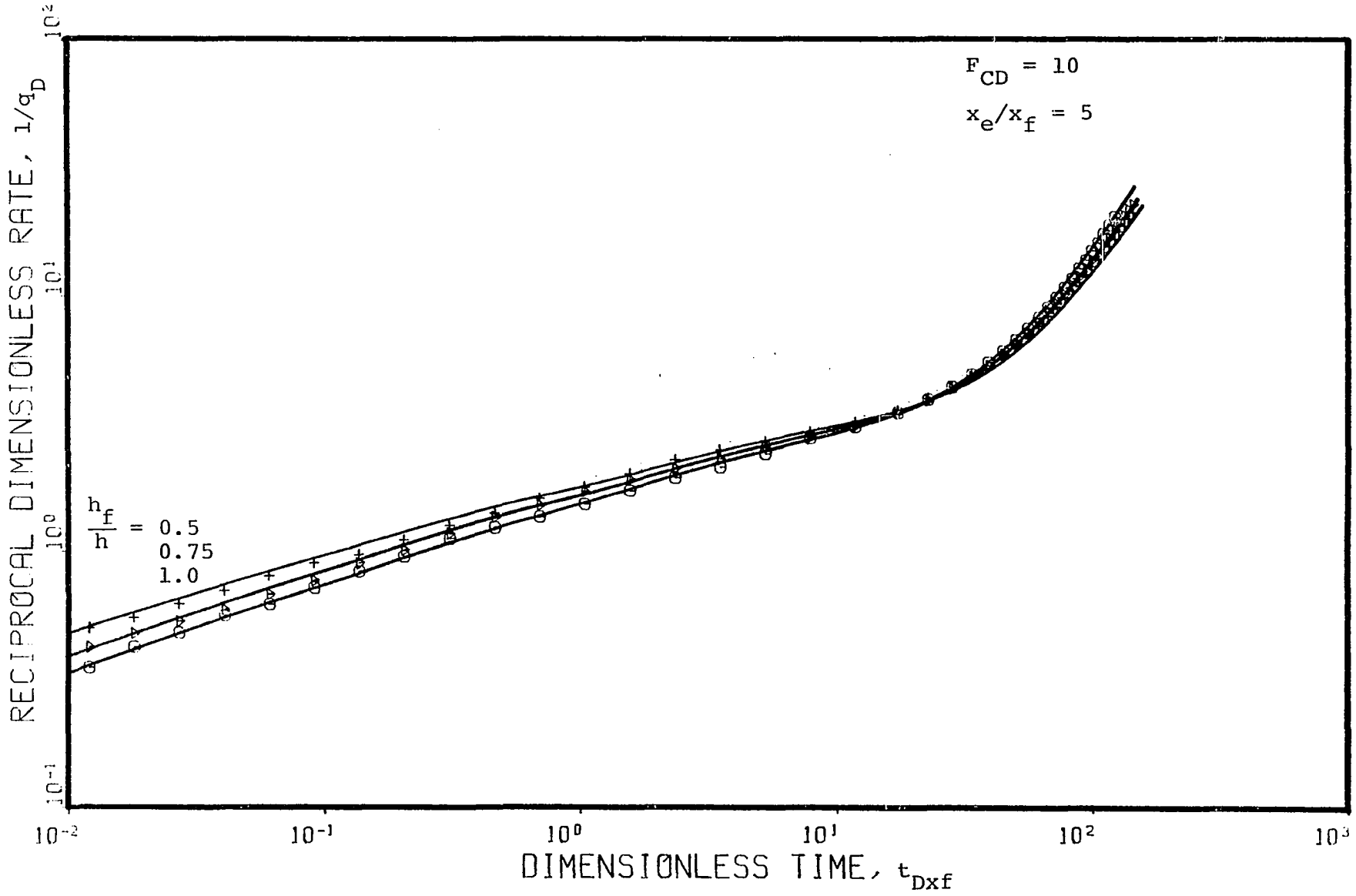


Figure 7.5: Log-log type curves for finite conductivity vertical fracture - effect of boundary.

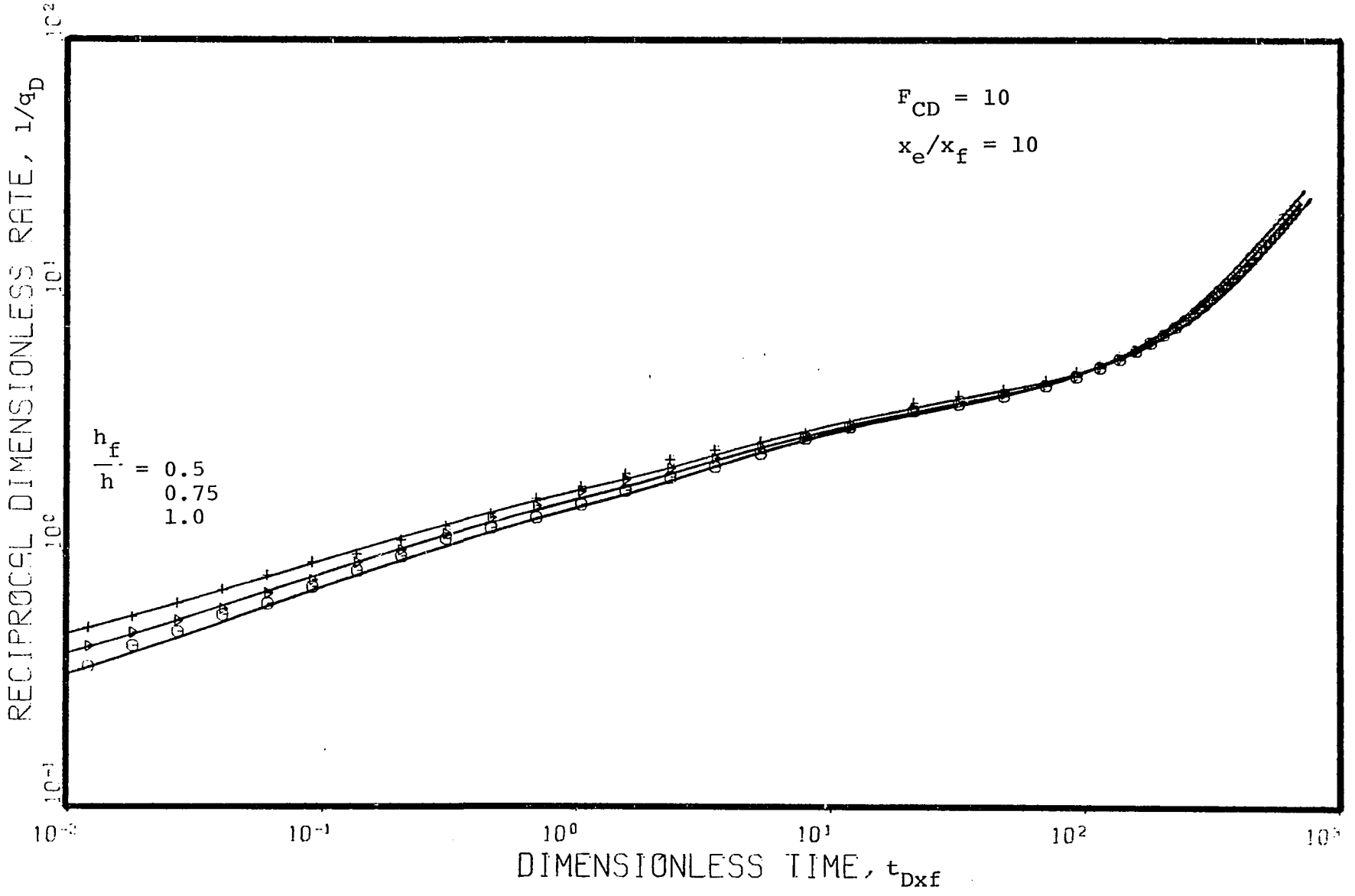


Figure 7.6: Log-log type curve for finite conductivity vertical fracture - effect of boundary

Guppy et al. This parameter takes into account the pseudo-pressure drop as well as the turbulent flow factor. The dimensionless pseudo-pressure drop for turbulence is defined as:

$$m_{DT} = \frac{\pi\beta M k_f k[m(p)_I - m(p)_{wf}]}{RT\mu_I w}$$

and in field units

$$m_{DT} = \frac{10.478 \times 10^{-12} M\beta k_f k[m(p)_I - m(p)_{wf}]}{T\mu_I w}$$

If m_{DT} is very small ($\simeq 0$), the flow in the fracture is laminar. In this case, the pressure drop must be very small. Consequently, the fluid velocity within the fracture is small. When m_{DT} is greater than zero, a non-Darcy flow takes place in the fracture.

In this section, the effect of turbulent flow within a finite conductivity vertical fracture in which the fracture height is less than formation thickness is examined. A quantitative result in terms of dimensionless parameters are obtained using the numerical model.

Figures 7-7 to 7-18 are the graphs of reciprocal dimensionless rate ($1/q_D$) for dimensionless fracture conductivity (F_{CD}) ranges from 1 to 100. In these runs, b is less than unit and m_{DT} varies from 0 to 1. It should

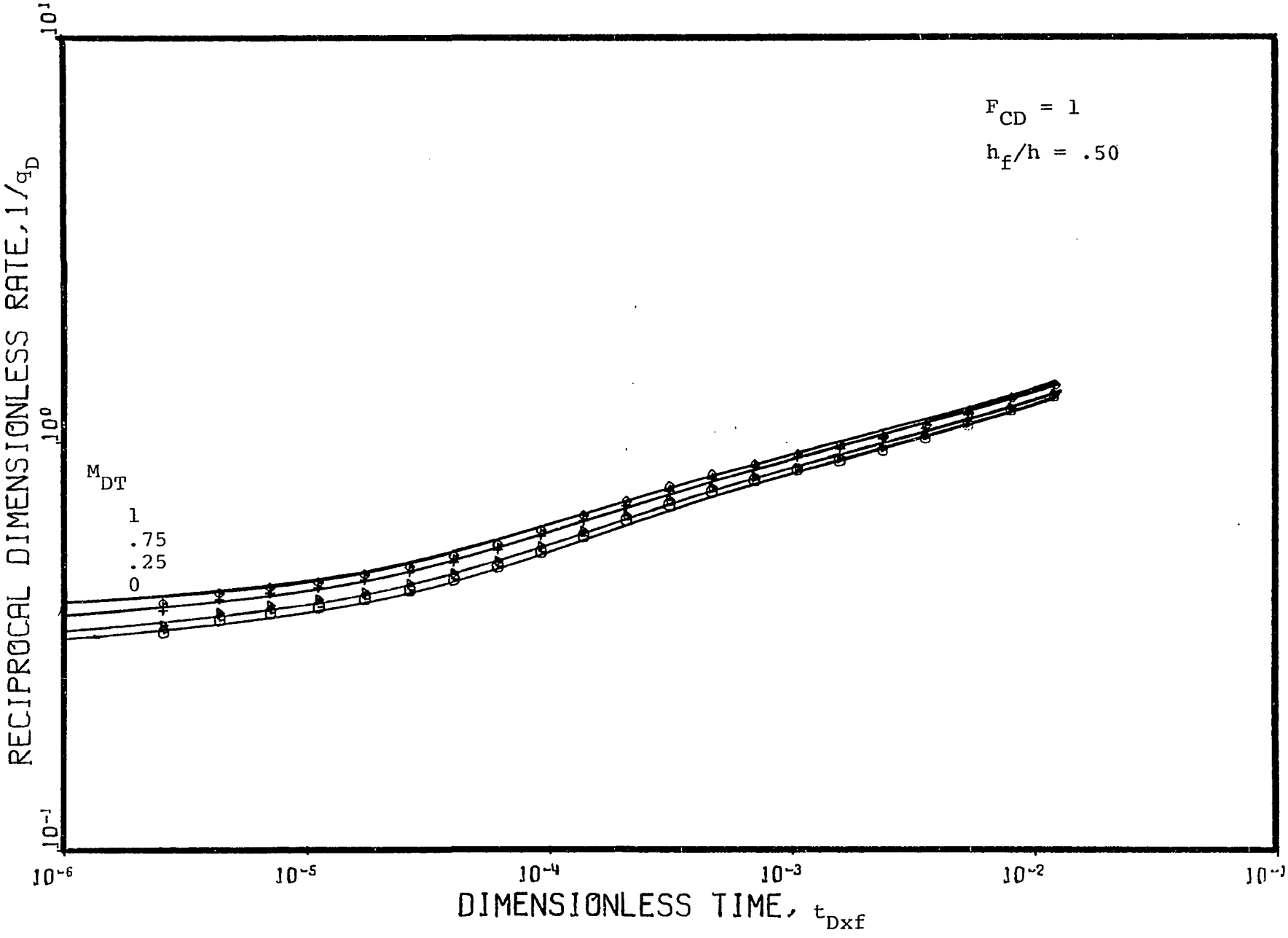


Figure 7.7: Log-log type curve for a vertically fractured well - effect of turbulent flow.

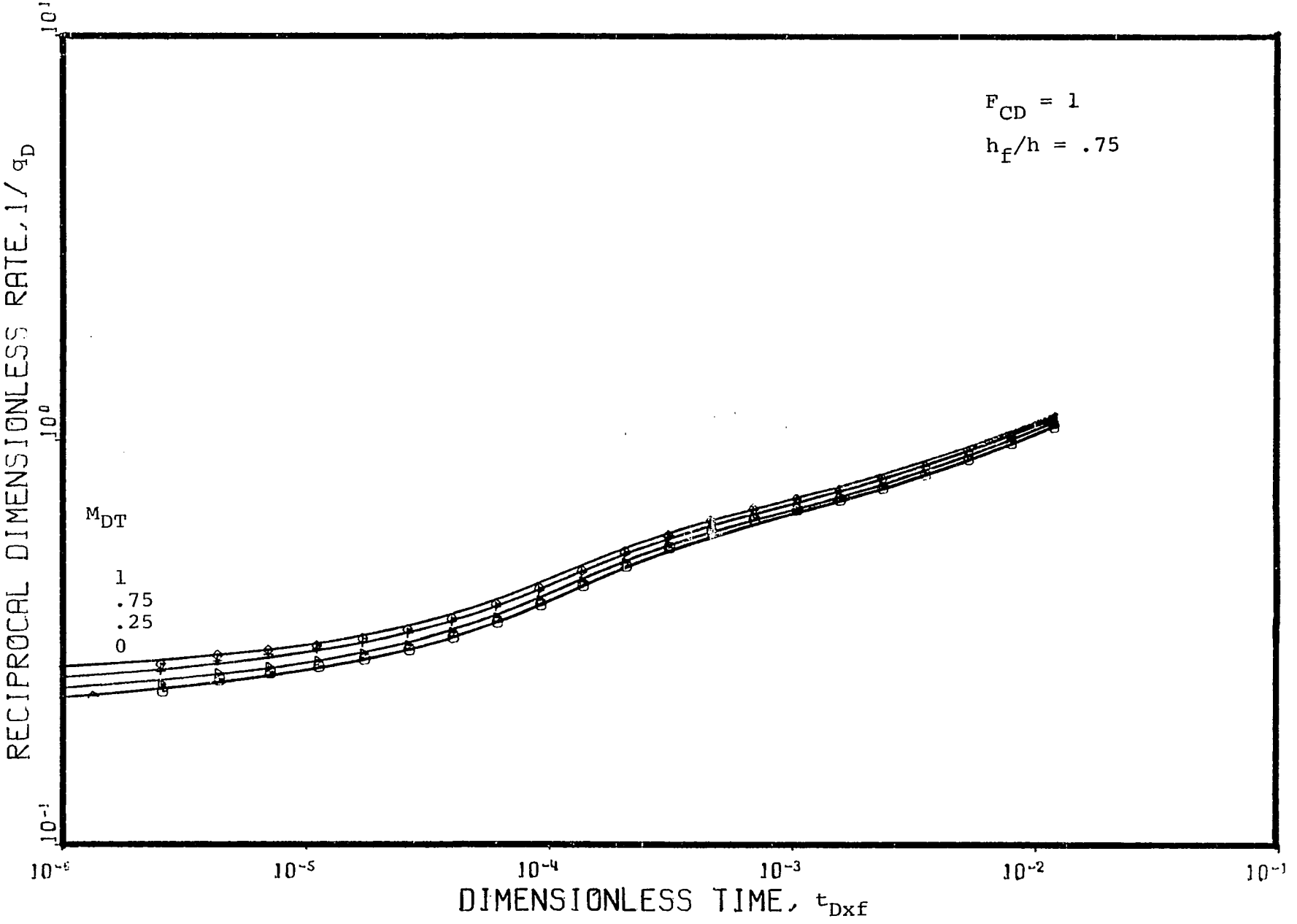


Figure 7.8: Log-log type curve for a vertically fractured well - effect of turbulent flow

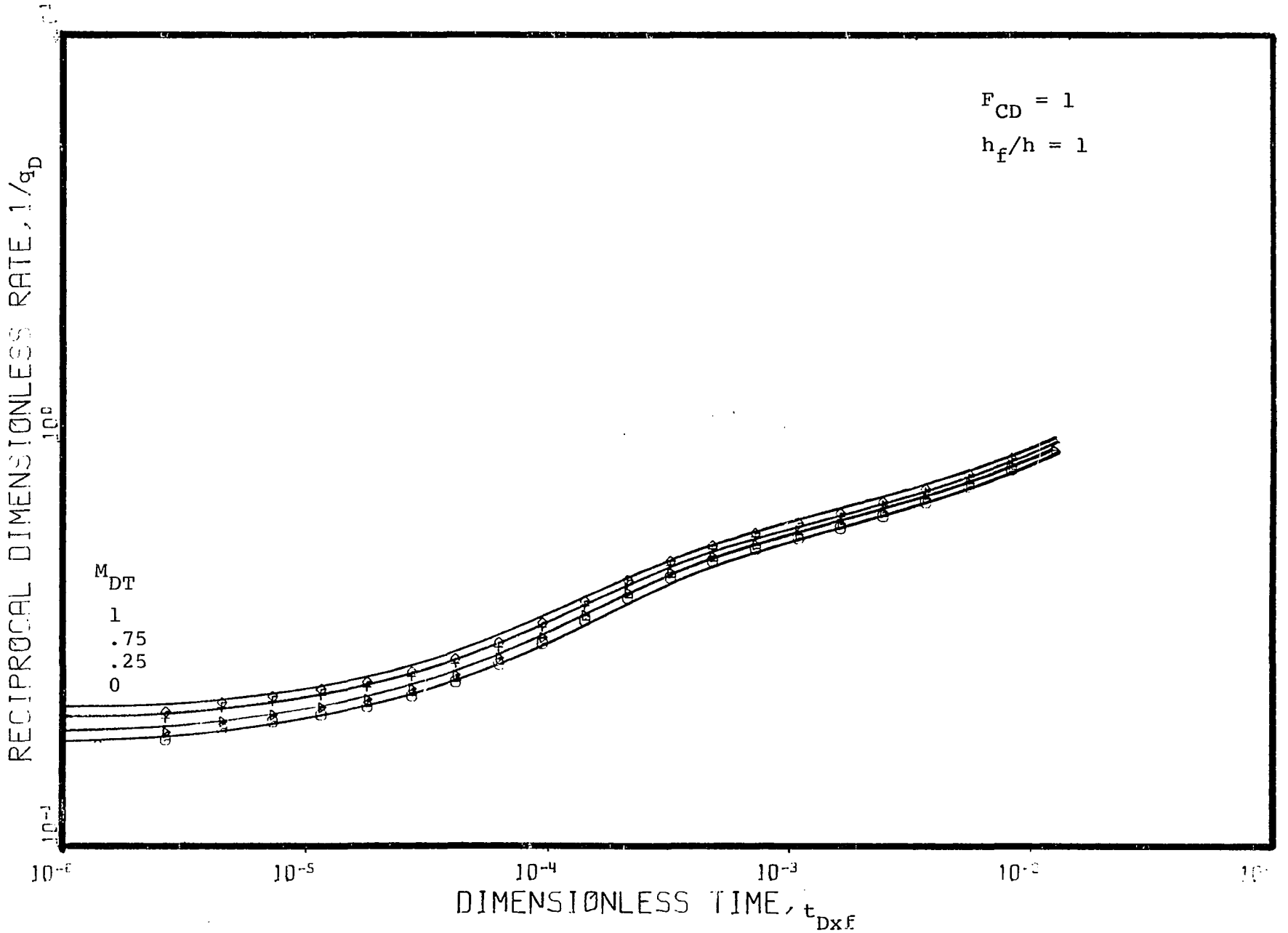


Figure 7.9: Log-log type curves for a v ertically fractured well - effect of turbulent flow.

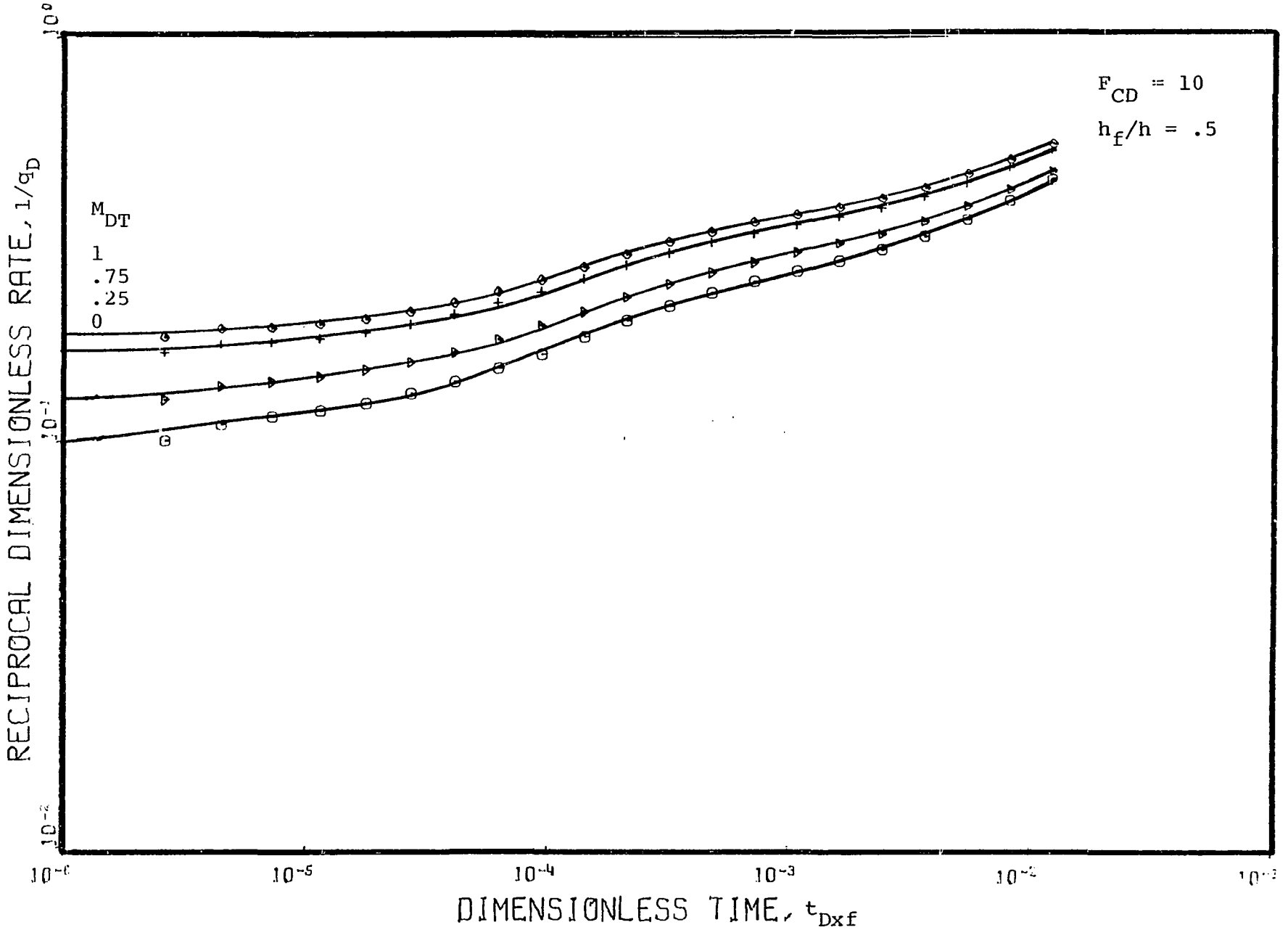


Figure 7.10: Log-log type c urve for a vertically fractured well - effect of turbulent flow.

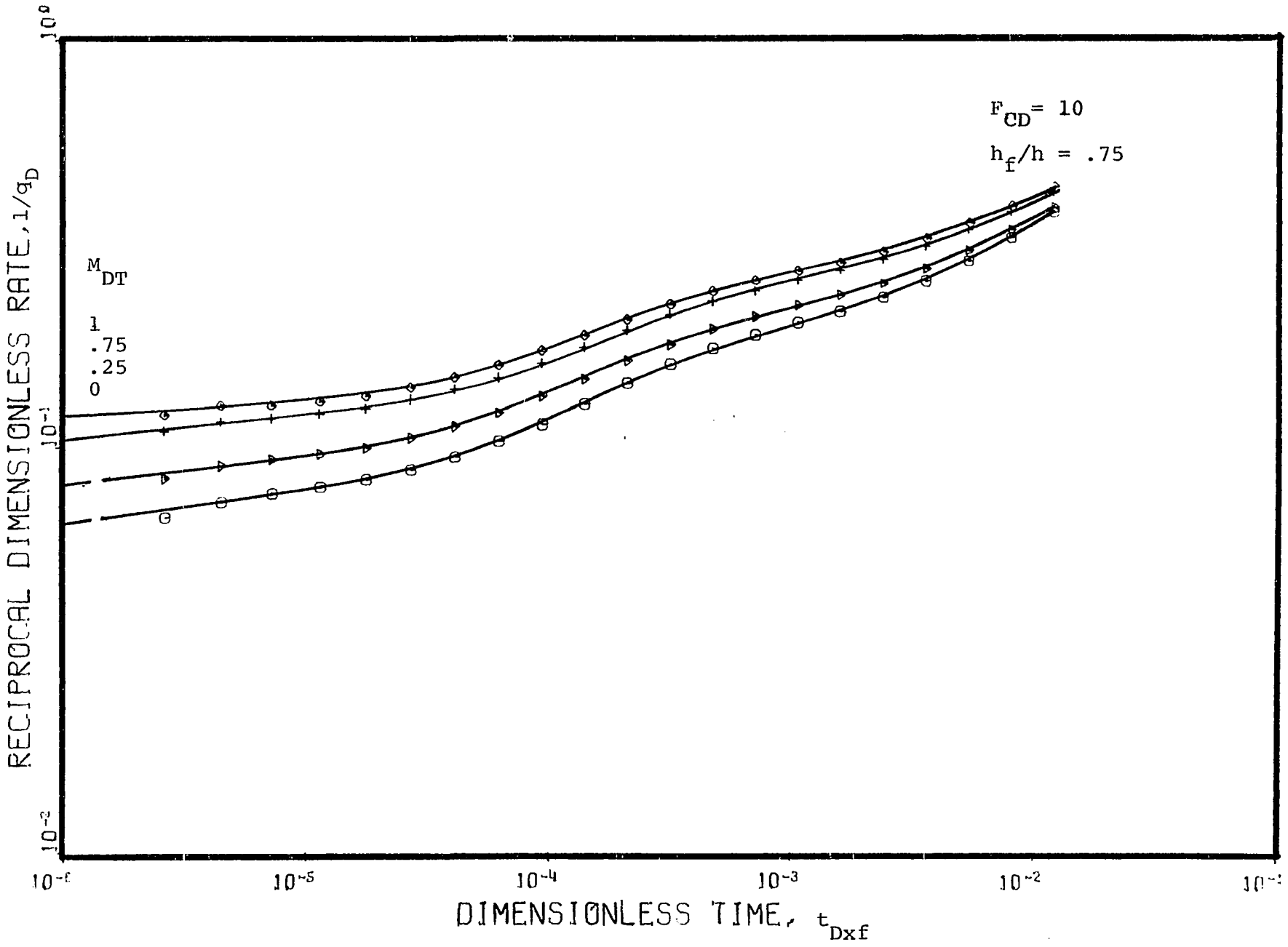


Figure 7.11: Log-log type curve for a vertically fractured well - effect of turbulent flow.

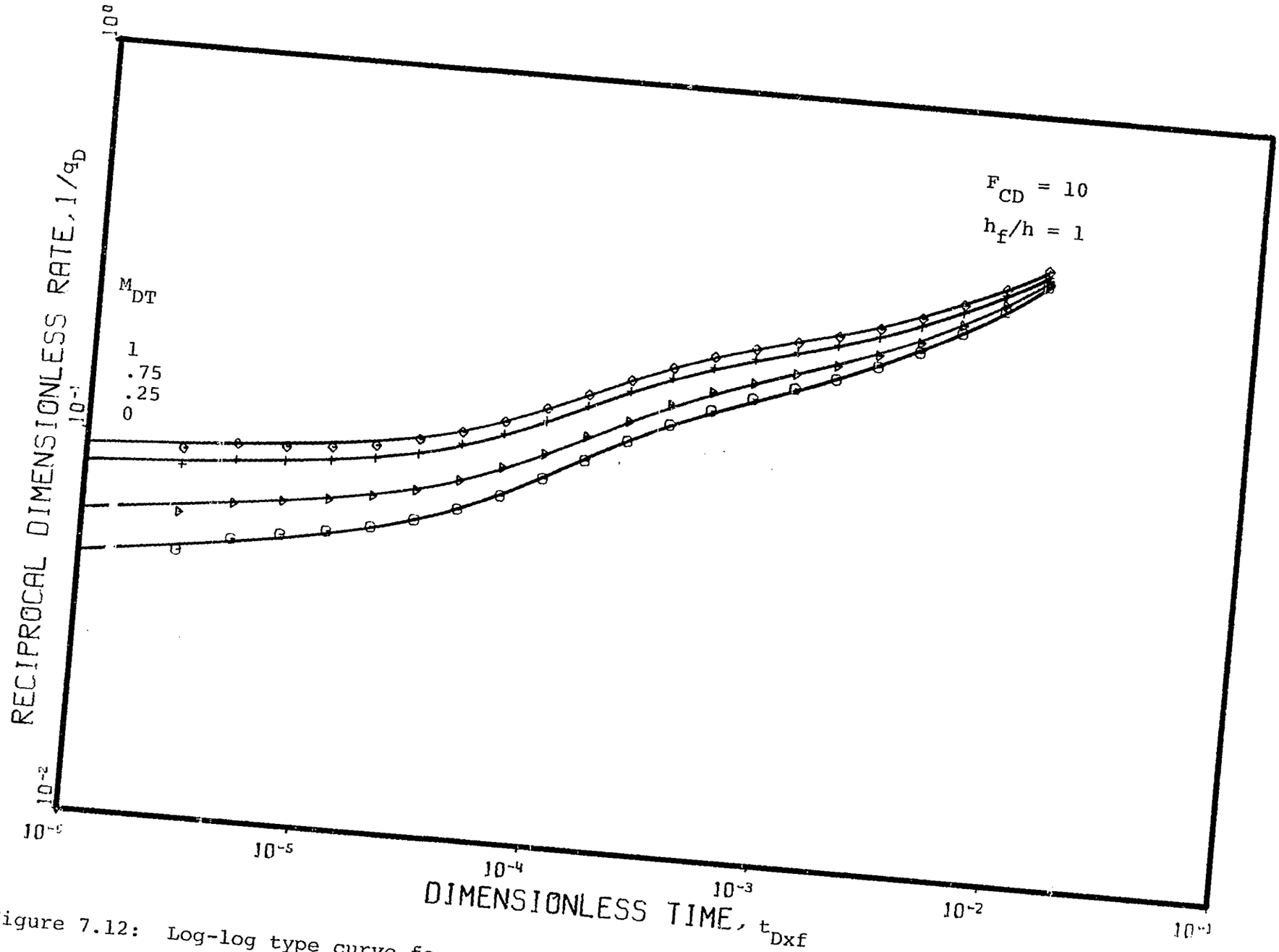


Figure 7.12: Log-log type curve for a vertically fractured well - effect of turbulent flow.

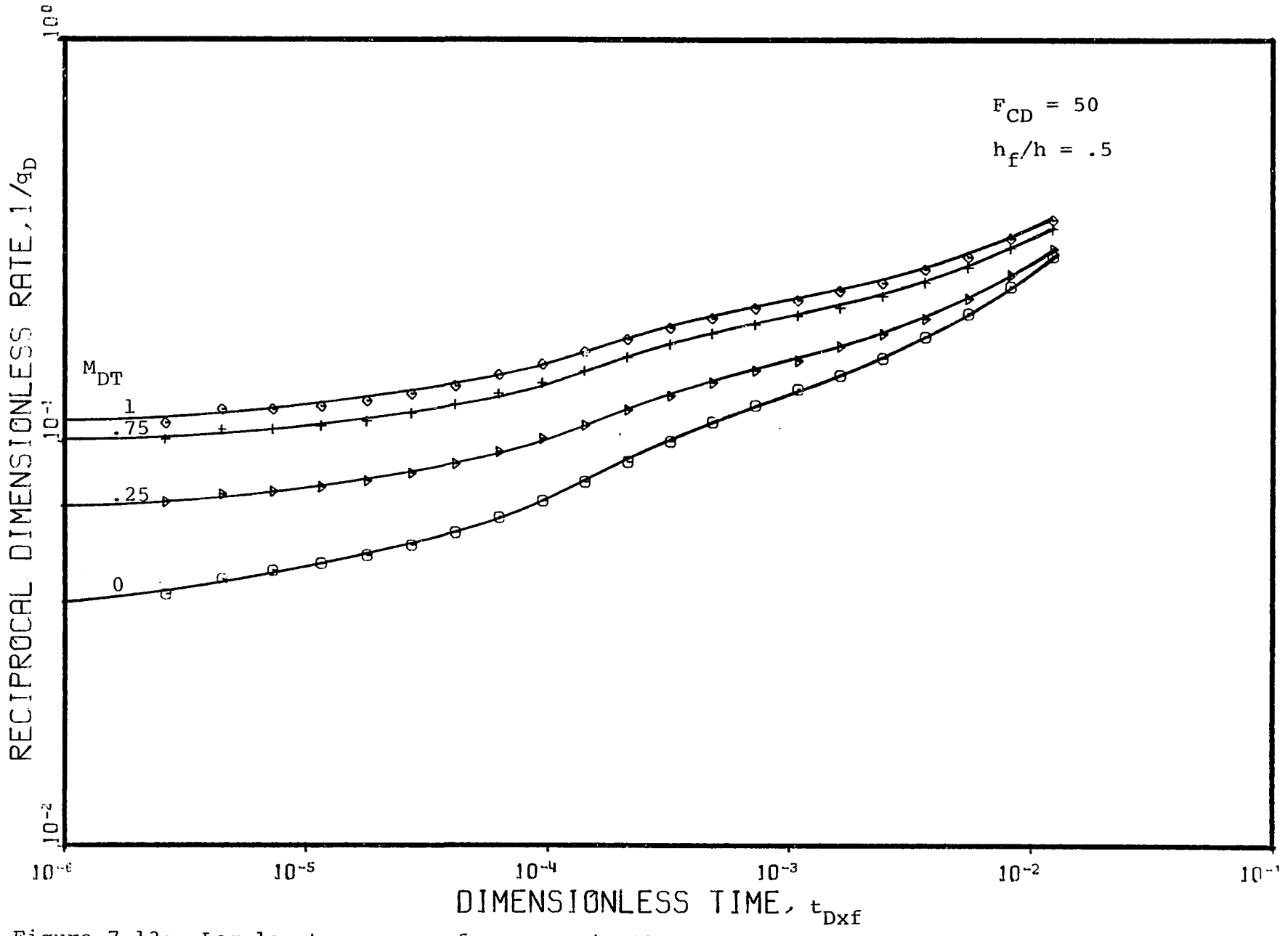


Figure 7.13: Log-log type curve for a vertically fractured well - effect of turbulent flow

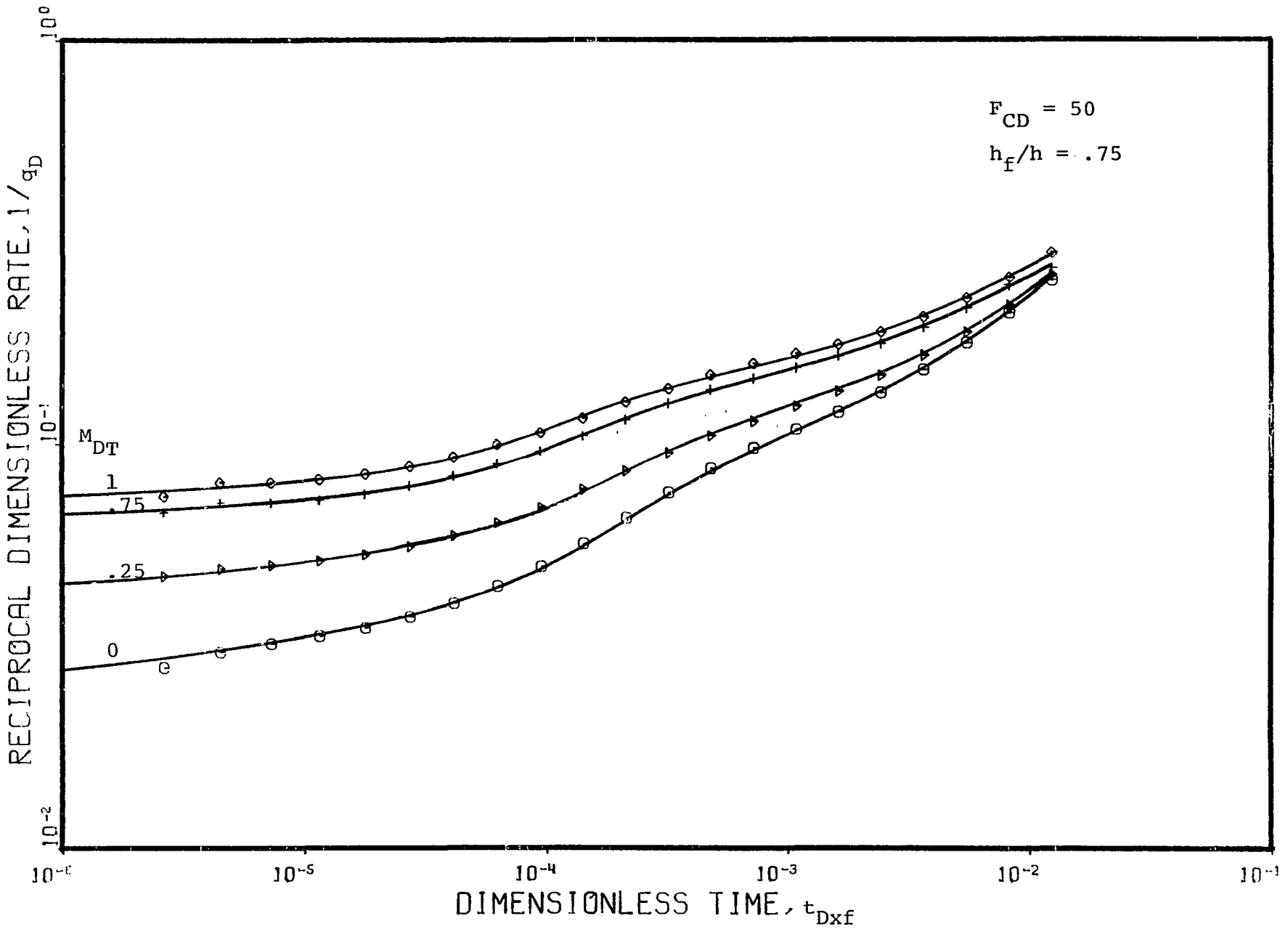


Figure 7.14: Log-log type curve for a vertically fractured well - effect of turbulent flow

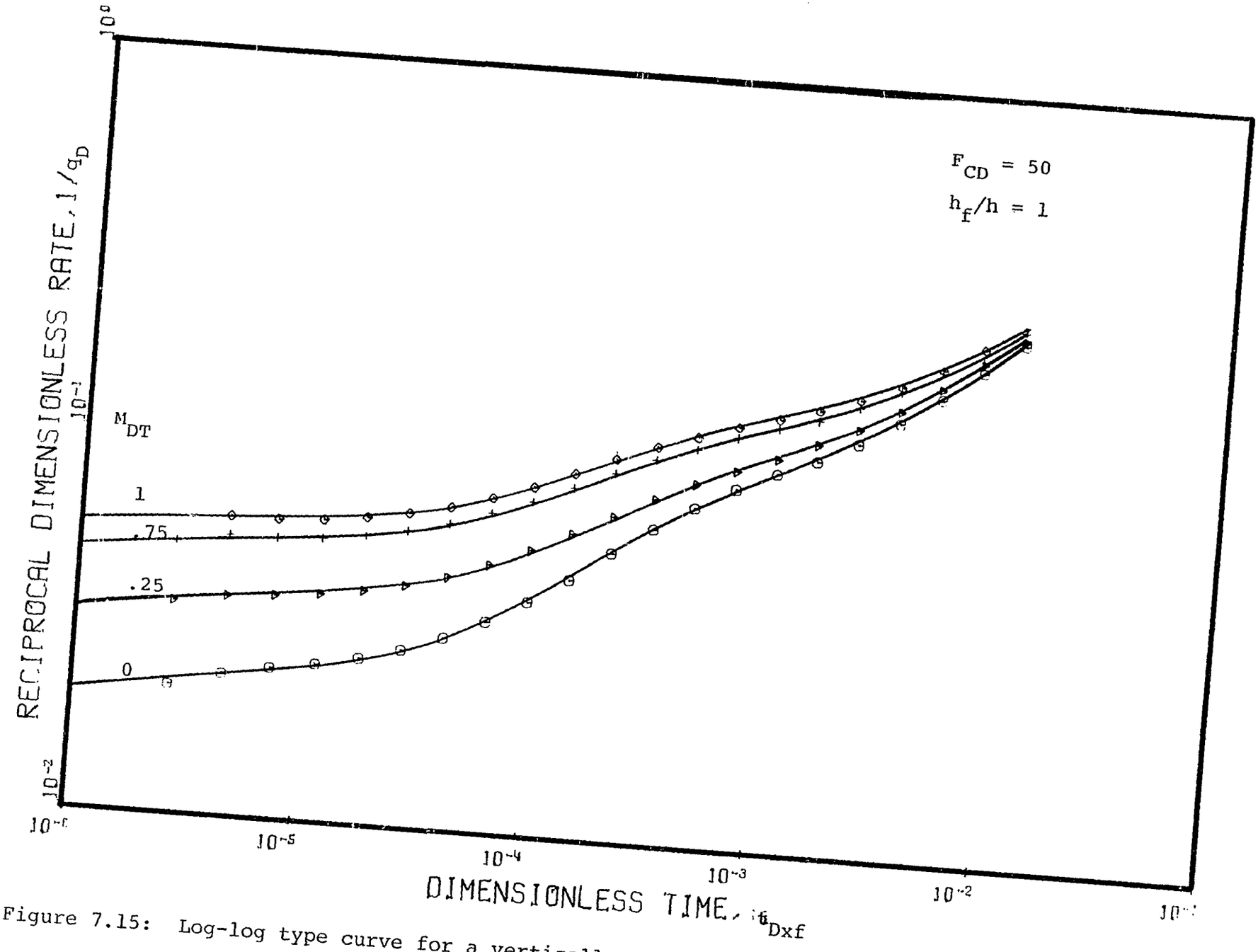


Figure 7.15: Log-log type curve for a vertically fractured well - effect of turbulent flow.

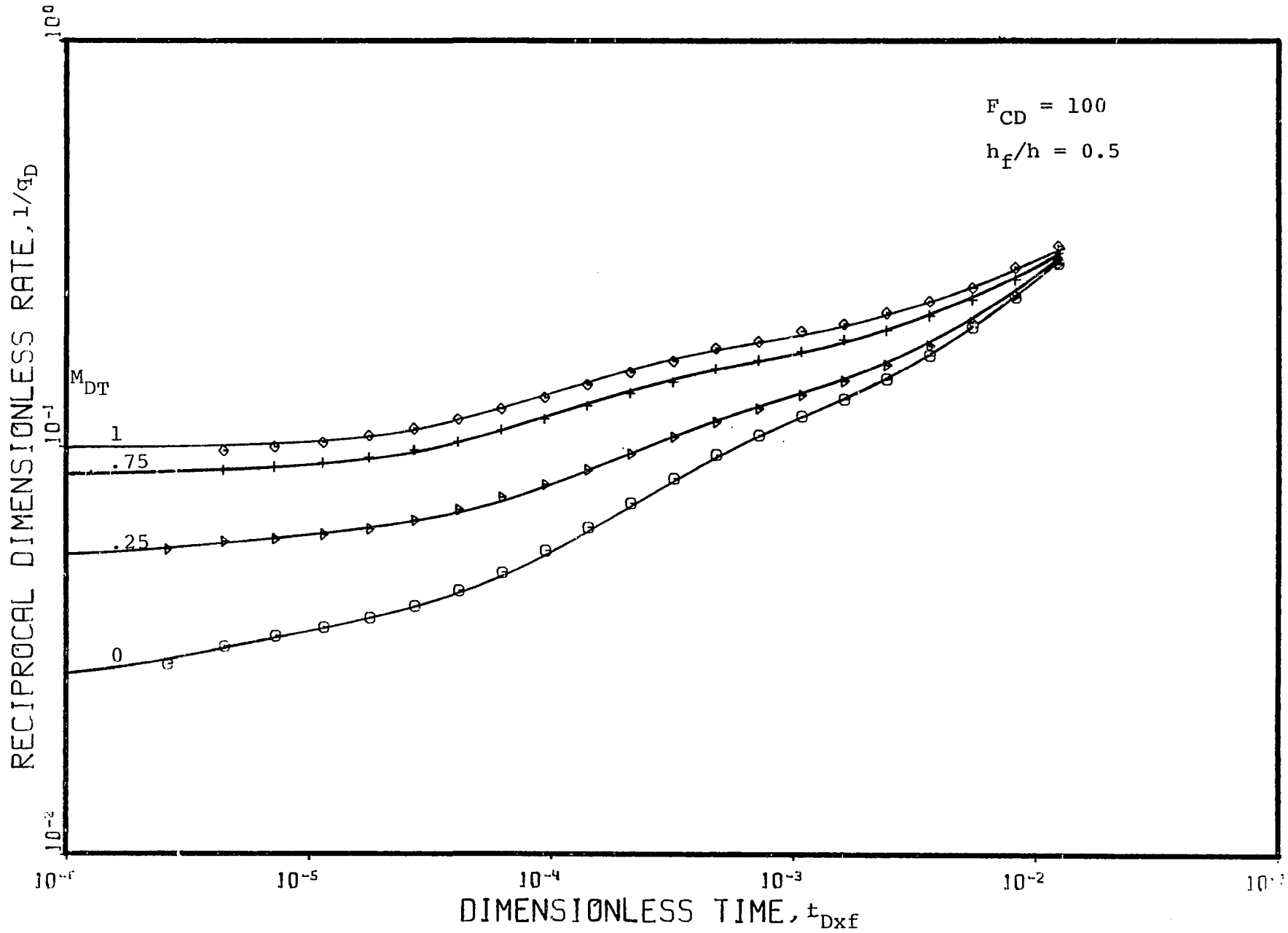


Figure 7.16: Log-log type curve for a vertically fractured well - effect of turbulent flow

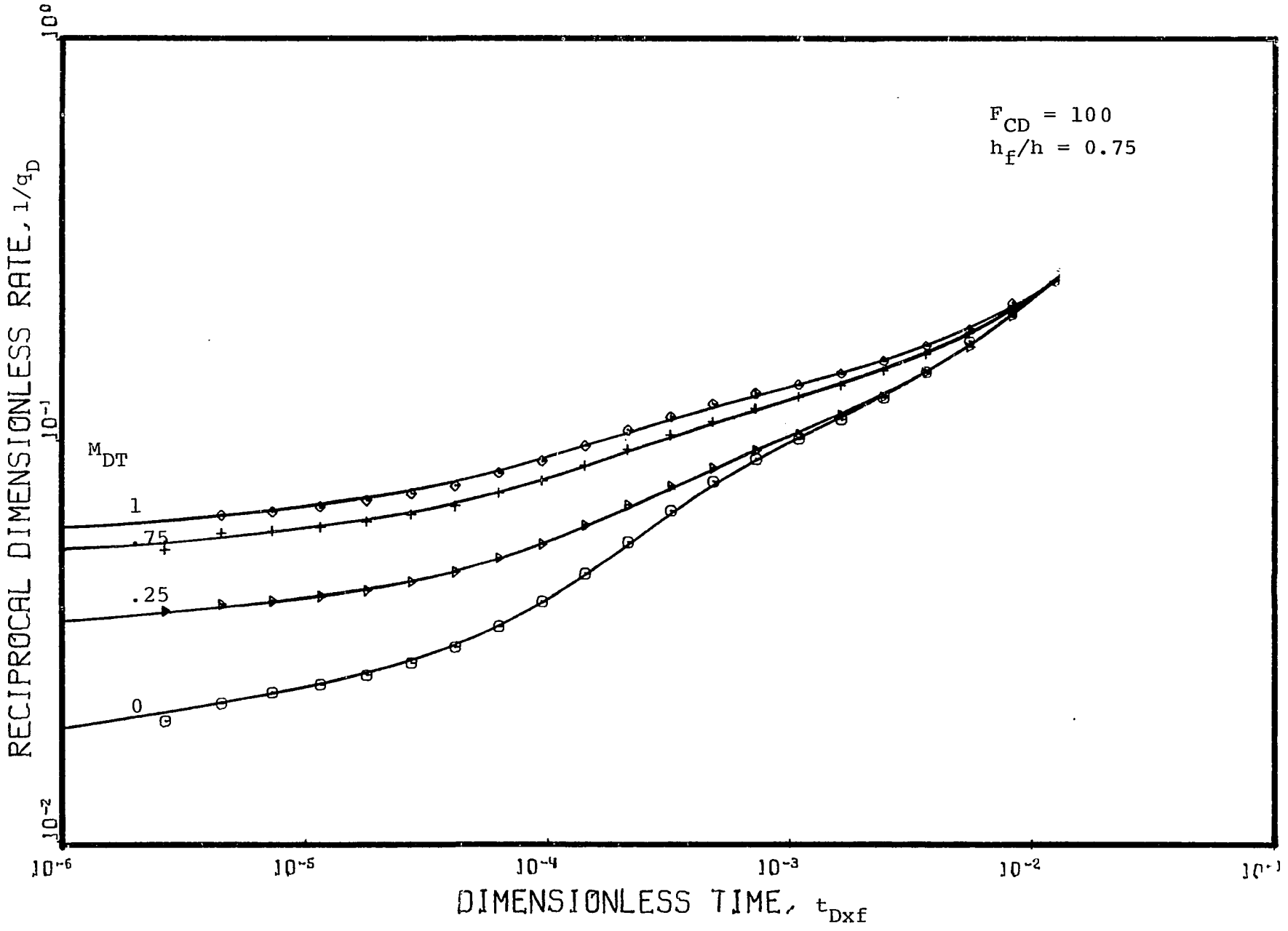


Figure 7.17: Log-log type curve for a vertically fractured well - effect of turbulent flow.

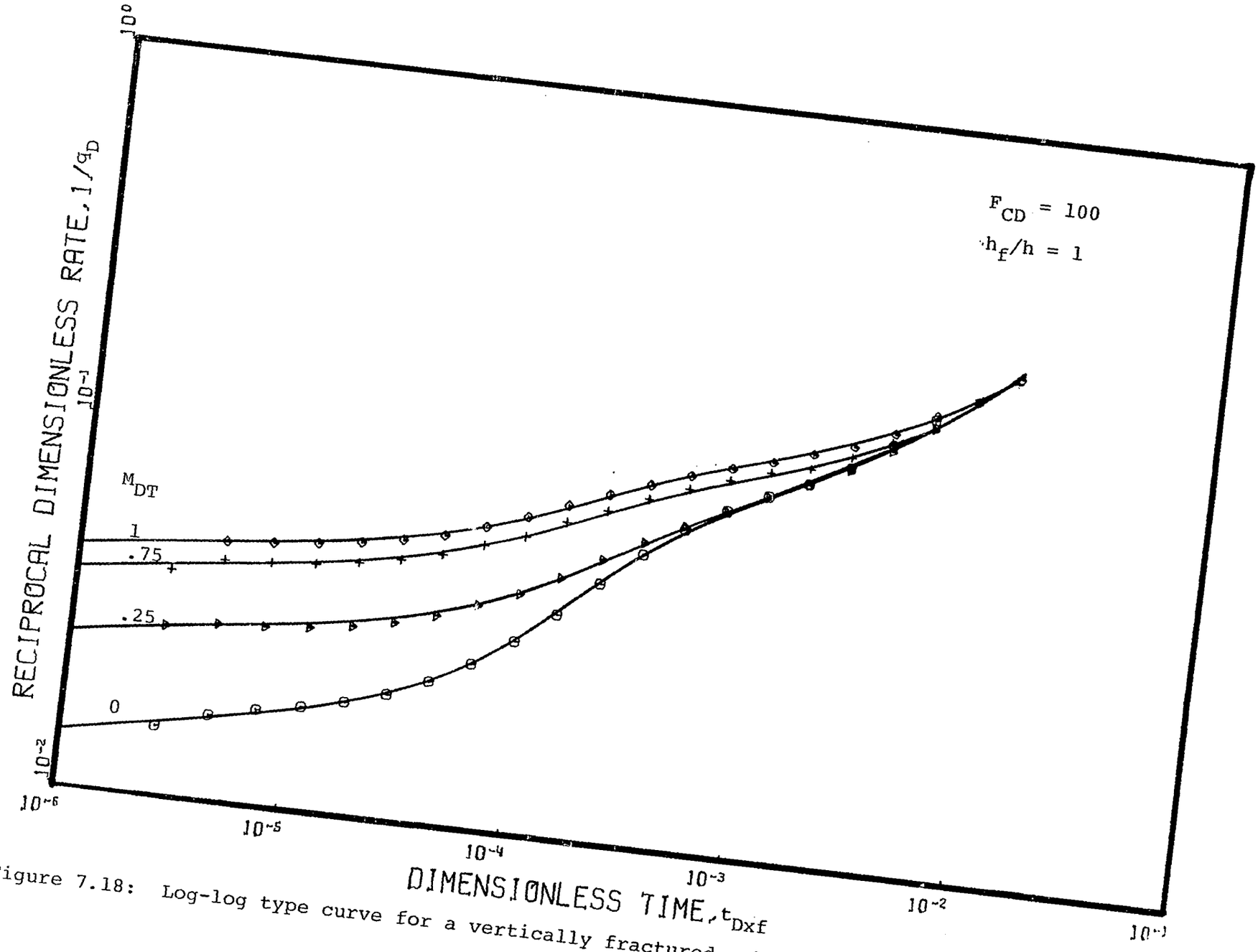


Figure 7.18: Log-log type curve for a vertically fractured well - effect of turbulent flow

be mentioned that for b = 1 and m_{DT} = 0, the results are comparable with type curves. When m_{DT} > 0, a significant reduction in the flow rate is obtained for any value of fracture conductivity. This non-Darcy flow effect is clearly noticeable at the early time data. Low and moderate fracture conductivities (F_{CD} from 1 to 10) showed relatively small turbulent effect when m_{DT} is greater than zero. On the other hand, high fracture conductivities yield a more significant turbulent effect for any value of b. This can be seen in Figures 7-16 to 7-18 at early time. Basically, a high conductivity fracture has a high fracture permeability which causes a very high fluid velocity. Since the turbulent effect depends on fluid velocity, it becomes more significant in the case of a high conductivity fracture.

As is evident from all results, when m_{DT} > 0, the fracture with non-Darcy flow effect behaves as if it had lower conductivity.

7.3 Closure Pressure Effect

The closure pressure is defined as the difference between bottom-hole treating pressure and the average pressure in the fracture. The closure pressure has a significant effect on the productivity of a fractured well and should be considered. As the fractured well starts production, the average pressure in the reservoir and fracture decreases. Thus, the closure pressure increases with time

causing crushing of the proppant, and therefore, the fracture flow capacity is reduced significantly. As a result of that, the fracture permeability decreases with time.

The model considers the effect of changing closure pressure as well as the effect of fracture height and turbulent flow. The closure pressure is determined at each cell in the fracture. Laboratory data for fracture conductivity versus closure pressure and proppant concentration for different proppants are used to calculate a new fracture permeability at each time step.

Using data of Table 7.1, computer run was made to study the effect of closure pressure when $b < 1$ in computing actual fracture flow capacity.

Figure 7-19 presents the results of this run. As can be seen, there is a significant reduction in the flow rate with time when the closure pressure effect is included. In this particular example, since the purpose is to study the effect of closure pressure, the flow in the fracture is assumed to be Laminar. This will eliminate the non-Darcy flow effect. In addition, the fracture height to the formation height ratio is 0.75 for both runs (with closure and without closure pressure effect). Thus, one may be able to justify that the reduction in the well productivity is caused by the closure pressure effect only as shown in Figure 7-19.

Table 7-1

Reservoir and Fluid Property Data

effective permeability, md	0.5
formation porosity	0.1
initial reservoir pressure, psi	5000
bottom-hole treating pressure, psi	6000
bottom-hole flowing pressure, psi	2500
bottom hole temperature, ^{o}F	250
well spacing, acres	160
wellbore radius, ft	0.5
gas gravity	0.65
gas viscosity, cps	0.021
fracture length, ft	1320
fracture flow capacity, md-ft	19800
proppant concentration, lb/1000 ft^2	1500
net pay, ft	40
fracture height, ft	30

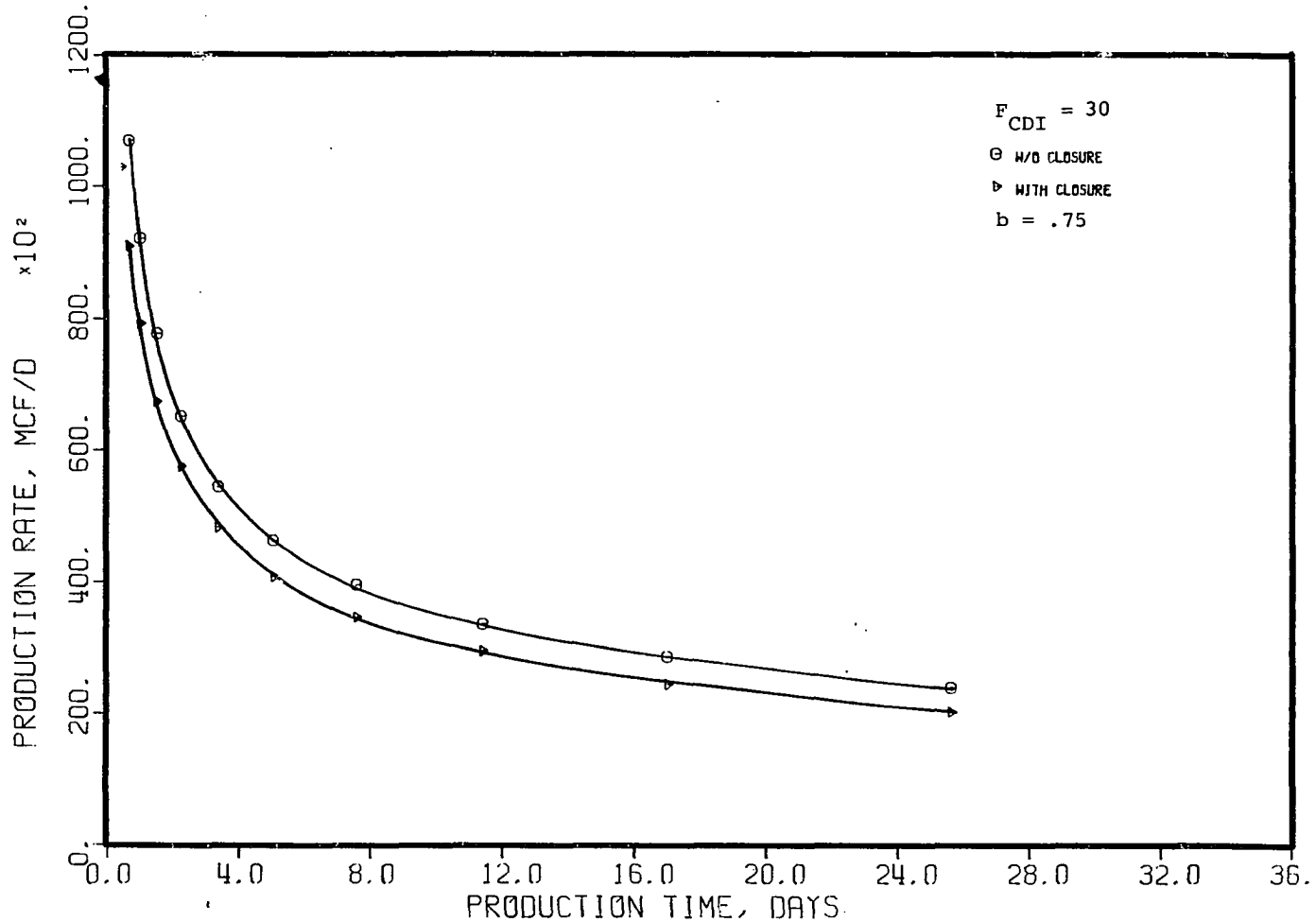


Figure 7.19: Predicted performance of a vertically fractured well - closure pressure effect

7.4 Layered Formations

The stratified formation is the most common type of heterogeneous reservoir. The hydraulic properties of porous media in them vary from one layer to another. Although the study of fluid behavior of multi-layered reservoirs is important, it becomes more complicated when the well is intercepted by a finitely conductive fracture.

A rather simple case is that of two layers in bounded reservoir. The interface boundary conditions between layers could be either with cross flow or without cross flow. In the first case, the only connection between layers occurs at the well and via the fracture. For the second boundary condition, there is a cross flow throughout the interface as well as the fracture. Each layer is homogeneous. In addition, the initial reservoir pressure is the same for the two layer system.

Many papers[47-55] have dealt with layered reservoirs with or without cross flow for unfractured formations. So far, no numerical studies of layered media in fractured system have been presented. Therefore, another objective of this work is to present the numerical results of layered formation in the fractured reservoirs.

Some of the dimensionless variables will be used throughout this discussion for convenience. These variables are defined as:

Dimensionless time

$$t_{Dxf} = \frac{.000264\ \bar{k}t}{\bar{\phi}\mu\ Cg\ X_f^2}$$

Dimensionless rate

$$q_D = \frac{1424\ qT}{\bar{k}\bar{h}\ \Delta m(p)}$$

Dimensionless fracture conductivity

$$F_{cD} = \frac{(wk)_f}{\bar{k}\ X_f}$$

where

$$\bar{h} = h_1 + h_2$$

$$\bar{k} = \frac{k_1h_1 + k_2h_2}{\bar{h}}$$

$$\bar{\phi} = \frac{\phi_1h_1 + \phi_2h_2}{\bar{h}}$$

Figure 7-20 is the plot of reciprocal dimensionless time, $1/q_D$, versus the dimensionless time, t_{Dxf}, on logarithmetic scale for h_1/h_2 of one and dimensionless fracture conductivity of F_{CD} of ten. The permeability ratio k_1/k_2 is the parameter of interest in this graph.

Figure 7-20 shows that for the early time period,

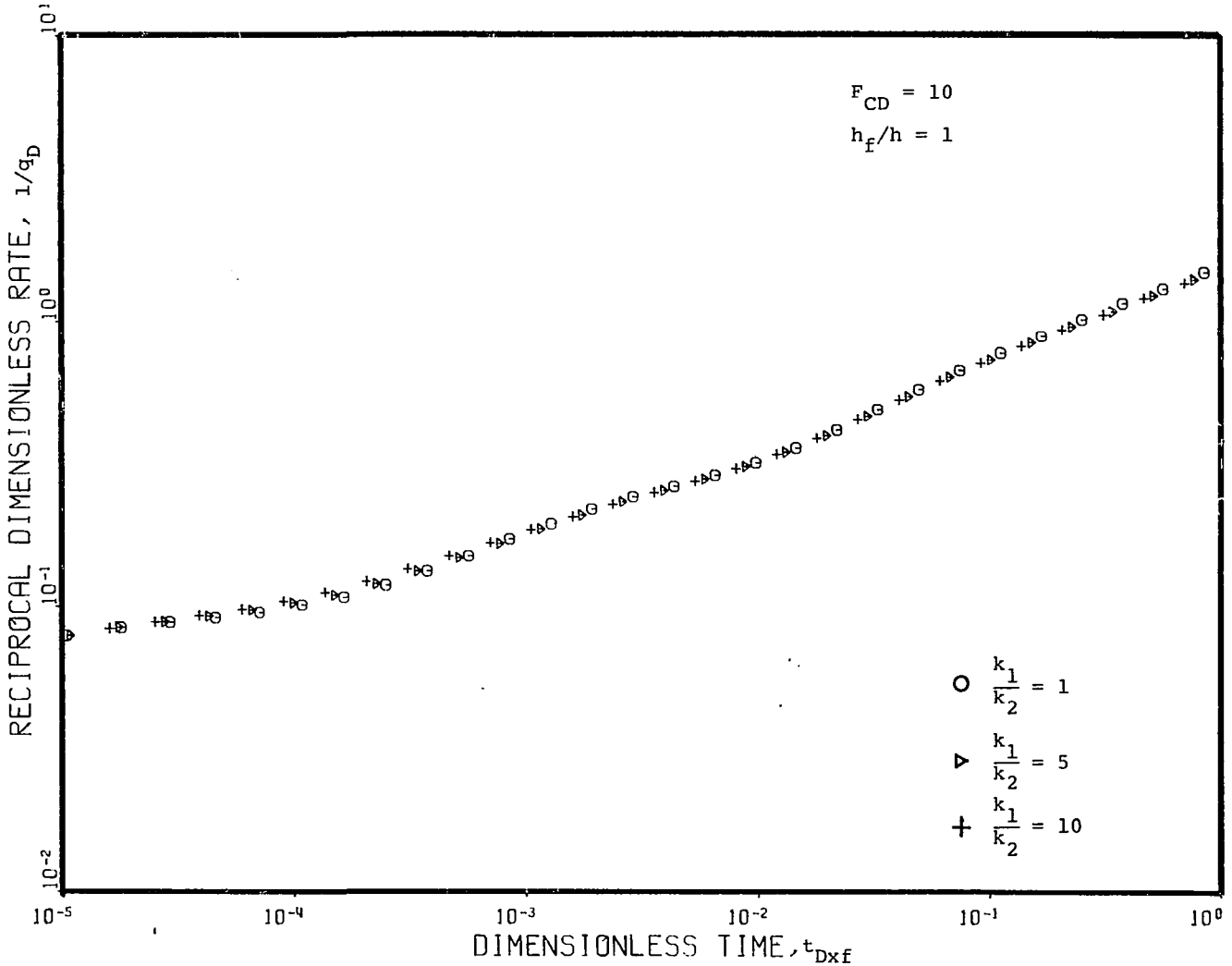


Figure 7.20: Type curves for layered formation with cross flow - using average parameters ($\overline{kh}$).

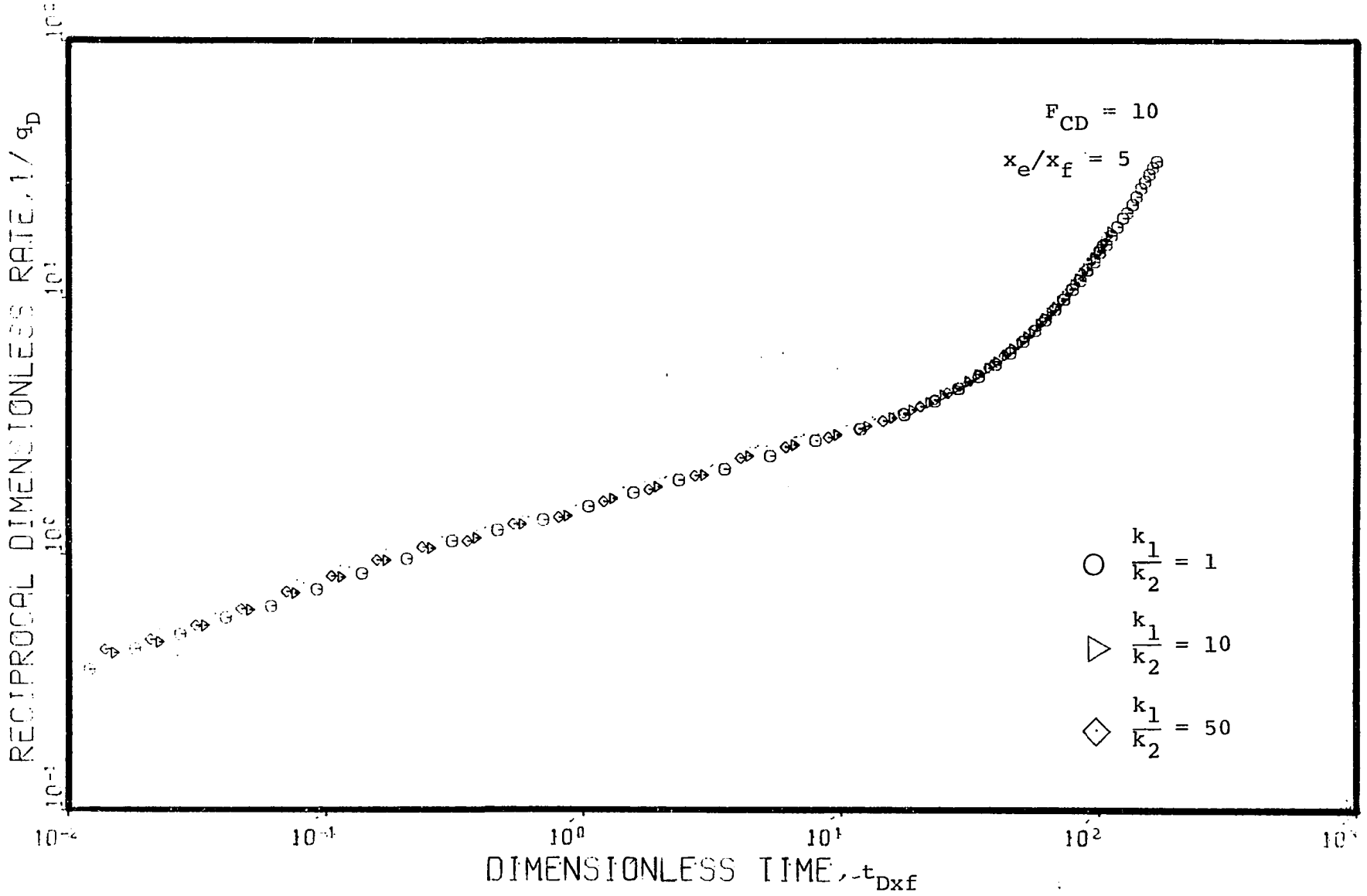


Figure 7.21: Type curve for layered formation - boundary effect.

permeability ratios at 1, 5 and 10 follow one curve. This indicates that the layered system behaves as an equivalent homogemeous system with average parameters, $\bar{\phi}$, $\bar{h}$, and $\bar{k}$. It also indicates that at the early time period, the flow behavior is independent of the permeability ratio for specific values of dimensionless fracture conductivity. It should be mentioned that this behavior was noticeable for all runs over a wide range of fracture conductivities.

Figure 7-21 presents the numerical results of the long time solution for a two layer system. This graph is for F_{cD} of 10 and x_e/x_f of 5. The permeability ratio k_1/k_2 is varied from 1 to 50. The late time data indicate the effect of boundary which is expected since the reservoir is assumed to be bounded. The late time solution also indicates that the fractured layered system behaves exactly as an equivalent homogeneous system. Similar results can be obtained for different values of dimensionless fracture conductivity and x_e/x_f.

On Figures 7-20 and 7-21 the effect of heterogeneity formation is shown for fractured system. Both the early and late time solutions yield the same results. The interesting observation is that the performance of a two-layer fractured reservoir with crossflow can be obtained by that of a single-layer reservoir. The equivalent single layer reservoir must have the same pore volume, wellhead and bottom hole conditions. In addition, the equivalent system must have

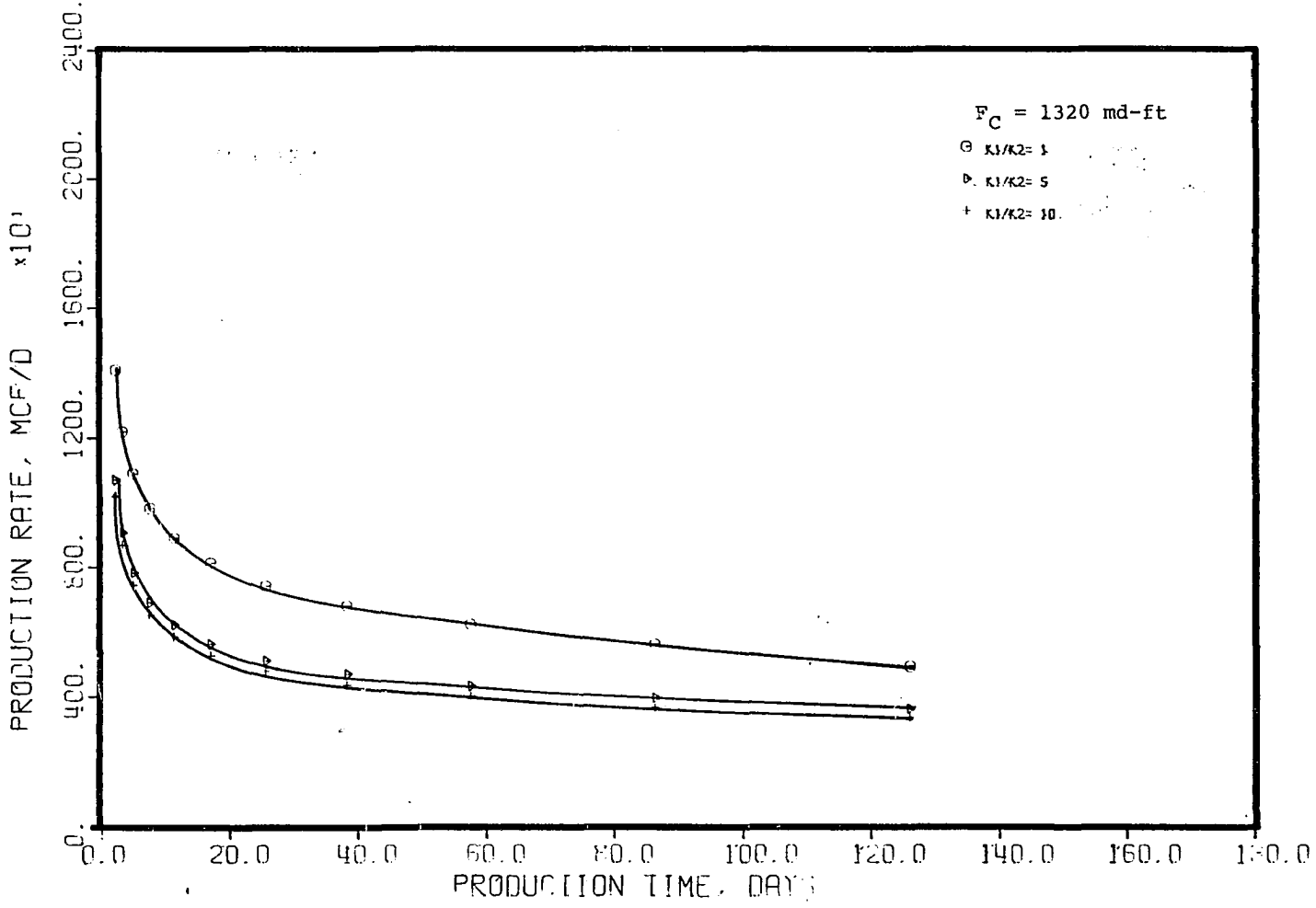


Figure 7.22: Effect of reservoir heterogenity on the production rate - with crossflow.

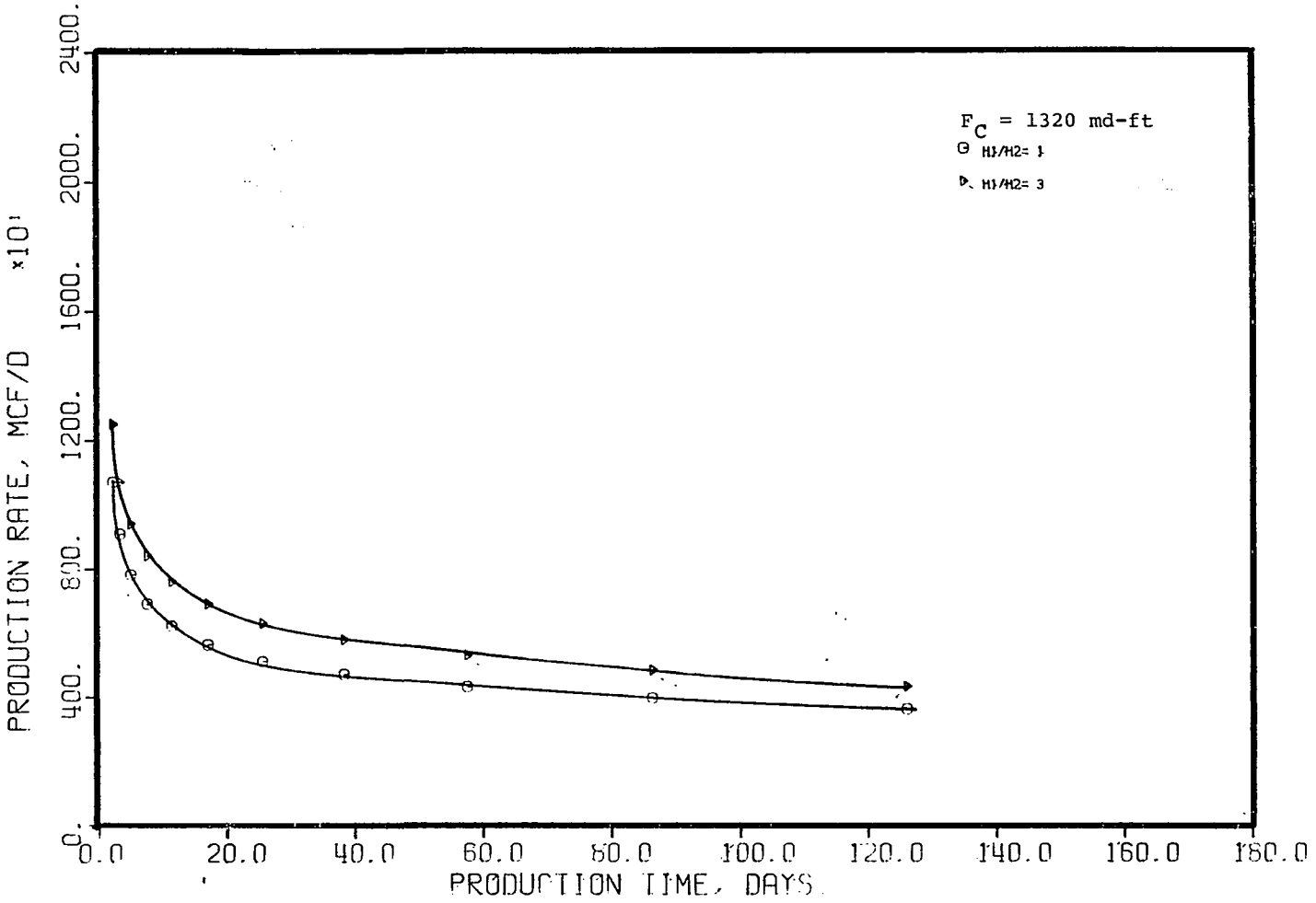


Figure 7.23: Effect of thickness ratio on the production rate - with crossflow

F_{cD}, $\bar{k}$, $\bar{\phi}$ and $\bar{h}$.

On Figure 7-22 the effect of the ratio k_1/k_2 on the actual well performance is shown. The flow rate is plotted versus production time for crossflow case. The permeability in one zone is decreased and the remaining parameters are held constant. As it can be seen on Figure 7-22 with increasing k_1/k_2 ratio the production rate is reduced significantly. This implies that with decreasing the permeability in one zone, the production rate is decreased.

The effect of varying the ratio h_1/h_2 for a particular set of parameters is shown on Figure 7-23. The permeability ratio is 1 and fracture flow capacity is held constant. The ratio of h_1/h_2 is changed while the total thickness remained constant. A higher flow rate at early time is obtained with increasing h_1/h_2 ratio as shown in Figure 7-23. The same results can be obtained for different permeability ratios. It should be mentioned that the communican between the layers is not that significant factor because there is a connection at the fracture faces.

Example output is presented in Appendix D.

CHAPTER VIII

CONCLUSIONS

In summary, the main objective of this study is to present the numerical results of the three-dimensional model for a fractured gas well. The behavior of a vertically fractured well is examined when the fracture height is less than the formation thickness for both one and two layers. For a single layer, the effects of non-Darcy flow and closure pressure as well as fracture heights are considered. For a two-layer system, the ratio of fracture height to formation thickness is assumed to be 1 and the flow in the fracture is laminar. The parameters of interest were the permeability ratio and the thickness ratio of the two layers.

Most of the results are presented in the general form of dimensionless variables. The following specific conclusions are based on this work.

1. A numerically stable three-dimensional simulator for a vertically fractured well with finite conductivity is developed.

2. A family of type curves for a well intercepting a vertical fracture with finite conductivity and producing at constant bottom hole flowing pressure is presented. The parameter of interest here is the ratio of fracture height to the formation height.
3. The effect of combining turbulent flow and fracture height on the performance of a vertically fractured well with finite conductivity is investigated. A set of type curves is presented.
4. Closure pressure stress decreases the productivity of fractured well significantly in case of high production rates.
5. For all times, the behavior of two layers in the fracture system is similar to the single layer when the average parameters ($\bar{k}$, $\bar{h}$, $\bar{\phi}$) are used.
6. The productivity of fractured well is decreased with increasing the permeability ratio k_1/k_2 in stratified system with crossflow.
7. Actual production rate of hydraulically fractured well increases with increasing the ratio of heights h_1/h_2 in heterogeneous reservoirs.
8. Quantitative analysis of well performance considering fracture height and type of flow can be obtained using type curves presented in this

study in conjunction with other available type curves.

NOMENCLATURE

C	transmissibility coefficient
C_g	gas compressibility
E	Young's modules of the materials
h	formation thickness
F_c	fracture conductivity
k	formation permeability
L	length
M	molecular weight
m(p)	pseudo-pressure function
m	abbreviation for pseudo-pressure function
P	pressure
q	flow rate
R	gas constant (10.73)
RHS	right hand side
T	temperature
t	time
w	fracture width
x	direction - x
y	direction - y
z	direction - z

Z	gas deviation factor
ν	velocity
ϕ	porosity
μ	viscosity
ρ	density
ϑ	turbulent factor
β	beta factor
Δ	change

Additional Subscripts

D	dimensionless
DT	dimensionless turbulence
e	boundary
f	fracture
I	reservoir conditions
i	cells in y-direction
j	cells in x-direction
ℓ	cells in z-direction
SC	standard conditions
n	old time step
n+1	new time step
w_f	wellbore conditions

REFERENCES

1. Clark, J. B.: "A Hydraulic Process for Increasing the Production of Wells," Trans., AIME 186 (1949), pp. 1-8.

2. Prats, M.: "Effect of Vertical Fractures on Reservoir Behavior - Incompressible Fluid Case," Soc. Pet. Eng. J., (June 1961), pp. 105-118.

3. Van Pollen, H. K., Tinsley, J. M., and Saunders, C. D.: "Hydraulic Fracturing: Fracture Flow Capacity vs. Well Productivity," Trans., AIME (1958), Vol. 213, p. 91.

4. Muskat, M.: Flow of Homogeneous Fluids Through Porous Media, McGraw-Hill Book Co., Inc., New York, (1937), p. 409.

5. Prats, M., Hazebrock, P., and Strickler, W. R.: "Effect of Vertical Fractures on Reservoir Behavior - Compressible Fluid Case," Soc. Pet. Eng. J., (June 1962), pp. 87-94.

6. Van Everdingen, A. F., and Meyer, F. J.: "Analysis of Buildup Curves Obtained After Well Treatment," J. Pet. Tech., (April 1971), pp. 513-524.

7. Gringarten, A. C., Ramey, H. J., and Raghavan, R.: "Unsteady-State Pressure Distributions Created By a Well With a Single Infinite Conductivity Vertical Fracture," Soc. Pet. Eng. J., (August 1974), pp. 347-359.

8. Newman, A. B., "Heating and Cooling Rectangular and Cylindrical Solids," Ind. and Eng. Chem., (1936), Vol. 28, p. 545.

9. Gringarten, A. C., and Ramey, H. J., Jr.: "The Use of Source and Green's Function in Solving Unsteady Flow Problems in Reservoirs," Soc. Pet. Eng. J., (Oct. 1973), pp. 285-296.

10. Ramye, H. J., Jr.: "Short Time Well Test Data Interpretation in the Prescence of Skin Effect and Wellbore Storage," J. Pet. Tech., (Jan. 1970), pp. 97-104.

11. Agarwal, Ram. G., Carter, R. D., and Pollock, C. B.: "Evaluation and Prediction of Performance of Low Permeability Gas Wells Stimulated by Massive Hydraulic Fracturing," SPE 6838, presented at the 52nd Annual Fall Technical Conference, Denver, Colorado, Oct. 9-12, 1977.

12. Cinco, L., Heber, Samaniego, U. F., and Dominiquez, A.N.: "Transient Pressure Behavior for a Well With a Finite Conductivity Vertical Fracture," Soc. Pet. Eng. J., (Aug. 1978).

13. Cinco, L., Heber, and Samaniego, U. F.: "Transient Pressure Analysis for Fractured Wells," SPE 7490, presented at the 53rd Annual Fall Technical Conference, Houston, Tex., Oct. 1-3, 1978.

14. Raghavan, R., Uraiet, A., and Thomas, G. W.: "Vertical Fracture Height - Effect on Transient Flow Behavior," Soc. Pet. Eng. J., (Aug. 1978), pp. 265-277.

15. Deyes, A. B., Kemp, C. L., and Caudle, B. H.: Effect of Fracutres on Sweep-out Pattern," Trans. AIME, Vol. 213, 1958, pp. 245-249.

16. McGuire, W. J., and Sikoura, U. J.: "The Effect of Vertical Fracutres on Well Productivity," Trans. AIME, (1960), 219, pp. 401-403.

17. Scott, J. O.: "The Effect of Vertical Fractures on Transient Pressure Behavior of Wells," J. Pet. Tech., (Dec. 1963), pp. 1365-1369.

18. Tinsley, J.M., Williams, J.R., Tiner, R. L., and Malone, W. T.: "Vertical Fracture Height - Its Effect on Steady-State Production Increase," J. Pet. Tech., (May 1969), pp. 633-638.

19. Ming-Lung Mao: "Performance of Vertically-Fractured Wells With Finite-Conductivity Fractures A dissertation submitted to the Department of Petroleum Engineering, School of Earth Science, Stanford University.

20. Raymond, L. R., and Binder, G. G., Jr.: "Productivity of Wells in Vertically Fractured, Damaged Formations," J. Pet. Tech., (Jan. 1967), pp. 120-130.

21. Russell, D. G., and Truitt, N. L.: "Transient Pressure Behavior in Vertically Fractured Reservoirs," J. Pet. Tech., (Oct. 1964), pp. 1159-1170.

22. Clark, K. K.: "Transient Pressure Testing of Fractured Water Injection Wells," J. Pet. Tech., (June 1968), pp. 639-643.

23. Wattenbarger, R. A., and Ramey, H. J.: Vertically Fractured Gas Wells," J. Pet. Tech., (May 1969), pp. 625-632.

24. Morse, R. A., and Von Gonten, W. D.: "Productivity of Vertically Fractured Wells Prior to Stabilized Flow," J. Pet. Tech., (July 1972), pp. 807-811.

25. Locke, C. D., and Sawyer, W. K.: "Constant Pressure Injection Test in a Fractured Reservoir - History Match Using Numerical Simulation and Type Curve Analysis," Paper SPE 5594, presented at the SPE-AIME 50th Annual Fall Technical Conference, Dallas, Texas., Oct. 1975.

26. Sawyer, W. K., Locke, C. D., Overbry, W. R., Jr.: "Simulation of a Finite Capacity Vertical Fracture in a Gas Reservoir," Paper SPE 4593, presented at the SPE-AIME 48th Annual Meeting, Las Vegas, Oct. 1973.

27. Narasimhan, T. N., and Polen, W. A.: "A Purely Numerical Approach for Analyzing Fluid Flow to a Well Intercepting A Vertical Fracture," SPE 7983, presented at the California Regional Meeting on April 20, 1979.

28. Howard, G. D., and Fast, C. R.: "Hydraulic Fracturing," Soc. Pet. Eng. J.,, Monograph Series, SPE (1970).

29. Hubbert, M. K., and Willis, D. G.: "Mechanics of Hydraulic Fracturing," Trans, AIME (1957), pp. 210, 153-166.

30. Deaneshy, A. A.: "Hydraulic Fracture Propagation in Layered Formation," Paper SPE 6088, was presented at the 51st Annual Fall Meeting of SPE in New Orleans.

31. Senddon, I. N.: "The Distribution of Stress in the Neighborhood of a Crack in an Infinite Solid," Proc. Roy. Soc. London, Series A, (Oct.-Dec. 1946), p. 187.

32. Perkins, T. K., and Kern, L. R.: "Widths of Hydraulic Fractures," J. Pet. Tech., (Sept. 1961), pp. 937-949.

33. Al-Husseiny, R., Ramey, H. J., and Crawford, P. B.: "The Flow of Real Gases Through Porous Media," J. Pet. Tech., (May 1966), p. 624.

34. Katz, D. L., Cornell, D., Kobayshi, R., Poettmann, F. H., Vary, J. A., Elenbaas, J. R., and Weinaug, C. F.: "Handbook of Natural Gas Engineering," McGraw-Hill Book, Co., Inc., New York, (1959).

35. Corneel, D., and Katz, D. L.: "Flow of Gases Through Porous Media," Ind. Eng. Chem., (1953), 43, 2145.

36. Cooke, C. L., Jr.: "Conductivity of Fracutre Proppants in Multiple Layers," J. Pet. Tech., (Sept. 1973), pp. 1101-1108; Trans., AIME, p. 255.

37. Wattenbarger, R.A., and Ramey, H. J., Jr.: "Well Test Interpretation of Vertically Fractured Gas Wells," J. Pet. Tech.,, (May 1969), pp. 625-632, Trans., AIME, p. 246.

38. Holditch, S. A., and Morse, R. A.: "The Effects of Non-Darcy Flow on the Behavior of Hydraulically Fractured Gas Wells," J. Pet. Tech., (Oct. 1976), pp. 1169-1179.

39. Guppy, K. H., Cinco, H., and Ramey, H. J.: "Effect of Non-Darcy Flow on the Constant Pressure Production of Fractured Wells," SPE paper presented at the 55th Annual Fall Technical Meeting of the SPE of AIME, Dallas, Tex., Sept. 21-24, 1980.

40. Guppy, K. H.: "Non-Darcy Flow in Wells With a Finite Conductivity Vertical Fracture," Ph.D. Dissertation, Stanford University, June, 1980.

41. "Fracturing Theory," Halliburton Services Book.

42. Bruce, G. A., Peaceman, D. W., and Rachford, H. H., and Rice, J. D.: "Calculations of Unsteady-State Gas Flow Through Porous Media," Trans., AIME, (1953), pp. 198, 79.

43. Todd, M. R., O'Dell, P. M., and Hirasaki, G. J.: "Methods for Increased Accuracy in Numerical Reservoir Simulators," Soc. Pet. Eng. J., (Dec. 1972), pp. 515-530.

44. Gustauson, F. G.: "Some Basic Techniques for Solving Sparse Systems of Linear Equations," Sparse Matrices and Their Applications, Plenum Press, New York, (1972), pp. 41-52.

45. Gustauson, F. G., Liniger, W. M., and Willoughly, R. A.: "Symbolic Generation of an Optimal Crent Algorithm for Sparse Systems of Linear Equations," J. Assoc. Comput., March 17, (1970), pp. 87-109.

46. Price, H. S., and Coats, K. H.: "Direct Methods in Reservoir Simulation," Paper 4278, 34th SPE Symposium on Numerical Simulation of Reservoir Performance, Houston, Texas (January, 1973).

47. Lefkovits, H. C., Hazebroek, P., Allen, E. E., and Matthews, C. S.: "A Study of the Behavior of Bounded Reservoirs Composed of Stratified Layers," Soc. Pet. Eng. J. (March, 1961): 43-58, Trans. AIME, 222.

48. Russell, D. G., and Prats, M.: "Performance of Layered Reservoirs with Crossflow - Single - Compressible - Fluid Case," Soc. Pet. Eng. J. (March, 1962): 53-67.

49. Katz, M. L., and Rasin, Tek, M.: "A Theoretical Study of Pressure Distribution and Fluid Flux in Bounded Stratified Porous Systems with Crossflow," Soc. Pet. Eng. J. (March, 1962): 68-82.

50. Russell, D. G. and Prats, M.: "The Practical Aspects of Interlayer Crossflow," J. Pet. Tech. (June, 1962): 589-594.

51 Kazemi, Hossein and Seth, Mohan S.: "Effect of Anisotropy and Stratification on Pressure Transient Analysis of Wells with Restricted Flow Entry," J. Pet. Tech. (May, 1969): 639-647.

52. Woods, E. G.: "Pulse-Test Response of a Two-Zone Reservoir," Soc. Pet. Eng. J. (Sept., 1970): 245-256; Trans. AIME, 249.

53. Cobb, William M., Ramey, H. J., Jr., and Miller, Frank G.: "Well-Test Analysis for Wells Producing Commingled Zones," J. Pet. Tech. (Jan., 1972): 27-30; Trans., AIME, 253.

54. Raghavan, R., Topalogly, H. N., Cobb, W. M., and Ramey, H. J., Jr.: "Well-Test Analysis for Wells Producing from Two Commingled Zones of Unequal Thickness," J. Pet. Tech. (Sept., 1974): 1035-1043; Trans., AIME, 257.

55. Earlougher, Robert C., Jr., Kersch, K. M., and Kunzman, W. J.: "Some Characteristics of Pressure Buildup Behavior in Bounded Multiple-Layer Reservoirs Without Crossflow," J. Pet. Tech. (Oct. 1974): 1178-1186; Trans., AIME, 257.

APPENDIX A

APPENDIX A

MATHEMATICAL FORMULATION

The equation governing the single-phase flow of a fluid through a porous medium can be developed by combining:

1. Conservation of Mass,
2. Darcy's flow equation, and
3. Equation of State.

Consider an element of a reservoir through which a single-phase fluid is flowing in one direction (x-direction), Figure A-1,

$$\text{Mass Flow In} = (\rho v)_x \, \Delta y \Delta z$$

$$\text{Mass Flow Out} = (\phi \rho)_{x+\Delta x} \, \Delta y \Delta z$$

$$\text{Mass Flow Accumulation} = (\phi \rho)_{t+\Delta t} - (\phi \rho)_t \, \Delta x \Delta y \Delta z$$

Then, at any instant;

$$\text{Mass Flow In} - \text{Mass Flow Out} = \text{Mass Flow Accumulation}$$

$$(\rho v)_x \, \Delta y \Delta t - (\rho v)_{x+\Delta x} \, \Delta y \Delta z = [(\phi \rho)_{t+\Delta t} - (\phi \rho)_t] \, \frac{\Delta x \Delta y \Delta z}{\Delta t}$$

Dividing by $\Delta x \Delta y \Delta z$, we get:

$$\frac{-(\rho v)_{x+\Delta x} - (\rho v)_x}{\Delta x} = \frac{\phi \, (-\rho_{t+\Delta t} - \rho_t)}{\Delta t}$$

Take the limit as Δx, Δt go to zero;

$$\frac{\partial (\rho v)}{\partial x} = - \partial \, \frac{\partial \rho}{\partial t} \qquad \text{(A-1)}$$

Similarly,

$$\frac{\partial(\rho v)}{\partial y} = - \phi \frac{\partial \rho}{\partial t} \tag{A-2}$$

$$\frac{\partial(\rho v)}{\partial z} = - \phi \frac{\partial \rho}{\partial t} \tag{A-3}$$

Then, for the three-dimensional flow

$$\frac{\partial(\rho v)}{\partial x} + \frac{\partial(\rho v)}{\partial y} + \frac{\partial(\rho v)}{\partial z} = - \phi \frac{\partial \rho}{\partial t} \tag{A-4}$$

But, from Darcy's law

$$v = - \frac{k}{\mu} \frac{\partial P}{\partial x} \tag{A-5}$$

Then, substituting in equation (A-4):

$$\frac{\partial\left(- \frac{k}{\mu} \frac{\partial P}{\partial x} \rho\right)}{\partial x} + \frac{\partial\left(- \frac{k}{\mu} \frac{\partial P}{\partial y} \rho\right)}{\partial y} + \frac{\partial\left(- \frac{k}{\mu} \frac{\partial P}{\partial z} \rho\right)}{\partial z} = -\phi\left(\frac{\partial \rho}{\partial t}\right) \tag{A-6}$$

Using the Gas Law for Real Gases:

$$\rho = \frac{PM}{ZRT} \tag{A-7}$$

we get

$$\frac{\partial\left(- \frac{kPM}{\mu ZRT} \frac{\partial P}{\partial x}\right)}{\partial x} + \frac{\partial\left(- \frac{kPM}{\mu ZRT} \frac{\partial P}{\partial x}\right)}{\partial y} + \frac{\partial\left(- \frac{kPM}{\mu ZRT} \frac{\partial P}{\partial x}\right)}{\partial z}$$

$$= \frac{\phi \partial\left(\frac{PM}{ZRT}\right)}{\partial t}$$

Dividing by M/RT which is assumed to be constant;

$$\frac{\partial(\frac{kP\partial P}{\mu Z\partial x})}{\partial x} + \frac{(\frac{kP\partial P}{\mu Z\partial y})}{\partial y} + \frac{(\frac{kP\partial P}{\mu Z\partial z})}{\partial z} = \frac{\partial}{\partial t}(\frac{P}{z}) \qquad \text{(A-8)}$$

the pseudo-pressure is defined as:

$$m(p) = \int_{P_m}^{P} \frac{2P}{\mu Z}\, dP \qquad \text{(A-9)}$$

then

$$\frac{m}{p} = \frac{2P}{\mu Z}$$

using chain rule:

$$\frac{\partial m}{\partial x} = \frac{\partial m}{\partial p}\frac{\partial p}{\partial x}$$

Then

$$\frac{\partial m}{\partial x} = \frac{\partial p\partial p}{\mu Z\partial x} \qquad \text{(A-10)}$$

$$\frac{\partial m}{\partial y} = \frac{2p\partial p}{\mu Z\partial y} \qquad \text{(A-11)}$$

$$\frac{\partial m}{\partial z} = \frac{2p\partial p}{\mu Z\partial t} \qquad \text{(A-12)}$$

$$\frac{\partial m}{\partial t} = \frac{2p\partial p}{\mu Z\partial t}$$

Now the right-hand size of Equation (A-8) can be written as:

$$\phi\,\frac{\partial(p/Z)}{\partial t} = \phi\,\left(\frac{1}{Z}\frac{\partial p}{\partial t} + p\,\frac{\partial(1/Z)}{\partial t}\right)$$

$$= \phi \left(\frac{1}{Z} + p \frac{\partial(1/Z)}{\partial p}\right) \frac{\partial p}{\partial t}$$

$$= \phi \frac{P}{Z} \left(\frac{1}{p} - \frac{1}{Z} \frac{\partial z}{\partial p}\right) \frac{\partial p}{\partial t} \qquad \text{(A-13)}$$

From the definition of the isothermal gas compressibility;

$$C_g = \frac{1}{p} - \frac{1}{Z} \frac{\partial z}{\partial p} \qquad \text{(A-14)}$$

Substituting equations (A-10) through (A-14) into equation (A-8), we have

$$\frac{\partial}{\partial x} \left(k_x \frac{\partial m}{\partial x}\right) + \frac{\partial}{\partial y} \left(k_y \frac{\partial m}{\partial y}\right) + \frac{\partial}{\partial z} \left(k_z \frac{\partial m}{\partial z}\right)$$

$$= \phi \mu C_g \frac{\partial m}{\partial t} + \frac{2qRT}{vM} \qquad \text{(A-15)}$$

For non-Darcy flow, the velocity of a fluid is given by

$$v = - \frac{\delta k}{\mu} \frac{\partial p}{\partial x} \qquad \text{(A-16)}$$

where δ is defined as:

$$\delta = \frac{1}{1 + \frac{k\beta\rho v}{\mu}} \qquad \text{(A-17)}$$

Thus, for the flow in the formation, we have:

$$\frac{\partial}{\partial x} \left(k_x \frac{\partial m}{\partial x}\right) + \frac{\partial}{\partial y} \left(k_y \frac{\partial m}{\partial y}\right) + \frac{\partial}{\partial z} \left(k_z \frac{\partial m}{\partial z}\right) =$$

$$\phi \mu C_g \frac{\partial m}{\partial t} \qquad \text{(A-18)}$$

and for non-Darcy flow in the fracture:

$$\frac{\partial}{\partial x}\left(\delta k \frac{\partial m}{\partial x}\right) + \frac{\partial}{\partial y}\left(\delta k \frac{\partial m}{\partial y}\right) + \frac{\partial}{\partial z}\left(\delta k \frac{\partial m}{\partial z}\right)$$

$$= \phi_f \mu C_g \frac{\partial m}{\partial t} + q \qquad \text{(A-19)}$$

The above equations represent the flow of gas in the formation and fracture at any point in the reservoir for any instant.

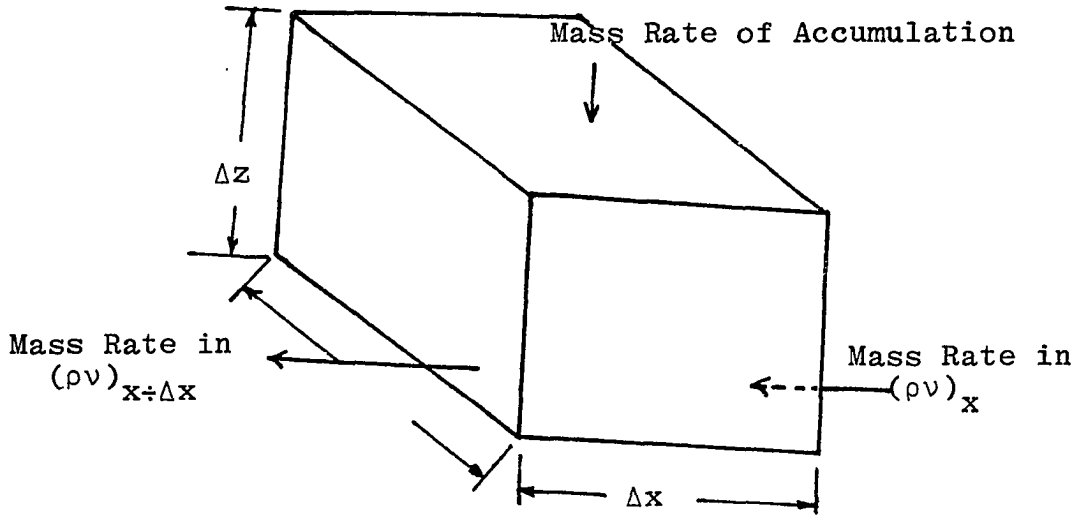


Figure A-1. Gas Mass Balance on Element.

APPENDIX B

APPENDIX B

B-1. FINITE DIFFERENCE MODEL

The flow equation can be expanded in fully implicit finite difference form as:

For formation:

$$\frac{1}{\Delta x_j}\left[k_{j+\frac{1}{2}}\frac{m_{j+1}-m_j}{\Delta x_{j+\frac{1}{2}}}-k_{j-\frac{1}{2}}\frac{m_j-m_{j-1}}{\Delta x_{j-\frac{1}{2}}}\right]^{n+1}$$

$$+\frac{1}{\Delta y_i}\left[k_{i+\frac{1}{2}}\frac{m_{i+1}-m_i}{\Delta y_{i+\frac{1}{2}}}-k_{i-\frac{1}{2}}\frac{m_i-m_{i-1}}{\Delta y_{i-\frac{1}{2}}}\right]^{n+1}$$

$$+\frac{1}{\Delta z_\ell}\left[k_{\ell+\frac{1}{2}}\frac{m_{\ell+1}-m_\ell}{2_{\ell+\frac{1}{2}}}-k_{\ell-\frac{1}{2}}\frac{m_\ell-m_{\ell-1}}{Z_{\ell-\frac{1}{2}}}\right]^{n+1}$$

$$=(\phi\ \mu\ C_g)^{n+1}_{j,i,\ell}\left[\frac{m^{n+1}_{i,j,\ell}-m^{n}_{i,j,\ell}}{\Delta t}\right] \qquad \text{(B-1)}$$

For the fracture cell:

$$\frac{1}{\Delta x_j}\left[(\delta k)_{j+\frac{1}{2}}\frac{m_{j+1}-m_j}{\Delta x_{j+\frac{1}{2}}}-(\delta K)_{j-\frac{1}{2}}\frac{m_j-m_{j-1}}{\Delta x_{j-\frac{1}{2}}}\right]^{n+1}$$

$$+\frac{1}{\Delta y_i}\left[(\delta k)_{i+\frac{1}{2}}\frac{m_{i+1}-m_i}{\Delta y_{i+\frac{1}{2}}}-(\delta k)_{i-\frac{1}{2}}\frac{m_i-m_{i-1}}{\Delta y_{i-\frac{1}{2}}}\right]^{n+1}$$

$$+\frac{1}{\Delta z}\left[(\delta k)_{\ell+\frac{1}{2}}\frac{m_{\ell H}-m_\ell}{\Delta Z_{\ell+\frac{1}{2}}}-(\delta k)_{\ell-\frac{1}{2}}\frac{m_\ell-m_{\ell-1}}{\Delta Z_{\ell-\frac{1}{2}}}\right]^{n+1}$$

$$= (\phi\ \mu\ C_g)^{n+1}_{ij\ell} \left[\frac{m^{n+1}_{ij\ell} - m^{n}_{ij_\ell}}{\Delta t} \right] \qquad \text{(B-2)}$$

Rearranging Equations B-1 and B-2, we have:

For formation cells:

$$C_1\ m_{j+1} + C_2\ m_{j-1} + C_3\ m_{i+1} + C_4\ m_{i-1} + C_5\ m_{\ell+1}$$

$$+ C_6\ m_{\ell-1} - C_7\ m_{ij\ell} = RHS \qquad \text{(B-3)}$$

where:

$$C_1 = \frac{k_{i+\frac{1}{2}}}{\Delta x_j\ \Delta x_{j+\frac{1}{2}}} \qquad \text{(B-4)}$$

$$C_2 = \frac{k_{j-\frac{1}{2}}}{\Delta x_j\ \Delta x_{j-\frac{1}{2}}} \qquad \text{(B-5)}$$

$$C_3 = \frac{k_{i+\frac{1}{2}}}{\Delta y_i\ \Delta y_{i+\frac{1}{2}}} \qquad \text{(B-6)}$$

$$C_4 = \frac{k_{i-\frac{1}{2}}}{\Delta y_i\ \Delta y_{i-\frac{1}{2}}} \qquad \text{(B-7)}$$

$$C_5 = \frac{k_{+\frac{1}{2}}}{\Delta z_\ell\ \Delta z_{\ell+\frac{1}{2}}} \qquad \text{(B-8)}$$

$$C_6 = \frac{k_{-\frac{1}{2}}}{\Delta z_\ell\ \Delta z_{\ell+\frac{1}{2}}} \qquad \text{(B-9)}$$

$$C_7 = C_1 + C_2 + C_3 + C_4 + C_5 + C_6 + C/\Delta t \qquad \text{(B-10)}$$

$$C = (\phi\ \mu\ C_g)^{n+1}_{ij\ell} \qquad \text{(B-11)}$$

$$RHS = -\frac{C}{\Delta t} m^{n}_{ij\ell} + Q \qquad \text{(B-12)}$$

$$Q = \frac{2\ qRT}{vM} \qquad \text{(B-13)}$$

Equation B-3 can be used for the fracture cells as well as formation cells. In case of fracture cells, the coefficients C_1-C_6 are modified to include the Non-Darcy flow factor (s).

$$C_{1f} = \frac{\delta k_{i+\frac{1}{2}}}{\Delta x_i\ \Delta x_{i+\frac{1}{2}}} \qquad \text{(B-14)}$$

$$C_{2f} = \frac{\delta k_{i-\frac{1}{2}}}{\Delta x_i\ \Delta x_{i-\frac{1}{2}}} \qquad \text{(B-15)}$$

$$C_{3f} = \frac{\delta k_{j+\frac{1}{2}}}{\Delta y_i\ \Delta y_{i+\frac{1}{2}}} \qquad \text{(B-16)}$$

$$C_{4f} = \frac{\delta k_{j-\frac{1}{2}}}{\Delta y_j \Delta y_{j-\frac{1}{2}}} \qquad \text{(B-17)}$$

$$C_{5f} = \frac{\delta k_{+\frac{1}{2}}}{\Delta z_k\ \Delta z_{k+\frac{1}{2}}} \qquad \text{(B-18)}$$

$$C_{6f} = \frac{\delta k_{-\frac{1}{2}}}{\Delta z_k\ \Delta z_{-\frac{1}{2}}} \qquad \text{(B-19)}$$

Also,

$$C_{7f} = C_{1f} + C_{2f} + C_{3f} + C_{45} + C_{5f} + C_{6f}$$

$$+ C/\Delta t - \qquad \text{(B-20)}$$

B-2. Two-Point Approximation for Fluid Permeability:

As fluid and reservoir properties are only defined at grid points, some technique must be used for approximating interblock flow coefficients based on values at the grid points. The term that makes up the flow coefficient is the fluid permeability. Permeability changes rapidly enough from grid block to grid block, especially at the fracture faces, to cause a significant difficulty. Although several weighting schemes have been tried for evaluating the permeability at the upstream block face, only the two-point upstream scheme[43] appears to be a useful tool in this model. The two-point scheme provides a reduction in numerical dispersion of the pressure and stability of the solution. Thus, at the planes $(i \pm \frac{1}{2})$ the following approximation is used:

For flow in the minus x-direction:

$$k_{j+\frac{1}{2}} = k_{j+1} - \frac{\Delta x_{j+1}}{\Delta x_{j+1} + \Delta x_{j+2}} (k_{j+2} - k_{j+1}) \qquad \text{(B-21)}$$

$$k_{j-\frac{1}{2}} = k_{j} - \frac{\Delta x}{\Delta x + \Delta x_{j+1}} (k_{j+1} - k_{j}) \qquad \text{(B-22)}$$

For flow in the plus x-direction:

$$k_{j+\frac{1}{2}} = k_{j} + \frac{\Delta x_{j}}{\Delta x_{j} + \Delta x_{j-1}} (k_{j} - k_{j-1}) \qquad \text{(B-23)}$$

$$k_{j-\frac{1}{2}} = k_{j-1} + \frac{\Delta x_{j-1}}{\Delta x_{j-1} + \Delta x_{j-2}} \qquad \text{(B-24)}$$

Equations B-21 through B-24 can be written for y and z directions. The above equations describe linear extrapolations for $k_{j \pm \frac{1}{2}}$ based on values at two upstream grid points.

B-3. Calculating the Real Gas Flow Rate:

Using Darcy's law for laminar flow,

$$v = - 1.127 \times 10^{-3} \frac{k}{\mu} \frac{dP}{dx} \tag{B-25}$$

From Gas law:

$$\frac{P_1 v_1}{Z_1 N T_1 R} = \frac{P_2 v_2}{Z_2 \, n \, R T_2} \tag{B-26}$$

Thus, in field units,

$$q = \frac{q_{SC} \, P_{SC} \, T \, Z}{5.615 \, T_{SC} \, P} \tag{B-27}$$

Substituting Equation B-27 in B-25,

$$\frac{q_{SC} \, P_{SC} \, T \, Z}{5.615 \, T_{SC} \, PA} = - 1.127 \, xp^{-3} \frac{k}{\mu} \frac{dP}{dx}$$

Separate variables,

$$\frac{q_{SC} \, P_{SV} \, T * 10^3}{5.615 * 1.127 \, k \, T_{SC} \, A} \int_0^L dx = - \int_{P_1}^{P_2} \frac{P}{\mu Z} \, dP$$

by definition, the pseudo-pressure function is

$$m(p) = 2 \int_{P_m}^{P} \frac{P}{\mu Z} \, dp \tag{B-28}$$

Then,

$$\frac{2\ q_{SC}\ P_{SC}\ T}{5.615\ x\ 1.127\ x\ 10^{-3}\ k\ T_{SC}\ A} \int_{o}^{L} dx$$

$$= -2 \int_{P_m}^{P_2} \frac{P}{\mu Z}\, dp - \int_{P_m}^{P_1} \frac{P}{\mu Z}\, dp$$

Integrate both sides,

$$\frac{2\ q_{SC}\ P_{SC}\ T\ L}{5.615\ *\ 1.127\ x\ 10^{-3}\ j\ T_x\ A} = m(p)_2 - m(p)_1$$

Thus,

$$q_{SC} = \frac{6.328\ x\ 10^{-3}\ k\ T_{SC}\ A\ \Delta m(p)}{2\ P_{SC}\ T\ L}\ scf/D$$

substituting P_{SC} and T_{SC}:

$$q_{SC} = \frac{0.111925\ k\ A\ \Delta m(p)}{T\ L} \qquad (B\text{-}29)$$

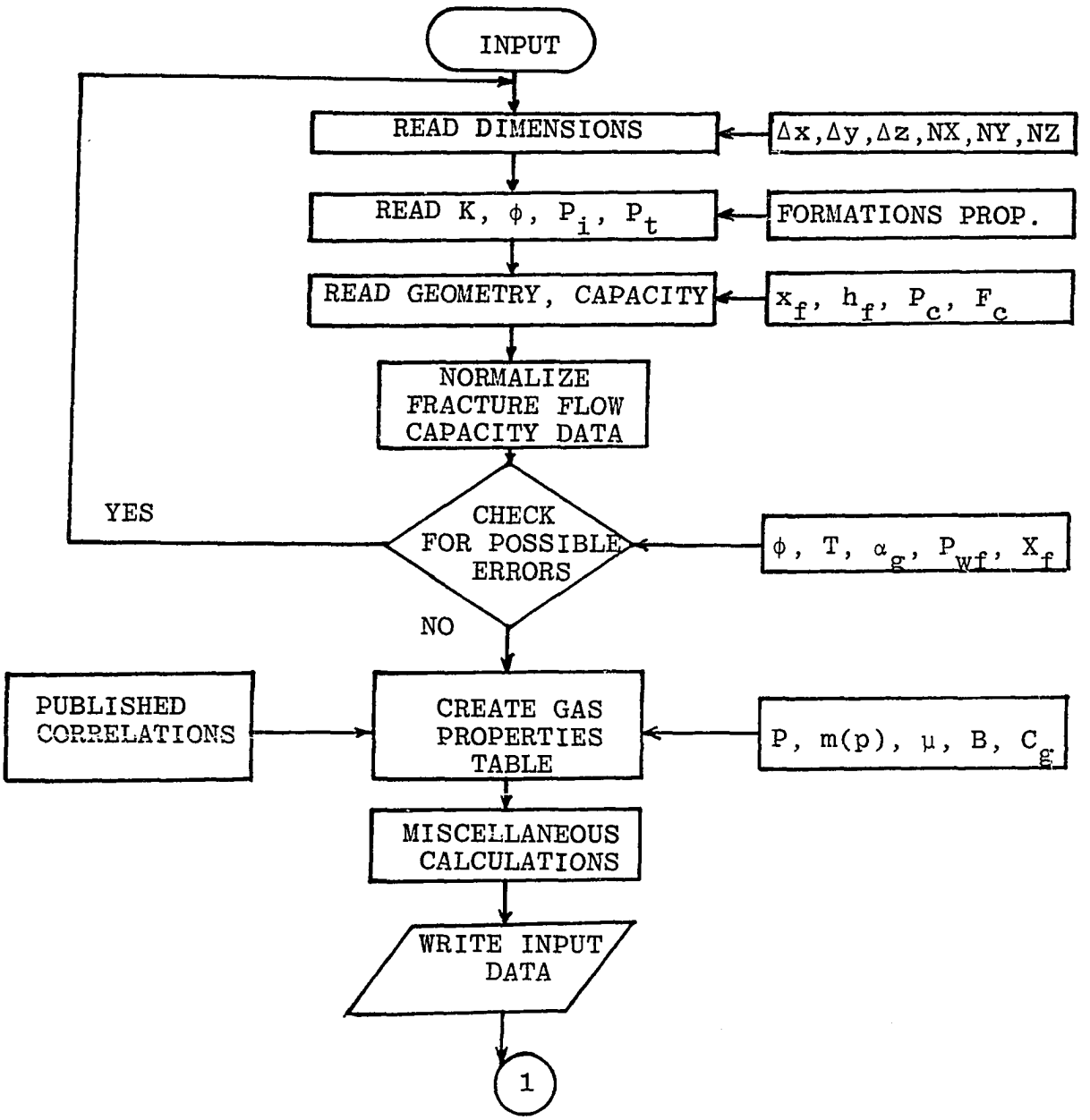
These above equations provide the flow rate of gas at each grid block around the wellbore.

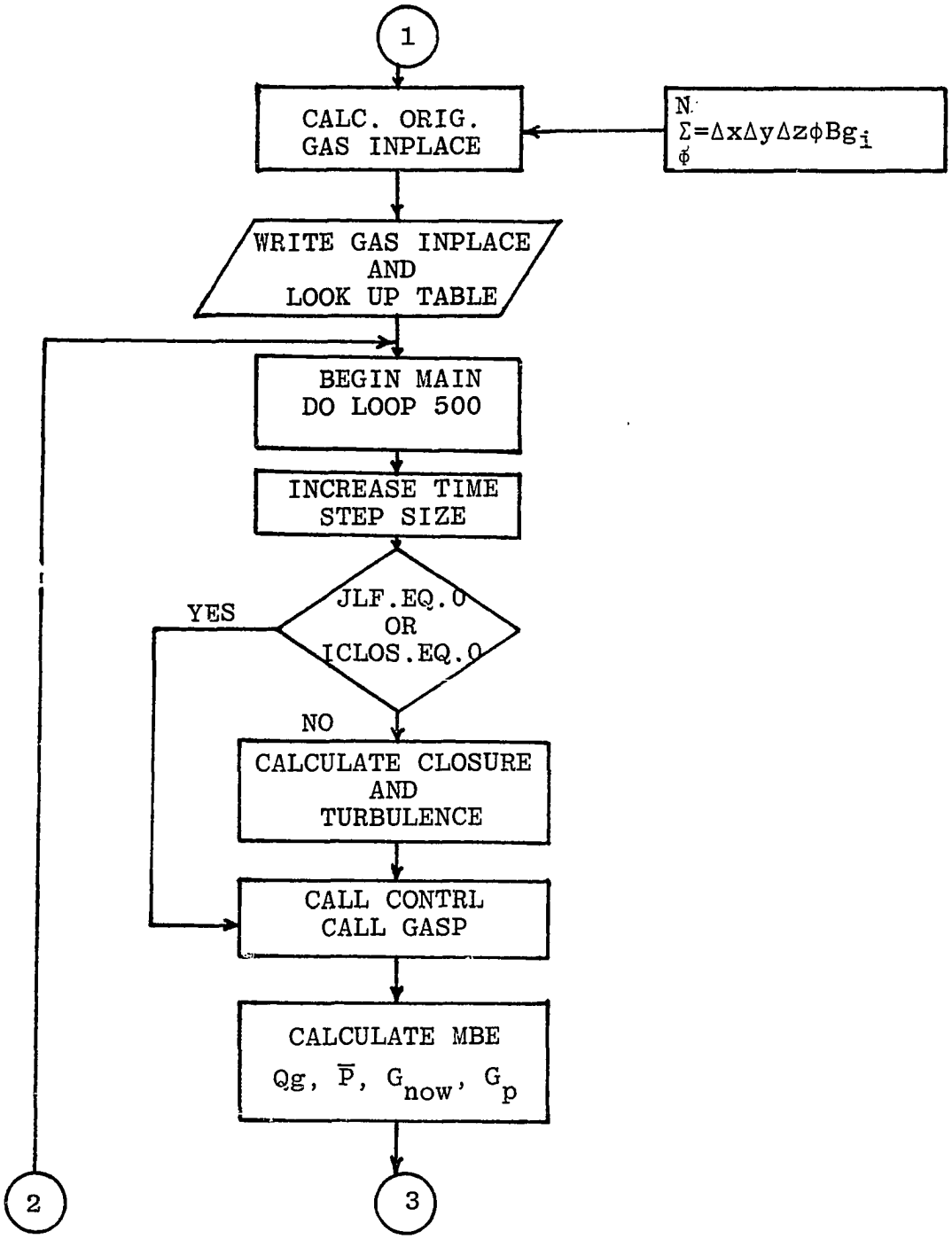
APPENDIX C

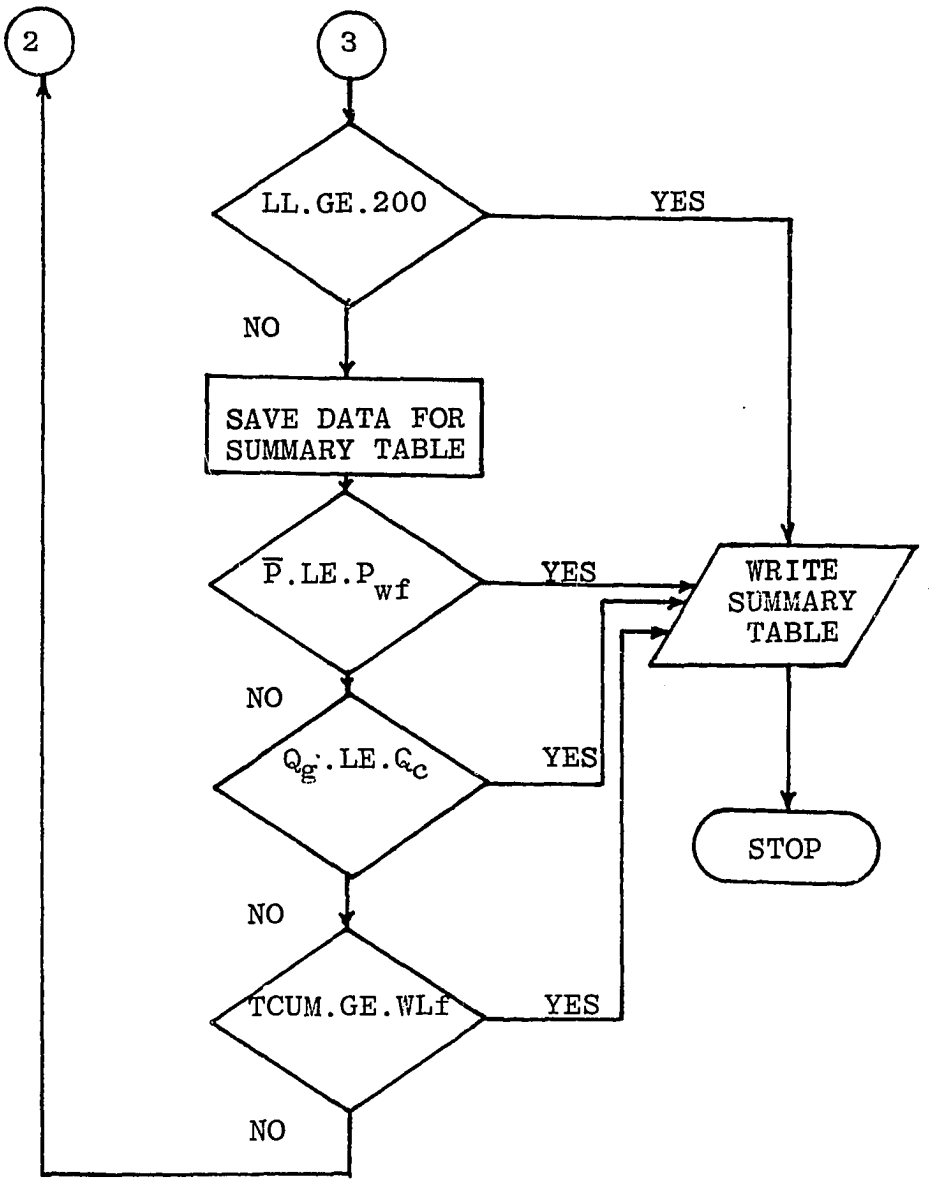
APPENDIX C

FLOW CHARTS

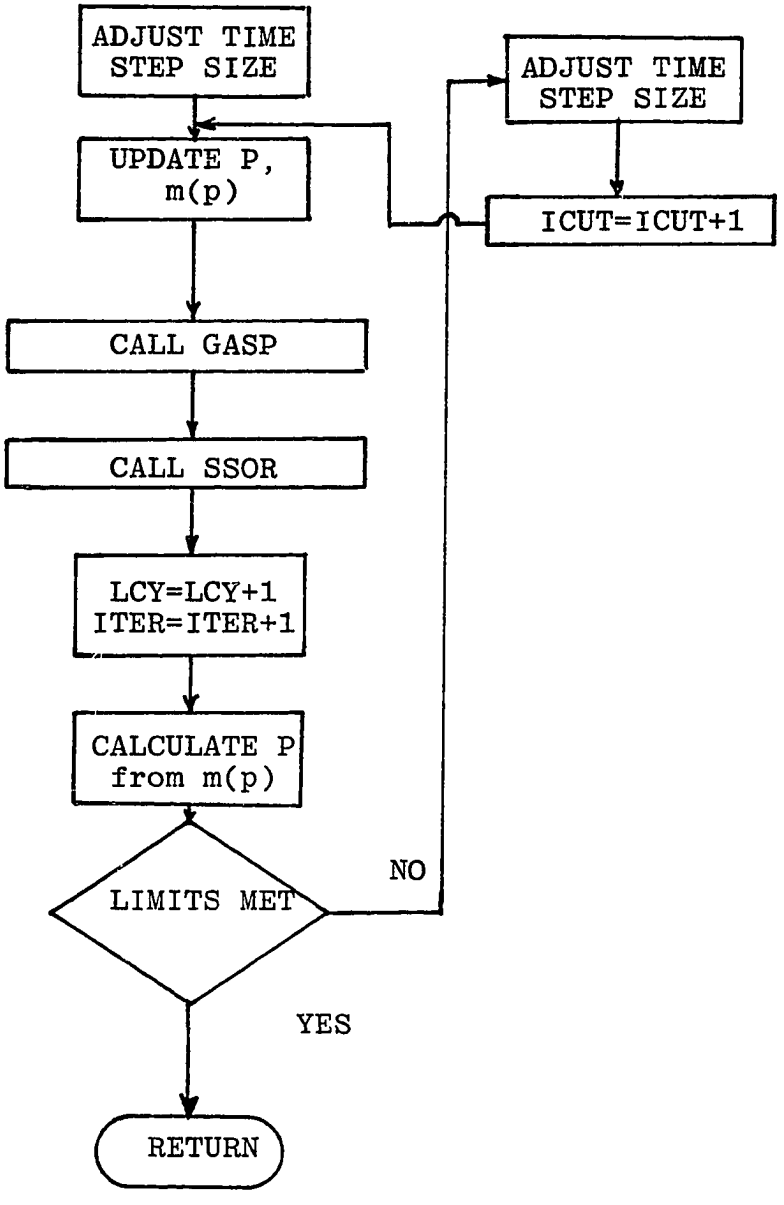
C.1 Flow Chart of Main Program



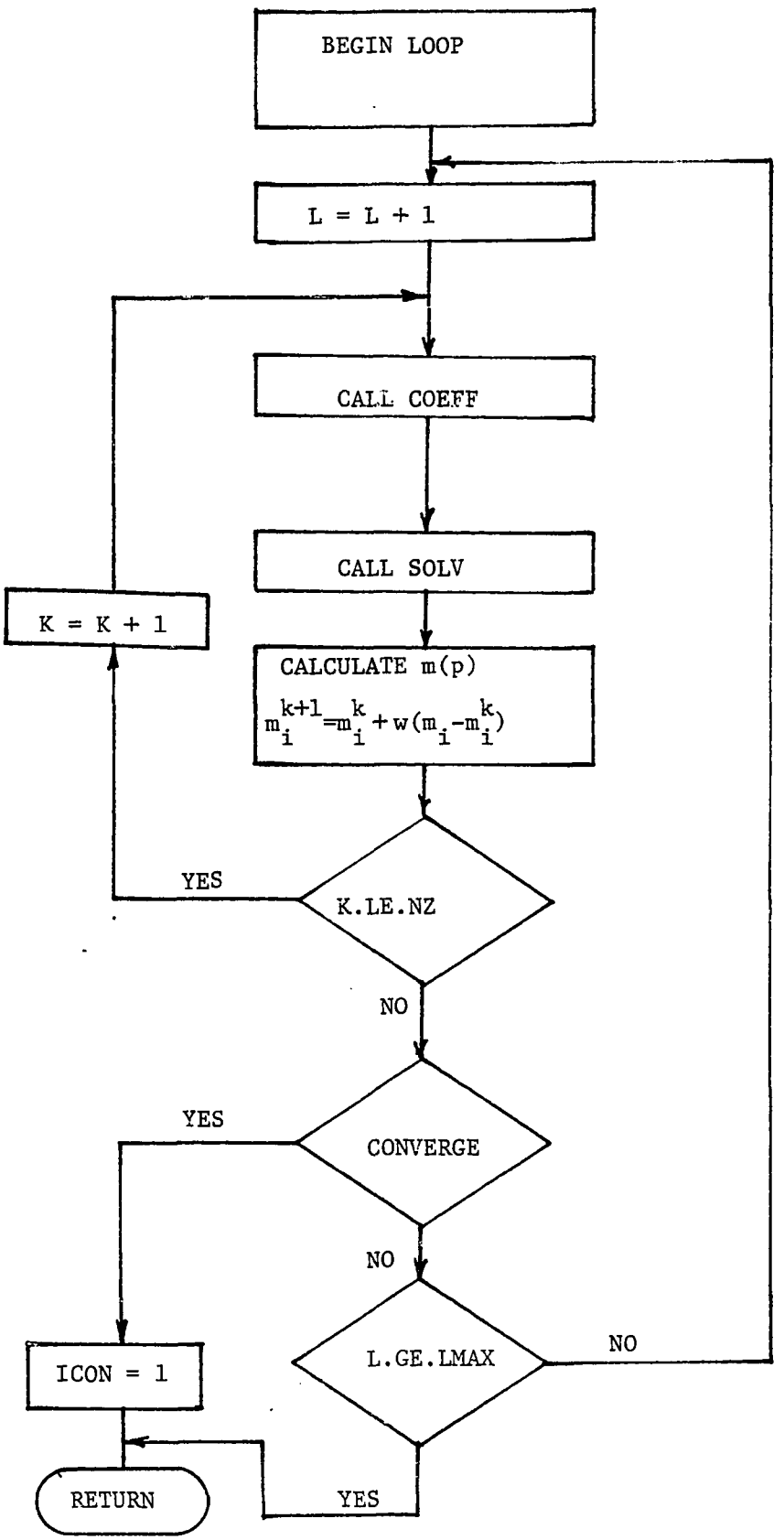

1
CALC. ORIG. GAS INPLACE
$\sum_{\phi}^{N} = \Delta x \Delta y \Delta z \phi Bg_i$
WRITE GAS INPLACE AND LOOK UP TABLE
BEGIN MAIN DO LOOP 500
INCREASE TIME STEP SIZE
JLF.EQ.0 OR ICLOS.EQ.0
YES
NO
CALCULATE CLOSURE AND TURBULENCE
CALL CONTRL
CALL GASP
CALCULATE MBE
Qg, $\overline{P}$, G_{now}, G_p
2
3


2
3
LL.GE.200
YES
NO
SAVE DATA FOR SUMMARY TABLE
$\overline{P}$.LE.P_{wf}
YES
WRITE SUMMARY TABLE
NO
Q_g.LE.Q_c
YES
STOP
NO
TCUM.GE.WLf
YES
NO

C.2 Flow Chart of Subroutine CONTRL



C.3 Flow chart of SSOR



APPENDIX D

APPENDIX D

SAMPLE OUTPUT

THREE DIMENSIONAL SIMULATOR FOR A FRACTURED LAYERED GAS RESERVOIR

HIS IS A TEST FOR FCD=10 ,K1/K2=50
CLOSURE PRESSURE EFFECT HAS BEEN NEGLECTED.
INPUT DATA IS NOT CHECKED FOR POSSIBLE ERRORS
TURBULENT EFFECT HAS BEEN CONSIDERED.

ZONE ONE :

EFFECTIVE PERMEABILITY	0.500	MD
FORMATION POROSITY	0.100	
INITIAL PRESSURE	5000.	PSIA

ZONE TOW :

EFFECTIVE PERMEABILITY	0.010	MD
FORMATION POROSITY	0.100	
INITIAL PRESSURE	5000.	PSIA

NET PAY	40.	FEET
BOTTOM HOLE FLOWING PRESSURE	3000.	PSIA
BOTTOM HOLE TEMPERATURE	250.	F
WELLBORE RADIUS	0.5	FEET
WELL SPACING	160.	ACRES
FRACTURE LENGTH	264.	FEET
FRACTURE FLOW CAPACITY	673.	MD-FT
PROPPANT CONCENTRATION	1500.	LB/1000 SQ.FT
GAS GRAVITY	0.650	

ORIGINAL GAS INPLACE, MMCF = 0.68E+05

FLUID PROPERTIES AND PSEUDO PRESSURE TABLE

	PRESSURE PSI	PSEUDO-PRES. MMPSI**2/CP	BG SCF/CU.FT.	VISCOSITY CPS	COMPRES. 1/PSI
1	.21000E+02	.33183E-01	.10477E+01	.13308E-01	.47684E-01
2	.42000E+02	.13282E+00	.20983E+01	.13308E-01	.23874E-01
3	.63000E+02	.29910E+00	.31517E+01	.13308E-01	.15938E-01
4	.84000E+02	.53209E+00	.42080E+01	.13319E-01	.11969E-01
5	.10500E+03	.83176E+00	.52671E+01	.13333E-01	.95878E-02
6	.12600E+03	.11981E+01	.63290E+01	.13347E-01	.80001E-02
7	.14700E+03	.16312E+01	.73937E+01	.13363E-01	.68660E-02
8	.16800E+03	.21310E+01	.84611E+01	.13381E-01	.60153E-02
9	.18900E+03	.26974E+01	.95313E+01	.13398E-01	.53536E-02
10	.21000E+03	.33303E+01	.10604E+02	.13419E-01	.48241E-02
11	.23100E+03	.40297E+01	.11680E+02	.13440E-01	.43908E-02
12	.25200E+03	.47955E+01	.12758E+02	.13462E-01	.40297E-02
13	.27300E+03	.56275E+01	.13839E+02	.13484E-01	.37240E-02
14	.29400E+03	.65259E+01	.14923E+02	.13506E-01	.34620E-02
15	.31500E+03	.74904E+01	.16009E+02	.13528E-01	.32348E-02
16	.33600E+03	.85210E+01	.17098E+02	.13550E-01	.30360E-02
17	.35700E+03	.96174E+01	.18189E+02	.13581E-01	.28605E-02
18	.37800E+03	.10779E+02	.19283E+02	.13613E-01	.27044E-02
19	.39900E+03	.12006E+02	.20379E+02	.13644E-01	.25647E-02
20	.42000E+03	.13298E+02	.21478E+02	.13665E-01	.24389E-02
21	.44100E+03	.14656E+02	.22579E+02	.13683E-01	.23251E-02
22	.46200E+03	.16080E+02	.23683E+02	.13700E-01	.22216E-02
23	.48300E+03	.17570E+02	.24789E+02	.13726E-01	.21270E-02
24	.50400E+03	.19124E+02	.25898E+02	.13756E-01	.20402E-02
25	.52500E+03	.20744E+02	.27008E+02	.13787E-01	.19604E-02
26	.54600E+03	.22427E+02	.28121E+02	.13823E-01	.18866E-02
27	.56700E+03	.24173E+02	.29237E+02	.13868E-01	.18183E-02
28	.58800E+03	.25981E+02	.30354E+02	.13913E-01	.17548E-02
29	.60900E+03	.27851E+02	.31474E+02	.13958E-01	.16956E-02
30	.63000E+03	.29782E+02	.32595E+02	.14002E-01	.16403E-02
31	.65100E+03	.31775E+02	.33719E+02	.14046E-01	.15886E-02
32	.67200E+03	.33830E+02	.34845E+02	.14090E-01	.15401E-02
33	.69300E+03	.35946E+02	.35973E+02	.14115E-01	.14944E-02
34	.71400E+03	.38126E+02	.37103E+02	.14140E-01	.14514E-02
35	.73500E+03	.40370E+02	.38235E+02	.14164E-01	.14108E-02
36	.75600E+03	.42677E+02	.39369E+02	.14189E-01	.13725E-02
37	.77700E+03	.45048E+02	.40504E+02	.14214E-01	.13361E-02
38	.79800E+03	.47482E+02	.41642E+02	.14239E-01	.13017E-02
39	.81900E+03	.49978E+02	.42781E+02	.14265E-01	.12689E-02
40	.84000E+03	.52538E+02	.43922E+02	.14292E-01	.12378E-02
41	.86100E+03	.55160E+02	.45064E+02	.14319E-01	.12081E-02
42	.88200E+03	.57844E+02	.46208E+02	.14345E-01	.11799E-02
43	.90300E+03	.60590E+02	.47354E+02	.14372E-01	.11529E-02
44	.92400E+03	.63399E+02	.48501E+02	.14399E-01	.11271E-02
45	.94500E+03	.66270E+02	.49650E+02	.14424E-01	.11024E-02
46	.96600E+03	.69203E+02	.50800E+02	.14445E-01	.10787E-02
47	.98700E+03	.72199E+02	.51951E+02	.14466E-01	.10561E-02
48	.10080E+04	.75257E+02	.53104E+02	.14486E-01	.10343E-02
49	.10290E+04	.78379E+02	.54258E+02	.14507E-01	.10134E-02
50	.10500E+04	.81563E+02	.55413E+02	.14528E-01	.99326E-03
51	.10710E+04	.84810E+02	.56570E+02	.14549E-01	.97390E-03
52	.10920E+04	.88117E+02	.57727E+02	.14580E-01	.95526E-03
53	.11130E+04	.91485E+02	.58886E+02	.14613E-01	.93728E-03
54	.11340E+04	.94911E+02	.60045E+02	.14646E-01	.91995E-03
55	.11550E+04	.98397E+02	.61206E+02	.14679E-01	.90321E-03
56	.11760E+04	.10194E+03	.62367E+02	.14711E-01	.88703E-03
57	.11970E+04	.10554E+03	.63529E+02	.14744E-01	.87140E-03
58	.12180E+04	.10921E+03	.64692E+02	.14777E-01	.85627E-03
59	.12390E+04	.11293E+03	.65856E+02	.14809E-01	.84163E-03

60	.12600E+04	.11670E+03	.67020E+02	-14840E-01	.82744E-03
61	.12810E+04	.12054E+03	.68185E+02	.14872E-01	.81369E-03
62	.13020E+04	.12443E+03	.69350E+02	.14904E-01	.80036E-03
63	.13230E+04	.12838E+03	.70516E+02	.14933E-01	.78742E-03
64	.13440E+04	.13239E+03	.71682E+02	.14967E-01	.77485E-03
65	.13650E+04	.13646E+03	.72849E+02	.15008E-01	.76265E-03
66	.13860E+04	.14058E+03	.74016E+02	.15049E-01	.75079E-03
67	.14070E+04	.14475E+03	.75183E+02	.15089E-01	.73925E-03
68	.14280E+04	.14898E+03	.76350E+02	.15130E-01	.72803E-03
69	.14490E+04	.15326E+03	.77517E+02	.15170E-01	.71711E-03
70	.14700E+04	.15759E+03	.78685E+02	.15211E-01	.70647E-03
71	.14910E+04	.16198E+03	.79852E+02	.15251E-01	.69611E-03
72	.15120E+04	.16642E+03	.81019E+02	.15292E-01	.68601E-03
73	.15330E+04	.17091E+03	.82186E+02	.15332E-01	.67616E-03
74	.15540E+04	.17546E+03	.83353E+02	.15373E-01	.66656E-03
75	.15750E+04	.18005E+03	.84520E+02	.15413E-01	.65718E-03
76	.15960E+04	.18470E+03	.85686E+02	.15454E-01	.64803E-03
77	.16170E+04	.18940E+03	.86852E+02	.15494E-01	.63910E-03
78	.16380E+04	.19415E+03	.88018E+02	.15535E-01	.63037E-03
79	.16590E+04	.19895E+03	.89182E+02	.15575E-01	.62184E-03
80	.16800E+04	.20381E+03	.90347E+02	.15616E-01	.61350E-03
81	.17010E+04	.20871E+03	.91510E+02	.15656E-01	.60535E-03
82	.17220E+04	.21366E+03	.92673E+02	.15697E-01	.59737E-03
83	.17430E+04	.21866E+03	.93835E+02	.15737E-01	.58957E-03
84	.17640E+04	.22371E+03	.94997E+02	.15778E-01	.58193E-03
85	.17850E+04	.22881E+03	.96157E+02	.15818E-01	.57445E-03
86	.18060E+04	.23396E+03	.97317E+02	.15859E-01	.56712E-03
87	.18270E+04	.23916E+03	.98475E+02	.15899E-01	.55995E-03
88	.18480E+04	.24440E+03	.99633E+02	.15940E-01	.55292E-03
89	.18690E+04	.24970E+03	.10079E+03	.15980E-01	.54603E-03
90	.18900E+04	.25504E+03	.10194E+03	.16021E-01	.53927E-03
91	.19110E+04	.26042E+03	.10310E+03	.16061E-01	.53265E-03
92	.19320E+04	.26586E+03	.10425E+03	.16102E-01	.52615E-03
93	.19530E+04	.27134E+03	.10540E+03	.16142E-01	.51978E-03
94	.19740E+04	.27687E+03	.10655E+03	.16183E-01	.51352E-03
95	.19950E+04	.28244E+03	.10770E+03	.16224E-01	.50738E-03
96	.20160E+04	.28806E+03	.10885E+03	.16264E-01	.50135E-03
97	.20370E+04	.29372E+03	.10999E+03	.16307E-01	.49544E-03
98	.20580E+04	.29943E+03	.11114E+03	.16351E-01	.48962E-03
99	.20790E+04	.30518E+03	.11228E+03	.16394E-01	.48392E-03
100	.21000E+04	.31098E+03	.11342E+03	.16437E-01	.47831E-03
101	.21210E+04	.31682E+03	.11456E+03	.16480E-01	.47280E-03
102	.21420E+04	.32270E+03	.11569E+03	.16524E-01	.46738E-03
103	.21630E+04	.32862E+03	.11683E+03	.16567E-01	.46206E-03
104	.21840E+04	.33458E+03	.11796E+03	.16610E-01	.45682E-03
105	.22050E+04	.34059E+03	.11909E+03	.16653E-01	.45168E-03
106	.22260E+04	.34664E+03	.12022E+03	.16697E-01	.44661E-03
107	.22470E+04	.35273E+03	.12134E+03	.16740E-01	.44164E-03
108	.22680E+04	.35886E+03	.12247E+03	.16783E-01	.43674E-03
109	.22890E+04	.36503E+03	.12359E+03	.16826E-01	.43192E-03
110	.23100E+04	.37125E+03	.12471E+03	.16869E-01	.42718E-03
111	.23310E+04	.37750E+03	.12583E+03	.16913E-01	.42252E-03
112	.23520E+04	.38379E+03	.12694E+03	.16956E-01	.41792E-03
113	.23730E+04	.39012E+03	.12806E+03	.16999E-01	.41340E-03
114	.23940E+04	.39649E+03	.12917E+03	.17042E-01	.40895E-03
115	.24150E+04	.40290E+03	.13028E+03	.17086E-01	.40457E-03
116	.24360E+04	.40934E+03	.13138E+03	.17129E-01	.40026E-03
117	.24570E+04	.41583E+03	.13248E+03	.17172E-01	.39601E-03
118	.24780E+04	.42235E+03	.13358E+03	.17215E-01	.39182E-03
119	.24990E+04	.42891E+03	.13468E+03	.17258E-01	.38770E-03
120	.25200E+04	.43551E+03	.13578E+03	.17302E-01	.38364E-03
121	.25410E+04	.44214E+03	.13687E+03	.17345E-01	.37964E-03
122	.25620E+04	.44881E+03	.13796E+03	.17388E-01	.37570E-03
123	.25830E+04	.45552E+03	.13905E+03	.17431E-01	.37182E-03
124	.26040E+04	.46226E+03	.14013E+03	.17475E-01	.36799E-03

125	.26250E+04	.46904E+03	.14121E+03	.17518E-01	.36422E-03
126	.26460E+04	.47585E+03	.14229E+03	.17561E-01	.36050E-03
127	.26670E+04	.48270E+03	.14337E+03	.17604E-01	.35683E-03
128	.26880E+04	.48958E+03	.14444E+03	.17648E-01	.35322E-03
129	.27090E+04	.49649E+03	.14551E+03	.17700E-01	.34966E-03
130	.27300E+04	.50344E+03	.14658E+03	.17751E-01	.34615E-03
131	.27510E+04	.51042E+03	.14764E+03	.17802E-01	.34268E-03
132	.27720E+04	.51742E+03	.14870E+03	.17853E-01	.33927E-03
133	.27930E+04	.52446E+03	.14976E+03	.17904E-01	.33590E-03
134	.28140E+04	.53152E+03	.15081E+03	.17955E-01	.33258E-03
135	.28350E+04	.53862E+03	.15187E+03	.18007E-01	.32931E-03
136	.28560E+04	.54574E+03	.15292E+03	.18058E-01	.32608E-03
137	.28770E+04	.55290E+03	.15396E+03	.18109E-01	.32289E-03
138	.28980E+04	.56008E+03	.15500E+03	.18160E-01	.31975E-03
139	.29190E+04	.56729E+03	.15604E+03	.18211E-01	.31665E-03
140	.29400E+04	.57452E+03	.15708E+03	.18262E-01	.31359E-03
141	.29610E+04	.58179E+03	.15811E+03	.18314E-01	.31057E-03
142	.29820E+04	.58908E+03	.15914E+03	.18365E-01	.30759E-03
143	.30030E+04	.59640E+03	.16017E+03	.18416E-01	.30465E-03
144	.30240E+04	.60374E+03	.16119E+03	.18467E-01	.30175E-03
145	.30450E+04	.61111E+03	.16221E+03	.18518E-01	.29889E-03
146	.30660E+04	.61851E+03	.16323E+03	.18569E-01	.29607E-03
147	.30870E+04	.62593E+03	.16424E+03	.18621E-01	.29328E-03
148	.31080E+04	.63338E+03	.16525E+03	.18672E-01	.29053E-03
149	.31290E+04	.64085E+03	.16626E+03	.18723E-01	.28781E-03
150	.31500E+04	.64835E+03	.16726E+03	.18774E-01	.28513E-03
151	.31710E+04	.65587E+03	.16826E+03	.18825E-01	.28249E-03
152	.31920E+04	.66342E+03	.16926E+03	.18876E-01	.27988E-03
153	.32130E+04	.67099E+03	.17025E+03	.18928E-01	.27730E-03
154	.32340E+04	.67858E+03	.17124E+03	.18979E-01	.27475E-03
155	.32550E+04	.68620E+03	.17222E+03	.19030E-01	.27224E-03
156	.32760E+04	.69384E+03	.17321E+03	.19081E-01	.26976E-03
157	.32970E+04	.70150E+03	.17419E+03	.19132E-01	.26731E-03
158	.33180E+04	.70919E+03	.17516E+03	.19183E-01	.26489E-03
159	.33390E+04	.71690E+03	.17614E+03	.19235E-01	.26251E-03
160	.33600E+04	.72463E+03	.17711E+03	.19286E-01	.26015E-03
161	.33810E+04	.73238E+03	.17807E+03	.19337E-01	.25782E-03
162	.34020E+04	.74015E+03	.17903E+03	.19388E-01	.25552E-03
163	.34230E+04	.74795E+03	.17999E+03	.19439E-01	.25325E-03
164	.34440E+04	.75576E+03	.18095E+03	.19490E-01	.25101E-03
165	.34650E+04	.76360E+03	.18190E+03	.19542E-01	.24879E-03
166	.34860E+04	.77146E+03	.18285E+03	.19593E-01	.24660E-03
167	.35070E+04	.77933E+03	.18379E+03	.19644E-01	.24444E-03
168	.35280E+04	.78723E+03	.18474E+03	.19695E-01	.24231E-03
169	.35490E+04	.79515E+03	.18567E+03	.19746E-01	.24020E-03
170	.35700E+04	.80308E+03	.18661E+03	.19797E-01	.23811E-03
171	.35910E+04	.81104E+03	.18754E+03	.19849E-01	.23606E-03
172	.36120E+04	.81901E+03	.18847E+03	.19900E-01	.23402E-03
173	.36330E+04	.82701E+03	.18939E+03	.19951E-01	.23202E-03
174	.36540E+04	.83502E+03	.19031E+03	.20002E-01	.23003E-03
175	.36750E+04	.84305E+03	.19123E+03	.20053E-01	.22807E-03
176	.36960E+04	.85110E+03	.19215E+03	.20104E-01	.22613E-03
177	.37170E+04	.85916E+03	.19306E+03	.20156E-01	.22422E-03
178	.37380E+04	.86725E+03	.19396E+03	.20207E-01	.22233E-03
179	.37590E+04	.87535E+03	.19487E+03	.20258E-01	.22046E-03
180	.37800E+04	.88346E+03	.19577E+03	.20309E-01	.21862E-03
181	.38010E+04	.89160E+03	.19666E+03	.20360E-01	.21679E-03
182	.38220E+04	.89975E+03	.19756E+03	.20411E-01	.21499E-03
183	.38430E+04	.90792E+03	.19845E+03	.20463E-01	.21321E-03
184	.38640E+04	.91610E+03	.19934E+03	.20514E-01	.21144E-03
185	.38850E+04	.92430E+03	.20022E+03	.20565E-01	.20970E-03
186	.39060E+04	.93251E+03	.20110E+03	.20616E-01	.20798E-03
187	.39270E+04	.94074E+03	.20198E+03	.20667E-01	.20628E-03
188	.39480E+04	.94899E+03	.20285E+03	.20718E-01	.20460E-03
189	.39690E+04	.95725E+03	.20372E+03	.20769E-01	.20294E-03

190	.39900E+04	.96953E+03	.20459E+03	.20821E-01	.20130E-03
191	.40110E+04	.97382E+03	.20545E+03	.20872E-01	.19968E-03
192	.40320E+04	.98212E+03	.20631E+03	.20923E-01	.19807E-03
193	.40530E+04	.99044E+03	.20716E+03	.20977E-01	.19649E-03
194	.40740E+04	.99877E+03	.20802E+03	.21030E-01	.19492E-03
195	.40950E+04	.10071E+04	.20887E+03	.21083E-01	.19337E-03
196	.41160E+04	.10155E+04	.20971E+03	.21136E-01	.19184E-03
197	.41370E+04	.10238E+04	.21056E+03	.21189E-01	.19032E-03
198	.41580E+04	.10322E+04	.21140E+03	.21243E-01	.18883E-03
199	.41790E+04	.10406E+04	.21223E+03	.21296E-01	.18734E-03
200	.42000E+04	.10490E+04	.21307E+03	.21349E-01	.18588E-03
201	.42210E+04	.10574E+04	.21390E+03	.21402E-01	.18443E-03
202	.42420E+04	.10659E+04	.21472E+03	.21456E-01	.18300E-03
203	.42630E+04	.10743E+04	.21555E+03	.21509E-01	.18159E-03
204	.42840E+04	.10828E+04	.21637E+03	.21562E-01	.18019E-03
205	.43050E+04	.10912E+04	.21719E+03	.21615E-01	.17880E-03
206	.43260E+04	.10997E+04	.21800E+03	.21668E-01	.17743E-03
207	.43470E+04	.11082E+04	.21881E+03	.21722E-01	.17608E-03
208	.43680E+04	.11167E+04	.21962E+03	.21775E-01	.17474E-03
209	.43890E+04	.11252E+04	.22042E+03	.21828E-01	.17341E-03
210	.44100E+04	.11337E+04	.22122E+03	.21881E-01	.17210E-03
211	.44310E+04	.11422E+04	.22202E+03	.21934E-01	.17081E-03
212	.44520E+04	.11508E+04	.22282E+03	.21988E-01	.16953E-03
213	.44730E+04	.11593E+04	.22361E+03	.22041E-01	.16826E-03
214	.44940E+04	.11679E+04	.22440E+03	.22094E-01	.16701E-03
215	.45150E+04	.11765E+04	.22518E+03	.22147E-01	.16576E-03
216	.45360E+04	.11850E+04	.22596E+03	.22201E-01	.16454E-03
217	.45570E+04	.11936E+04	.22674E+03	.22254E-01	.16332E-03
218	.45780E+04	.12022E+04	.22752E+03	.22307E-01	.16212E-03
219	.45990E+04	.12108E+04	.22829E+03	.22360E-01	.16094E-03
220	.46200E+04	.12194E+04	.22906E+03	.22413E-01	.15976E-03
221	.46410E+04	.12280E+04	.22983E+03	.22467E-01	.15860E-03
222	.46620E+04	.12367E+04	.23059E+03	.22520E-01	.15745E-03
223	.46830E+04	.12453E+04	.23135E+03	.22573E-01	.15631E-03
224	.47040E+04	.12539E+04	.23211E+03	.22626E-01	.15518E-03
225	.47250E+04	.12626E+04	.23287E+03	.22680E-01	.15407E-03
226	.47460E+04	.12713E+04	.23362E+03	.22733E-01	.15297E-03
227	.47670E+04	.12799E+04	.23437E+03	.22786E-01	.15187E-03
228	.47880E+04	.12886E+04	.23511E+03	.22839E-01	.15079E-03
229	.48090E+04	.12973E+04	.23586E+03	.22892E-01	.14973E-03
230	.48300E+04	.13060E+04	.23660E+03	.22946E-01	.14867E-03
231	.48510E+04	.13147E+04	.23733E+03	.22999E-01	.14762E-03
232	.48720E+04	.13234E+04	.23807E+03	.23052E-01	.14659E-03
233	.48930E+04	.13321E+04	.23880E+03	.23105E-01	.14556E-03
234	.49140E+04	.13408E+04	.23953E+03	.23159E-01	.14455E-03
235	.49350E+04	.13495E+04	.24025E+03	.23212E-01	.14354E-03
236	.49560E+04	.13582E+04	.24098E+03	.23265E-01	.14255E-03
237	.49770E+04	.13670E+04	.24170E+03	.23318E-01	.14157E-03
238	.49980E+04	.13757E+04	.24241E+03	.23371E-01	.14059E-03
239	.50190E+04	.13845E+04	.24313E+03	.23425E-01	.13963E-03
240	.50400E+04	.13932E+04	.24384E+03	.23478E-01	.13867E-03
241	.50610E+04	.14020E+04	.24455E+03	.23531E-01	.13773E-03
242	.50820E+04	.14107E+04	.24525E+03	.23584E-01	.13680E-03
243	.51030E+04	.14195E+04	.24596E+03	.23638E-01	.13587E-03

SUMMARY OF THE RESULTS

TIME DAYS	FLOW RATE MCF/D	CUM. PRODUCTION MMCF	AVG. PRESSURE PSIA	1/QD	TD
0.0001	0.13316E+06	0.13316E-01	4999.91	0.5918596E-01	0.7050101E-05
0.0002	0.86621E+05	0.26309E-01	4999.88	0.9098548E-01	0.1762524E-04
0.0005	0.73655E+05	0.42882E-01	4999.85	0.1070030E+00	0.3348796E-04
0.0008	0.68036E+05	0.65844E-01	4999.83	0.1158401E+00	0.5728203E-04
0.0013	0.63988E+05	0.98238E-01	4999.80	0.1231676E+00	0.9297318E-04
0.0021	0.60308E+05	0.14403E+00	4999.75	0.1306830E+00	0.1465098E-03
0.0032	0.56584E+05	0.20849E+00	4999.68	0.1392841E+00	0.2268149E-03
0.0049	0.52701E+05	0.29853E+00	4999.59	0.1495467E+00	0.3472720E-03
0.0075	0.48320E+05	0.42237E+00	4999.46	0.1631064E+00	0.5279584E-03
0.0113	0.43542E+05	0.58976E+00	4999.30	0.1810042E+00	0.7989875E-03
0.0171	0.38401E+05	0.81120E+00	4999.07	0.2052361E+00	0.1205532E-02
0.0257	0.33236E+05	0.10987E+01	4998.79	0.2371296E+00	0.1815347E-02
0.0387	0.28404E+05	0.14672E+01	4998.43	0.2774681E+00	0.2730071E-02
0.0582	0.24325E+05	0.19406E+01	4997.96	0.3240038E+00	0.4102156E-02
0.0874	0.21196E+05	0.25594E+01	4997.35	0.3718207E+00	0.6160282E-02
0.1312	0.18873E+05	0.33858E+01	4996.53	0.4175958E+00	0.9247471E-02
0.1969	0.17075E+05	0.45074E+01	4995.41	0.4615787E+00	0.1387825E-01
0.2954	0.15485E+05	0.60351E+01	4993.90	0.5089564E+00	0.2082444E-01
0.4432	0.13943E+05	0.80937E+01	4991.89	0.5652505E+00	0.3124370E-01
0.6648	0.12399E+05	0.10842E+02	4989.25	0.6356291E+00	0.4687260E-01
0.9974	0.10915E+05	0.14472E+02	4985.75	0.7220758E+00	0.7031590E-01
1.4962	0.95346E+04	0.19228E+02	4981.19	0.8265942E+00	0.1054809E+00
2.2443	0.82992E+04	0.25437E+02	4975.27	0.9496382E+00	0.1582284E+00
3.3666	0.72135E+04	0.33532E+02	4967.50	0.1092575E+01	0.2373497E+00
5.0500	0.62921E+04	0.44125E+02	4957.31	0.1252561E+01	0.3560315E+00
7.5751	0.55260E+04	0.58078E+02	4943.81	0.1426224E+01	0.5340543E+00
11.3628	0.49106E+04	0.76678E+02	4925.77	0.1604948E+01	0.8010886E+00
17.0443	0.44115E+04	0.10174E+03	4901.56	0.1786536E+01	0.1201639E+01
25.5665	0.39944E+04	0.13578E+03	4868.94	0.1973067E+01	0.1802465E+01
38.3499	0.36346E+04	0.18225E+03	4824.46	0.2168423E+01	0.2703705E+01
57.5249	0.33143E+04	0.24580E+03	4763.51	0.2377970E+01	0.4055565E+01
86.2875	0.30294E+04	0.33293E+03	4680.10	0.2601586E+01	0.6083354E+01
126.2875	0.27779E+04	0.44405E+03	4576.93	0.2837137E+01	0.8903395E+01
166.2875	0.25752E+04	0.54706E+03	4481.57	0.3060420E+01	0.1172344E+02
206.2875	0.24043E+04	0.64323E+03	4393.43	0.3278038E+01	0.1454348E+02
246.2875	0.22543E+04	0.73340E+03	4313.68	0.3496175E+01	0.1736351E+02
286.2874	0.21179E+04	0.81811E+03	4239.05	0.3721197E+01	0.2018355E+02
326.2874	0.19911E+04	0.89770E+03	4170.28	0.3958201E+01	0.2300359E+02
366.2874	0.18749E+04	0.97275E+03	4106.01	0.4203659E+01	0.2582362E+02
406.2874	0.17674E+04	0.10434E+04	4046.36	0.4459163E+01	0.2864366E+02
446.2874	0.16694E+04	0.11102E+04	3991.32	0.4721134E+01	0.3146371E+02
486.2874	0.15791E+04	0.11734E+04	3940.11	0.4990943E+01	0.3428375E+02
526.2874	0.14957E+04	0.12332E+04	3891.92	0.5269249E+01	0.3710379E+02
566.2874	0.14166E+04	0.12899E+04	3846.00	0.5563544E+01	0.3992383E+02
606.2874	0.13412E+04	0.13435E+04	3802.83	0.5876255E+01	0.4274387E+02
646.2874	0.12702E+04	0.13943E+04	3763.90	0.6204881E+01	0.4556389E+02
686.2874	0.12052E+04	0.14425E+04	3726.81	0.6539446E+01	0.4838394E+02
726.2874	0.11462E+04	0.14884E+04	3691.08	0.6875872E+01	0.5120396E+02
766.2874	0.10885E+04	0.15319E+04	3657.26	0.7240344E+01	0.5402403E+02
806.2874	0.10347E+04	0.15733E+04	3626.14	0.7616955E+01	0.5684406E+02
846.2874	0.98403E+03	0.16127E+04	3596.47	0.8009151E+01	0.5966411E+02
886.2874	0.93536E+03	0.16501E+04	3568.86	0.8425914E+01	0.6248413E+02
926.2874	0.89183E+03	0.16858E+04	3543.00	0.8837161E+01	0.6530420E+02
966.2874	0.85102E+03	0.17198E+04	3518.71	0.9260962E+01	0.6812421E+02
1006.2874	0.81058E+03	0.17522E+04	3495.30	0.9723057E+01	0.7094427E+02

1046.2874	0.77357E+03	0.17832E+04	3473.02	0.1018818E+02	0.7376430E+02
1086.2874	0.73621E+03	0.18126E+04	3451.28	0.1070525E+02	0.7658435E+02
1126.2874	0.70348E+03	0.18408E+04	3431.36	0.1120330E+02	0.7940437E+02
1166.2874	0.67104E+03	0.18676E+04	3412.21	0.1174484E+02	0.8222444E+02
1206.2874	0.64009E+03	0.18932E+04	3393.43	0.1231275E+02	0.8504446E+02
1246.2874	0.61182E+03	0.19177E+04	3376.07	0.1288169E+02	0.8786452E+02
1286.2874	0.58460E+03	0.19411E+04	3359.49	0.1348147E+02	0.9068454E+02
1326.2874	0.55880E+03	0.19634E+04	3343.65	0.1410405E+02	0.9350461E+02
1366.2874	0.53473E+03	0.19848E+04	3328.96	0.1473880E+02	0.9632463E+02
1406.2874	0.51175E+03	0.20053E+04	3315.17	0.1540062E+02	0.9914468E+02
1446.2874	0.49004E+03	0.20249E+04	3302.09	0.1608282E+02	0.1019647E+03